# *The Development of the (U-Th)/He Thermochronometer*

Thesis by

Richmond A. Wolf

In Partial Fulfillment of the Requirements

for the Degree of

Doctor of Philosophy

California Institute of Technology

Pasadena, California

1997

(submitted May 28, 1997)

*To Kitty, Mom, and Dad*

# Acknowledgments

I am pleased to have an opportunity to acknowledge the many people who were a part of this dissertation. My primary advisors, Dr. Ken Farley and Dr. Lee Silver, provided me with academic, intellectual, and financial support. Dr. Farley taught me a great deal about noble gas geochemistry, and I appreciate the opportunity to have worked in his laboratory. Dr. Silver expanded my knowledge of geology and taught me the importance of breadth as an earth scientist. I would also like to express my gratitude to the National Science Foundation for providing funding for our research.

I would like to thank Dr. Brian Wernicke and Dr. Don Burnett for serving on my academic committee and engaging in many helpful discussions, as well as thank Dr. Sam Epstein for his support and encouragement. I am also grateful to Dr. Brian Wernicke and Dr. Kerry Sieh for sponsoring my research during my first year at Caltech.

Dave Kass, who was collaborator on the modeling of helium diffusion, and Dr. Paul Fitzgerald, who provided samples in a collaborative effort to study Gold Butte, Nevada, were an important part of this work. I would like to thank Paul Asimow, Dr. Mark Harrison, Dr. Marty Grove, Dr. Oscar Lovera, and Phil Watts for helpful discussions. I am appreciative of the technical training I received from Dr. Des Patterson and Vic Nenow. Dr. Gary Clow provided a heat flow model used in our study of Cajon Pass. Paul Carpenter and Dr. Peter Green were helpful while using the analytical facilities that are in their respective charge.

Dr. Don Porcelli read many drafts of my thesis and offered much support, only having to be bribed by a cup of coffee and an occasional whisky.

I would like to thank all my friends and colleagues who made this a more enriching experience, with special thanks to Donna Sackett and Tom Mannion for help in the closing weeks and to Mark Wild, Dr. Kim West, Dr. Doug Yule, and Tom Lloyd for their encouragement along the way.

I am grateful to Dr. Nick Cull, Dr. Jamie Shanley, Dr. John Suppe, and Dr. Robert Hargraves for their encouragement to pursue a Ph.D. Dr. Suppe and Dr. Hargraves served as my undergraduate mentors and instilled in me an everlasting appreciation of geology.

I would be remiss in not thanking my family, for they are the chief source of my ambitions. My grandmother, Becky, and my great aunts, Edna and Helen, have always been a source of reassurance in whatever path I have chosen. I cannot thank my parents enough for what they have given me. Not only are they kind, generous, and forgiving, but they are truly my friends. I dedicate the thesis to my parents, for they instilled in me the motivation to complete the task and supported me every step of the way.

Finally, I would like to thank the person who stood by me as I completed this work, and gave me the courage to do it, Kitty Erkkila. W. H. Auden would appreciate that she is "my north, my south, my east and west; my working week and my Sunday rest." I also dedicate the thesis to her because she takes the time to listen to all of me.

# Abstract

(U-Th)/He dating of apatite provides a tool for recording the low temperature (<100°C) history of the crust. A model based on stopping distances in apatite relates the fraction of alpha particles emitted from the crystal during U and Th decay to crystal size. Helium ages for different sized apatite aliquots are indistinguishable when corrected for the effects of alpha emission. Diffusion coefficients were measured by the incremental outgassing of helium from apatite. The measured range of diffusion parameters is nearly identical for apatites of different chemical composition, grain size, and grain morphology. Isothermal experiments are consistent with spherical diffusion domains which are smaller than the physical grain size.

Helium ages may reflect complex thermal histories where samples spend considerable amounts of time in the region where helium is only partially retained. Therefore, the solution to the full radiogenic helium diffusion/production equation is used to interpret helium ages instead of Dodson's (1973) closure temperature formulation. The time required to achieve a steady state between helium production and diffusion at various temperatures can be determined, as well as the range of temperatures defining the helium partial retention zone (the region where helium retentivity is most sensitive to temperature). In general, this zone resides at ~40-80°C (~2±1 km depth for typical continental geothermal gradients). This is ~35°C cooler than the analogous apatite fission track partial annealing zone.

Application of the (U-Th)/He method to natural systems has provided consistent results and useful geologic information. Helium ages from the Cajon Pass Drillhole decline from 41.1 to 0.3 Ma between 526 and 2018 m depth, and appear to be in equilibrium with the present thermal gradient. This is in contrast to the previous assertion that the region is in a thermal transient resulting from recent erosion. Helium ages from Mt. San Jacinto, California, decrease monotonically from 79 to 17 Ma with sample elevation, and suggest a modest (~7°) westward tilting of the block with no evidence of rapid exhumation during this period. Helium ages from Mt. San Jacinto and Cajon Pass are younger than other available thermochronometric techniques, consistent with predictions from laboratory diffusion data.

# Table of Contents

# Introduction

The ability to date events in the geologic record is a critical aspect of understanding Earth Science. The most widely utilized methods of geochronometry use radioactive parent nuclides which decay to produce a radiogenic daughter nuclide at a known rate. Some of the methods which have been employed are U/Pb, Sm/Nd, Rb/Sr, K/Ar, and Ar/Ar. Different crystal phases which concentrate the desired parent nuclide are chosen for analysis. However, with each of these systems, the geochronometric clock does not begin to tick until the parent and daughter are effectively in a closed system (i.e., parent or daughter do not diffuse out of the crystal). In the K/Ar system, the daughter diffuses at a faster rate than the parent at the same temperature. For instance, Ar diffuses rapidly from biotite in excess of ~310°C, but K remains in the silicate framework at temperatures where Ar is completely lost from the crystal by diffusion (Harrison and McDougall, 1985).

With the use of the K/Ar system in different mineral phases, the concept of thermochronology was developed (McDougall and Harrison, 1989). In a rapidly cooling pluton, the Ar in biotite will not effectively be retained until the rock cools below ~310°C (Harrison and McDougall, 1985). Thus, the K/Ar apparent age measured on biotite effectively recalls the time since the pluton cooled below this temperature. Dodson (1973) suggested that there is an effective temperature, the closure temperature (defined by the diffusion parameters measured during incremental outgassing experiments), below which quantitative retention of the diffusant effectively occurs, assuming the rock cools

at a constant rate. For geologic environments which cool at a constant rate, the closure temperature is one method for creating a thermal framework for thermochronometers.

The concept of dating the last time a sample was at a given temperature is a powerful one for understanding metamorphism, migmatism, plutonism, and even uplift. Since there are natural thermal gradients in the Earth's crust, the thermochronometer with the lowest closure temperature will record geologic events occurring nearest the surface. Moreover, the lowest temperature thermochronometer will also record the most recent thermal history. These lowest temperature thermochronometers are useful for understanding recent uplift histories and neotectonics, and can be used in thermal maturation studies which investigate hydrocarbon potential in a sedimentary basin.

Although the K/Ar and Ar/Ar methods have been used for thermochronology, they are primarily useful for studies concerned with thermal histories in excess of ~200°C (McDougall and Harrison, 1989). Another type of thermochronometer, the fission track thermochronometer, has been used to record low temperature histories. The fission track thermochronometer uses the fact that the spontaneous fission of $^{238}U$ occurs at a known rate and leaves a damage track in the crystal phase (~15 μm long in the mineral apatite when etched in acid) (Fleischer et al., 1975). The number of fission tracks present is a function of the U concentration and the fission track age. The precision of an analysis depends primarily on the number of tracks appearing in the etched crystal. Since the determination of fission tracks is somewhat subjective, track

counters standardize themselves by counting fission tracks in a mineral standard of known age (Fleischer et al., 1975). The annealing of fission tracks is analogous to the diffusion of the radiogenic daughter. For most igneous apatite compositions, complete fission track annealing occurs above ~100-120°C over geologic timescales (Green et al., 1985; Green et al., 1986; Green et al., 1988; Green, 1988; Crowley et al., 1991). Many studies have utilized the low annealing temperature in apatite to characterize the timing and rate of uplift on mountain blocks by looking at fission track age as a function of sample position (Wagner and Reimer, 1972; Fitzgerald and Gleadow, 1990; Fitzgerald et al., 1991; Holm and Dokka, 1993; Roberts and Burbank, 1993; Fitzgerald et al., 1995; Osullivan and Currie, 1996). However, compared to radiometric methods, the precision on fission track dating is quite poor. Because low temperature thermochronometers are so important to neotectonics and the recent thermal history of the crust, there is a need for newer high precision low temperature radiometric thermochronometers in addition to apatite fission track dating.

As early as 1905, Rutherford had suggested that measurements of the number of alpha particles (helium nuclei) and their parent uranium atoms could be used as a geochronometer. Other investigators attempted to develop the (U-Th)/He method, but these attempts were considered failures until very recently (Strutt, 1908, 1909; Hurley, 1954; Damon and Green, 1963; Fanale and Kulp, 1962; Fanale and Schaeffer, 1965; Turekian et al., 1970; Bender, 1973; Ferreira et al., 1975). In an attempt to find a new low temperature thermochronometer with potentially higher precision than fission track dating, Zeitler et al. (1987)

explored the possibility of using the (U-Th)/He system in apatite by performing helium diffusion experiments on Durango apatite, a ~31 million year old pyrothermal apatite from Mexico (McDowell et al., 1979). Although the low precision on their diffusion experiments resulted in a broad range of calculated closure temperatures (100°±30°C, assuming a cooling rate of 10°C/Ma), they suggested that this might be a valuable low temperature thermochronometer. The work on apatite was continued by Lippolt et al. (1994), who drew essentially the same conclusions as Zeitler et al. (1987) with roughly the same uncertainties. Since then, the method has been further developed and applied to natural systems, and this volume is a description of the development and primary application of the apatite (U-Th)/He thermochronometer.

The thesis is divided into six chapters and two appendices. Chapter 1 addresses the problem of alpha emission from apatite crystals during radioactive decay using a model created by Dr. Ken Farley which relates the fraction of alphas retained to crystal size. This model was tested by analyzing (U-Th)/He ages on four different sized populations of apatite and showing that their ages are indistinguishable when corrected with the alpha emission model. This work was recently published (Farley et al., 1996a). Chapter 2 describes the incremental outgassing experiments which were used to determine the diffusion coefficients for helium in apatite. This chapter explains the (U-Th)/He method and the potential applicability to geologic problems. This study was also recently published (Wolf et al., 1996a). Chapter 3 uses the measured diffusion parameters from chapter 2 and the solution to the time dependent radiogenic

production/diffusion equation to learn more about the sensitivity of (U-Th)/He ages to thermal history and diffusivity. Because samples do not tend to cool at a constant rate at low temperatures, this approach is a more adequate characterization of (U-Th)/He ages than the closure temperature formulation (Dodson, 1973), which assumes a constant rate of cooling. Instead of discussing the (U-Th)/He method in terms of its closure temperature, we present a discussion of the helium partial retention zone which is a zone of temperatures where helium retentivity is a sensitive function of temperature and the transition from effective retention to effective loss occurs. The helium partial retention zone is analogous to the fission track partial annealing zone and is compared to it in this chapter. This chapter is currently being prepared for publication. Chapter 4 contains observed variations in helium age with depth and temperature in the Cajon Pass Drillhole. The study involves an attempt to relate model predictions of the helium partial retention zone with observed variations in a borehole. This work is also currently being prepared for publication. Chapter 5 is an application of the (U-Th)/He method to a steep mountain block adjacent to the San Andreas fault, southern California. Samples were collected on vertical and lateral transects in an attempt to reconstruct the recent thermal history of the block. This work was also recently published (Wolf et al., 1997). Chapter 6 describes in more detail the analytical instrumentation specifically designed to make helium analyses. This chapter describes the hardware used to make the incremental outgassing experiments in chapter 2,

and describes the quadrupole vacuum line used to make helium analyses described in chapter 4 and Appendix A.

Appendix A is a project which intended to compare helium results with fission track results in the tilted Gold Butte block, Nevada. The pertinent observation in this work is that samples which were determined to be apatite with micron sized monazite inclusions (mineral identification was done by electron microprobe and SEM analysis) yielded helium at temperatures where helium has, in every other case, been completely extracted. SEM and microprobe analyses showed the presence of monazite and xenotyme inclusions in some samples, but it is difficult to reconcile whether these inclusions are responsible for the additional helium and the higher retentivity. These samples come from amphibolite grade metamorphic rocks, and previous diffusion studies have been on igneous rocks with little or no metamorphic alteration. These observations may indicate complications in analyzing apatites from high grade metamorphic rocks. Appendix B presents results from a reconnaissance study of helium isotopes in basalts from the central Great Basin, United States. This work was published in an abstract for the 1994 Fall American Geophysical Union meeting.

# Chapter 1

## The Effects of Long Alpha-Stopping Distances on (U-Th)/He Ages

K.A. Farley
R.A. Wolf
L.T. Silver

(This chapter was reprinted from *Geochimica et Cosmochimica Acta* (1996), 60, 4223-4230)

**Abstract** - A mathematical framework for quantitative evaluation of alpha stopping effects on (U-Th)/He ages has been developed. Alpha stopping ranges in the $^{238}U$, $^{235}U$ and $^{232}Th$ chains vary between ~10 and ~30 μm, depending on decay energy and density/composition of the stopping medium. In the case of U and Th rich accessory minerals (e.g., apatite, zircon, titanite), the dominant effect of long stopping distances is alpha ejection to adjacent minerals. For grains smaller than a few hundred microns in minimum dimension, ejection effects will cause measured helium ages to substantially underestimate true ages. For example, a sphere of 100 μm radius retains only ~82% of its alphas. For a homogeneous distribution of parent nuclides, the fraction of alphas ejected is ~1/4 of the mean alpha range multiplied by the crystal surface to volume ratio, independent of geometry. Removal of the outer 20 μm of a crystal prior to dating eliminates the region which has experienced alpha loss, but may lead to erroneous ages when crystals are strongly zoned with respect to U and Th. By careful characterization of four sieved apatite

separates from a single sample, we show that it is possible to accurately correct (U-Th)/He ages for alpha ejection even when ejection exceeds 35% of total decays. Our results are useful for identifying the size and shape of grains which are best suited for (U-Th)/He dating and provide the basis for correcting ages when ejection effects are significant. This work underscores that meaningful (U-Th)/He ages require either large crystals, or correction of measured ages for alpha ejection.

## 1.1 Introduction

After being essentially abandoned two decades ago, renewed attention has been directed to the development of dating via the decay of U and Th series nuclides to $^4$He (Zeitler et al., 1987; Lippolt and Weigel, 1988; Lippolt et al., 1994; Wolf et al., 1996). The appeal of the (U-Th)/He system is its rapid evolution in common accessory minerals, low analytical blanks, and, in apatite, a uniquely low closure temperature of potentially great value for thermochronological studies (Zeitler et al., 1987; Wolf et al., 1996). However, one drawback of the technique which has not previously been quantitatively explored is the effect of long alpha-stopping distances on measured helium ages. Alpha particles from U and Th series decay are emitted with high kinetic energies and typically require tens of microns to come to rest within solid matter. These long stopping distances can cause substantial spatial fractionation of the parent/daughter ratio in systems (such as rocks) where the parent nuclides are not uniformly distributed. This effect has important

implications for (U-Th)/He dating of fine-grained minerals. Here we calculate stopping distances in crystals likely to be of use in helium dating, predict the effects of alpha stopping in crystals of various geometries, and test these predictions by measuring helium ages on natural samples.

The stopping distance of energetic alpha particles is a function of their initial energy and the elemental composition and density of the medium through which they travel. As shown in Table 1, alphas of the $^{238}U$, $^{235}U$ and $^{232}Th$ decay series are emitted with a large range in energies, from about 4 to almost 8 MeV. Using these energies and the stoichiometric composition and typical density of the common accessory minerals most useful for helium dating (apatite, titanite, zircon), stopping distances for each nuclide have been computed from published formulae and alpha stopping data in pure elemental targets (Ziegler, 1977). To a good approximation the computed stopping distances represent the straight-line distance from the parent nuclide to the rest site of the alpha particle (Ziegler, 1977). These distances range from a minimum of ~11 μm to a maximum of ~34 μm. Note that the relationship between decay energy and stopping distance is non-linear. The series-averaged mean stopping distance is shortest in the $^{238}U$ chain, followed by $^{232}Th$ and $^{235}U$, reflecting the total alpha energy of each series. For most common minerals, density (rather than chemistry) is the strongest control on the alpha stopping distance at a given energy. For example, as density increases from apatite (3.2 g/cm$^3$) to titanite (3.6) to zircon (4.4) the mean stopping distance in the $^{238}U$ series drops from 19.7 to 17.8 to 16.6 μm.

By assuming ideal crystal geometry, it is possible to quantitatively assess the effects of long stopping distances on the parent/daughter ratio of minerals separated from their host rocks. We have developed an analytical model for spherical geometry, and present results of a Monte Carlo simulation for cylinders and cubes. The results obtained are general enough to be applied to other geometries as well.

## 1.2 Procedures and Results

### *1.2.1 Analytical Model*

Alpha particles will come to rest after traveling the stopping distance ("S") from the site $X_0$ of the decaying parent, so they will reside on the surface of a sphere of radius S centered at $X_0$. The probability that decays from $X_0$ will come to rest within a spherical crystal of radius R depends both on S and on how close $X_0$ is to the surface of the crystal. Using rectangular coordinates with the origin at the center of the crystal sphere "R," and with the parent nuclide located at some distance $X_0$ on the x-axis, the equations of the crystal and stopping spheres are:

$$X^2 + Y^2 + Z^2 = R^2$$

$$(X-X_0)^2 + Y^2 + Z^2 = S^2$$

| Isotope | Alpha Energy (MeV) | Stopping Distances (μm) Apatite | Titanite | Zircon |
|---|---|---|---|---|
| **$^{238}$U** | 4.18 | 13.54 | 12.51 | 11.78 |
| $^{234}$U | 4.76 | 16.26 | 14.99 | 14.09 |
| $^{230}$Th | 4.67 | 15.84 | 14.61 | 13.73 |
| $^{226}$Ra | 4.77 | 16.31 | 15.04 | 14.13 |
| $^{222}$Rn | 5.49 | 20.09 | 18.49 | 17.32 |
| $^{218}$Po | 6.00 | 22.89 | 21.06 | 19.69 |
| $^{214}$Bi | 7.69 | 33.39 | 30.71 | 28.56 |
| $^{210}$Po | 5.31 | 19.10 | 17.59 | 16.48 |
| *$^{238}$U Average* | 5.36 | 19.68 | 17.78 | 16.65 |
| **$^{235}$U** | 4.38 | 14.48 | 13.36 | 12.58 |
| $^{231}$Pa | 5.00 | 17.39 | 16.02 | 15.04 |
| $^{227}$Th | 5.93 | 22.50 | 20.71 | 19.36 |
| $^{223}$Ra | 5.65 | 20.97 | 19.30 | 18.06 |
| $^{219}$Ra | 6.68 | 26.89 | 24.74 | 23.07 |
| $^{215}$Po | 7.38 | 31.40 | 28.88 | 26.87 |
| $^{211}$Bi | 6.57 | 26.18 | 24.08 | 22.47 |
| *$^{235}$U Average* | 5.94 | 22.83 | 21.01 | 19.64 |
| **$^{232}$Th** | 3.98 | 12.60 | 11.65 | 10.99 |
| $^{228}$Th | 5.35 | 19.32 | 17.79 | 16.67 |
| $^{224}$Ra | 5.67 | 21.08 | 19.40 | 18.16 |
| $^{220}$Rn | 5.49 | 20.09 | 18.49 | 17.32 |
| $^{216}$Po | 6.78 | 27.53 | 25.33 | 23.61 |
| $^{212}$Bi/$^{212}$Po | 6.0/8.7 | 34.14 | 31.40 | 29.19 |
| *$^{232}$Th Average* | 5.85 | 22.46 | 20.68 | 19.32 |

**Table 1.**

Alpha-Stopping Distances.

The fraction of decays from point $X_o$ which come to rest in the volume of R, $F(X_o)$, is unity when the sphere S is completely internal to R, and is zero when $X_o$ is more than one stopping distance greater than R. When $(R-S)<X_o<(R+S)$, the two spheres intersect along a plane, at:

$$X^* = \frac{1}{(2X_o)}(X_o^2 + R^2 - S^2)$$

and $F(X_o)$ is equal to the surface area of S lying within sphere R. Thus:

$$F(X_o) = \frac{1}{2} + \frac{X^* - X_o}{2S} \qquad (1)$$

$$\text{for} \quad (R - S) \leq X_o \leq (R+S)$$

To calculate the total fraction of alpha decays which come to rest within the sphere R, we must find the mean value of $F(X_o)$ throughout space, weighted for the distribution of the parent nuclide. Given a radially-symmetric distribution U(r) of parent nuclide, we can switch to polar coordinates, and the mean value can be found by integrating the expression:

$$F_T = \frac{\int_0^{R+S} (4\pi r^2) F(r) U(r) dr}{\int_0^{R+S} (4\pi r^2) U(r) dr} \qquad (2)$$

In the minerals most appropriate for helium dating, the concentration contrast in U and Th between the dated mineral and the host rock is so large (typically >20) that the weighting factor U(r) is negligible when r>R, i.e., outside of the crystal of interest. In addition, we observe that the spacing between parent-rich accessory grains is large in most rocks, so implantation from nearby grains can also be

ignored. As a consequence, the only effect we need to consider is ejection of alpha particles from the crystal, and thus we can integrate from 0 to R instead of 0 to (R+S).

Assuming a homogeneous parent nuclide distribution within the grain (U(r)=a constant), equation (2) integrated from 0 to R is solved analytically as:

$$F_T = 1 - \frac{3S}{4R} + \frac{S^3}{16R^3} \qquad (3)$$

This is the same result previously asserted for recoil of Rn nuclei from spheres (Gilleti and Kulp, 1955). In Figure 1, Equation 3 is plotted as a function of radius for U and Th series decays in apatite and zircon spheres. These curves were computed by averaging the retentivities of all the decays within each chain. For the stopping distances in these chains, Equation (3) is characterized by a rapid rise in retention up to a radius of about 60 μm, followed by an asymptotic approach to unity. Even in crystals up to 250 μm in radius, on the order of 5% of alpha decays are lost. Loss exceeds 50% for crystals with radii smaller than 30 μm.

At small crystal radii, the different decay energy in each chain leads to different mean retentivities. For example, at 40 μm radius in apatite, 64% of $^{238}U$ decays are retained, but only 58% of $^{235}U$ decays. Thus the mean retentivity in a natural crystal will depend on the source of the alpha particles. At larger radii the mean retentivities converge; at 500 μm radius, 97.0% and 96.6% of $^{238}U$ and $^{235}U$ decays are retained, respectively.

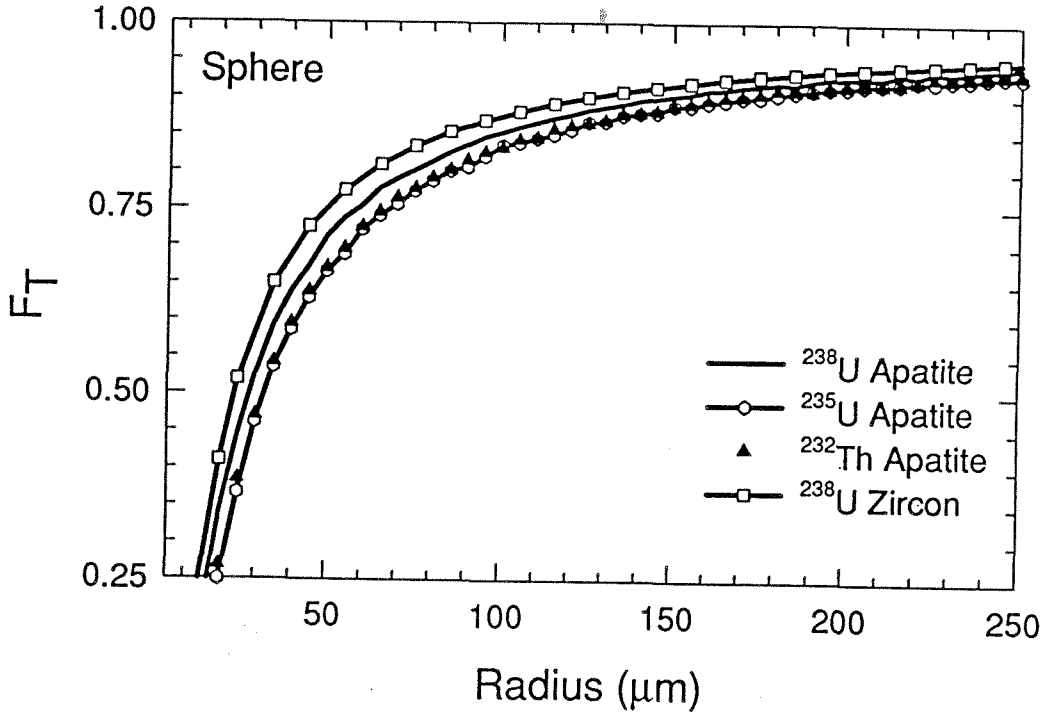


**Figure 1.**

Retentivity ($F_T$) of alpha particles in a sphere of varying radius for the $^{238}U$, $^{235}U$, and $^{232}Th$ decay chains in apatite and zircon, computed from Equation 3. A homogeneous distribution of the parent nuclides is assumed.

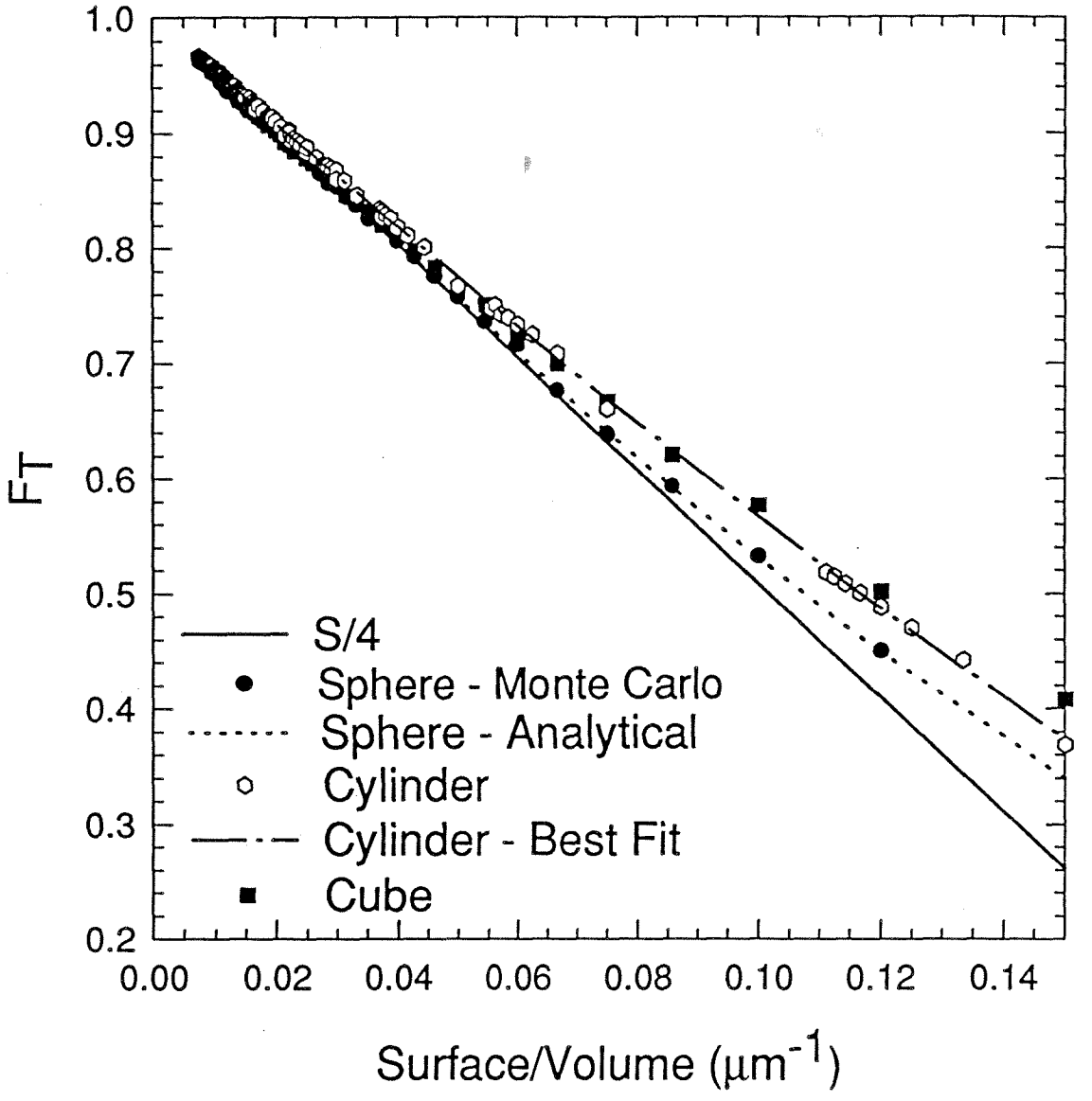


**Figure 2.**

Relationship between retentivity and the surface/volume ratio of spheres, cylinders and cubes, computed for the series decay of $^{238}U$ in apatite (i.e., for S=19.68 mm). The equation for the best fit to the cylindrical results is given in the text. At high retentivities (>~0.8), retentivity can be approximated by 1-(S/4)(surface area/volume) regardless of geometry, as indicated by the line labeled "S/4."

Because Equation (3) is essentially linear in S for crystals larger than a few tens of microns in radius (i.e., the cubic term disappears for reasonably large values of R), mean retentivities within a decay chain can be approximated from the mean stopping distance of all the alphas in a series. Thus the retentivity in apatite for the $^{238}U$, $^{235}U$ and $^{232}Th$ series can be computed using S values of 19.68, 22.83 and 22.46 μm, respectively, when R is greater than about 35 μm.

When the crystal is significantly larger than the stopping distance, i.e., $S^3 << R^3$, the fraction of alphas ejected ($1-F_T$) is proportional to the surface to volume ratio of the sphere (β, =3/R, Figure 2). The constant of proportionality is 1/4 of the stopping distance S. As shown below, this is a general result independent of geometry.

Equation 3 and Figure 1 demonstrate that alpha ejection is extremely important for small grains, and because in our experience the accessory minerals in most rocks are in the size range shown in Figure 1, *alpha ejection effects will in general be significant in helium geochronometry.* It is clearly advantageous to analyze the largest crystals available.

### *1.2.2 Monte Carlo Modeling*

Although relatively simple, the spherical solution is not relevant for most datable minerals, which are more likely to be prismatic (zircon, apatite) or wedge-shaped (titanite). These geometries are far more difficult to model analytically, so we have developed a Monte Carlo procedure to calculate alpha

retentivity. The simulation works as follows. A geometric model of the crystal is defined, specifying the coordinates of the grain surfaces. A point "P" within the crystal is selected at random. This point is the locus of emission for alpha particles for a single chain of decays. The final location "A" of each alpha in the chain is computed by adding a vector of length S (from Table 1) to point P, in a random orientation. It is then determined whether point A lies within the confines of the crystal. At each point P either 8, 7 or 6 alpha decays (of the appropriate energies) are simulated depending on whether $^{238}U$, $^{235}U$ or $^{232}Th$ decay is being considered. The process is then repeated with a new location P. Retentivity is simply the number of decays which remain confined in the grain divided by the total number of decays simulated. 50,000 decays yielded satisfactory convergence for the retentivity. This model assumes a homogeneous distribution of parent nuclides within the crystal.

To test the results of the Monte Carlo model, we have simulated the emission of alpha particles from a sphere, for which Equation 3 provides an independent check. As shown in Figure 2, there is excellent agreement between the analytic and simulated retentivities. The results of Monte Carlo simulation of retention in a cylinder are shown in Figure 3. Retentivity curves are similar to those for the sphere, but define a family of curves depending on the length/radius (L/R) ratio. Longer cylinders are more retentive than shorter cylinders of the same radius. These variations again demonstrate dominant control from the surface to volume ratio, which for a cylinder is given by $\beta=2(R+L)/(RL)$. As the cylinders become more elongate at a given radius, $\beta$

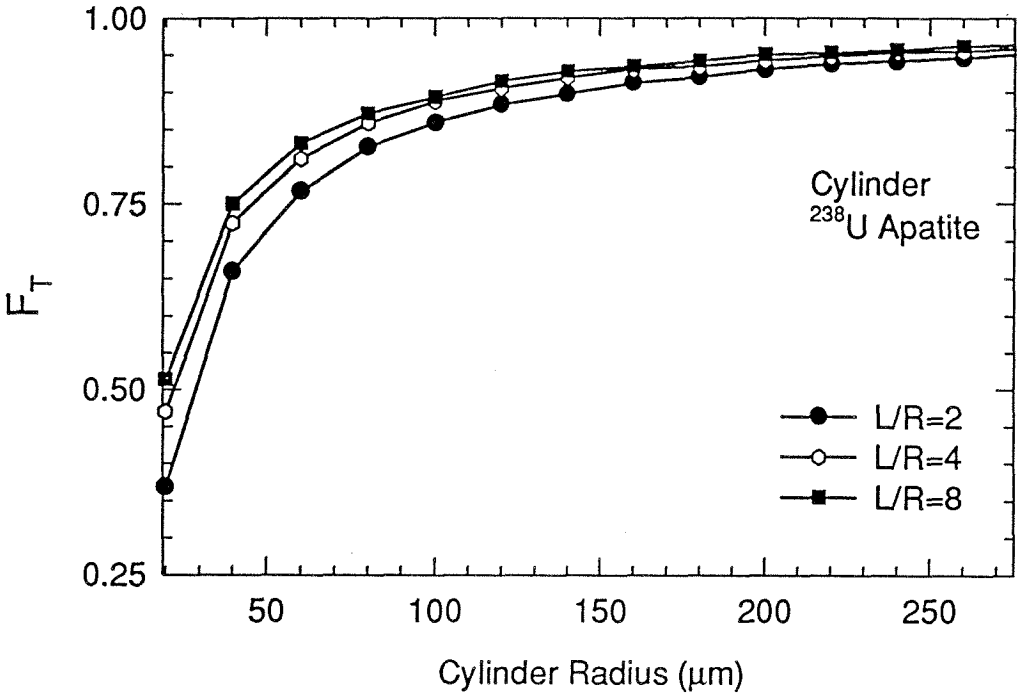


**Figure 3.**

Monte Carlo results for retentivity in cylinders with varying radius and length/radius (L/R) ratio. These are computed for $^{238}$U series decay in apatite assuming a homogeneous distribution of U. As suggested by Figure 1, the curves would be only slightly shifted for $^{232}$Th and $^{235}$U series decay.

asymptotically approaches 2/R, and retentivity increases proportionally. For cylinders which are either "flat" (L approaching zero) or needle-like (R approaching zero), β approaches infinity, and retentivity approaches zero. Needle-like morphologies are common in apatite, and are inappropriate for helium dating for this reason.

Figure 2 demonstrates that the relationship between β and $F_T$ for a sphere also holds for cylindrical and cubic geometry (details not shown). When the stopping distance is significantly smaller than the minimum crystal dimension, retentivity can be approximated by $F_T=1-(S/4)*\beta$. At smaller crystal sizes, geometry dependent factors become significant; for the cylinder the expression $F_T=1-4.695\beta+3.381\beta^2$ fits the $^{238}U$ series retentivity very well. The general relationship between β and $F_T$ shown in Figure 2 is useful for evaluating retentivity in more complex morphologies which are analytically intractable or which require lengthy calculations for Monte Carlo simulation. For example, we can compare the results for the cylinder with the results for a symmetrical hexagonal prism, which may more closely describe natural apatite and zircon. Such a prism has $\beta= (2.31L+2R)/(RL)$, so at a length to radius ratio of 5 (typical of some plutonic apatites, see below), the prism has a β (and thus a relative alpha loss) that is 13% higher than a cylinder of the same radius.

| Description of Parent Nuclide Distribution | U(r) | $F_T$ | $F_T$ (80μm) |
|---|---|---|---|
| Homogeneous | c | 0.85 | 1.00 |
| Increasing linearly by 11x from core to rim | c+c(r/100) | 0.83 | 1.01 |
| Increasing linearly by 2x from core to rim | c+c(r/10) | 0.82 | 1.03 |
| Increasing exponentially by 10x from core to rim | $ce^{0.023r}$ | 0.79 | 1.08 |
| Increasing exponentially by 50x from core to rim | $ce^{0.039r}$ | 0.75 | 1.18 |
| Decreasing linearly by 11x from core to rim | 2c-c(r/100) | 0.87 | 0.98 |
| Decreasing linearly by 2x from core to rim | 110c-c(r/10) | 0.93 | 0.95 |
| Decreasing exponentially by 10x from core to rim | $ce^{0.023(100-r)}$ | 0.91 | 0.96 |
| Decreasing exponentially by 50x from core to rim | $ce^{0.039(100-r)}$ | 0.95 | 0.96 |

**Table 2.**

Retentivity in a sphere of R=100 mm for S=19.68 mm (i.e., $^{238}U$ series in apatite). c is an arbitrary constant. $F_T$ is retention in entire crystal, and $F_T$ (80 μm) is "effective retentivity" in a crystal in which the outer 20 mm has been removed.

*1.2.3 Effects of Zonation*

The previous discussion has assumed a homogeneous distribution of parent nuclides within the crystal. If the crystal is compositionally zoned, deviations from the calculated retentivity can be expected. For example, zircons often have U and Th concentrations which increase from core to rim, and such grains clearly must have poorer retentivity than if the parent nuclides were homogeneously distributed. If 100% of the parent lies on the rim, $F_T$ will achieve its minimum value, which depends on grain size and morphology. In the case of a 100 μm sphere, for example, this minimum value is 0.45, compared with 0.85 in the homogeneous case. At the opposite extreme, if 100% of the parent lies at a distance >S from the crystal rim, the retentivity will be unity. In most cases zonation is less extreme than these limits and requires a more detailed treatment. In the case of spherical grains, Equation 3 can be used to directly calculate the consequences of zonation. This equation has been solved numerically for a variety of different parent distributions as described in Table 2.

Although an infinite variety of parent distributions can be envisioned, Table 2 is useful in that it demonstrates the sensitivity of $F_T$ to U(r). The most important observation is that retentivity is relatively insensitive even to rather extreme zonation. For example, an 11-fold increase of parent concentration from core to rim reduces retention by only 3%, from 85% to 82%, and even a 50-fold exponential increase from core to rim produces only a 12% drop in retention.

*1.2.4 Correcting (U-Th)/He Ages*

The previous discussion demonstrates that selection of appropriate size and morphology of crystals is critical for obtaining meaningful (U-Th)/He ages, and that for small crystals, ejection effects must be considered. When the size, morphology, and parent distribution of grains have been determined, values of $F_T$ can be calculated and used to correct measured helium ages:

$$\text{Corrected Age} = \frac{\text{Measured Age}}{F_T} \qquad (4)$$

To test our ability to make corrections for alpha ejection using Equation 4, we have obtained (U-Th)/He ages on four fractions of apatite which span a range of grain sizes and shapes. The fractions are from a single tonalite sample ("CL") from the Peninsular Ranges Batholith, and are part of a study of the helium ages of the San Jacinto Mountains (Wolf et al., 1996; Wolf et al., 1997). Prior to helium analysis, several hundred grains from each fraction were microscopically examined and measured with an optical micrometer in order to characterize the size and shape of grains present within the original rock. The grains were then analyzed for He, U, and Th using techniques described elsewhere (Wolf et al., 1996).

The apatites examined fall into one of several morphologic classes: (1) euhedral, hexagonal grains with two flat-topped pyramidal terminations, (2) prismatic grains with one pyramidal termination and one irregular end sub-perpendicular to the long axis of the crystal, (3) prismatic grains with two ends sub-perpendicular to the long axis, and (4) rare grains that have very poor

| | | 2 pyramidal terminations | 1 pyramidal termination | 2 broken terminations | poor crystal form | $F_T$ | Measured Age | Corrected Age |
|---|---|---|---|---|---|---|---|---|
| Fraction "A" | Mean Diameter (μm) | 60 | 63 | 63 | 68 | 0.648 | 30.8±0.9 | 47.5±1.4 |
| | Uncorrected Mean Length (μm) | 122 | 101 | 96 | 98 | | | |
| | Mass Fraction | 0.46 | 0.33 | 0.09 | 0.12 | | | |
| | Number fraction | 0.45 | 0.37 | 0.1 | 0.08 | | | |
| Fraction "B" | Mean Diameter (μm) | 93 | 123 | 123 | 122 | 0.805 | 38.2±1.1 | 47.5±1.4 |
| | Uncorrected Mean Length (μm) | 191 | 179 | 150 | 156 | | | |
| | Mass Fraction | 0.19 | 0.54 | 0.11 | 0.16 | | | |
| | Number fraction | 0.3 | 0.45 | 0.11 | 0.14 | | | |
| Fraction "C" | Mean Diameter (μm) | 114 | 126 | 136 | 127 | 0.81 | 39.35±1.2 | 48.6±1.5 |
| | Uncorrected Mean Length (μm) | 225 | 182 | 156 | 155 | | | |
| | Mass Fraction | 0.28 | 0.54 | 0.11 | 0.07 | | | |
| | Number fraction | 0.24 | 0.54 | 0.08 | 0.14 | | | |
| Fraction "D" | Mean Diameter (μm) | 106 | 147 | 165 | 150 | 0.848 | 40.7±1.2 | 48.0±1.4 |
| | Uncorrected Mean Length (μm) | 204 | 209 | 220 | 209 | | | |
| | Mass Fraction | 0.15 | 0.61 | 0.12 | 0.12 | | | |
| | Number fraction | 0.22 | 0.56 | 0.105 | 0.115 | | | |

**Table 3.**

Dating of sieved apatite grains to test alpha emission corrections. Fractions A, B, C, and D were sieved from a single apatite population separated from a tonalite from Mt. San Jacinto ("CL," Wolf et al., 1996). The mean size and relative abundances of grain morphologies is indicated, along with the computed $F_T$ value and the measured and emission-corrected helium ages. "Uncorrected Mean Length" is the measured length, uncorrected for grain breakage during sample preparation. As described in the text, the actual grain population (rather than the mean values indicated here) was used to compute $F_T$.

crystal form. The relative abundance of these classes within each fraction is shown in Table 3. In thin section nearly all apatites in this rock have two well developed pyramidal terminations, and we infer that the abundance of grains with irregular ends is an artifact of grain breakage during sample preparation. Anear complete absence of conchoidally fractured grains suggests that chips of larger grains are extremely rare. The grains range between 25 and 150 μm in prism radius (Figure 4).

Our observations demonstrate that these apatites are most commonly prismatic, and we have chosen to model them as symmetrical hexagonal prisms with flat terminations. To calculate $F_T$ we must establish the original size of the crystals prior to mineral separation. In practice this requires that we estimate the original length of grains with one or two broken ends, i.e., we must add the broken bits back together. Because grain diameter and length are likely to be correlated, we wish to add together only broken pieces of similar diameter. This was accomplished by sorting by diameter the grains with a single broken end, then adding them together two by two to get a statistical estimate of the original lengths. To calculate the original length of the relatively rare grains with two broken terminations, we assumed they obey the same relationship between diameter and length as these reconstituted grains. Although this procedure may not predict exactly the original lengths, it is important to note that the grains are all relatively long, with corrected length to radius ratios averaging about 5. At length/radius ratios this high, the alpha-retentivity is no longer a strong function of length (Figure 4). From these dimensions we calculated $F_T$ for each of the

measured grains using their surface/volume ratio (and using the U and Th abundances measured in the bulk sample). The average retentivity of each fraction was then computed by taking an average of all the measured grains weighted by their mass contribution to the fraction. In the four aliquots the mean retentivity ranges from 65% to 85% (Table 3).

The measured (U-Th)/He ages on these fractions are shown in Table 3 and are plotted against $F_T$ in Figure 5. The ages range from 30.8 to 40.7 Ma and are strongly correlated with $F_T$. A single line can be drawn through the origin and all of these data points, demonstrating that the measured ages are consistent with a single "true" helium age variably affected by alpha ejection. The true helium age (i.e., corrected for ejection effects) is given when $F_T$=1. These data show that at least in the case of this sample, alpha ejection effects can be modeled and corrected for with a precision comparable to the parent/daughter measurements themselves.

*1.2.5 Alternative Approaches*

One alternative to the correction of He ages for alpha ejection using Equation 4 is to remove the outer skin of the crystal, where ejection effects are confined, prior to analysis of parent and daughter concentrations. This could be accomplished either by chemical dissolution or by mechanical abrasion. Given a homogeneous distribution of parent nuclides, removal of the outer 20 μm of a crystal would increase the fractional retention to unity and obviate the need for a correction.

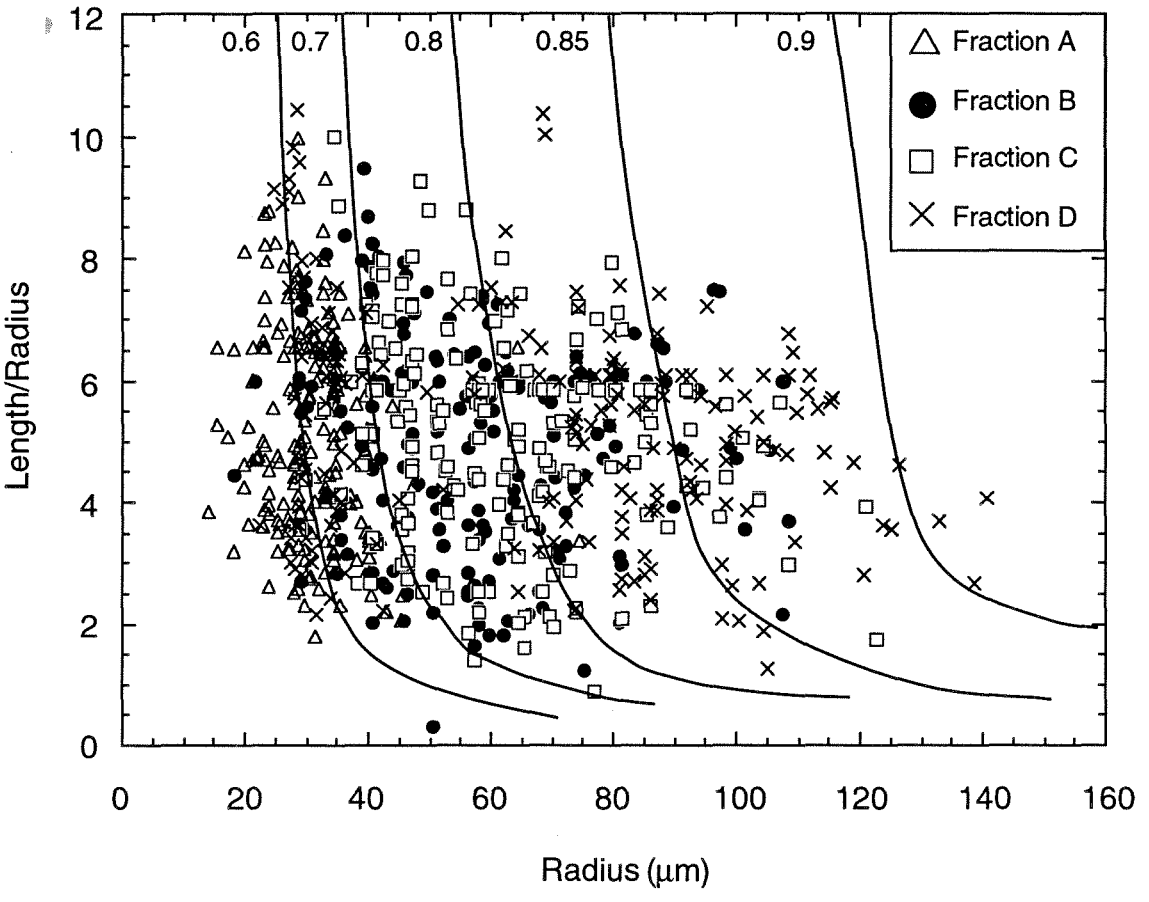


**Figure 4.**

The distribution of radii and corrected length/radius ratios in the four dated fractions. Note that the fractions are not perfectly sieved, but instead represent various ranges of grain sizes. Curves are contours of $F_T$ computed for a hexagonal prism assuming a stopping distance of 20 mm. Once L/R exceeds about 3, the retentivity is relatively insensitive to the L/R ratio.

In a zoned crystal, the effects of skin removal are less obvious, but in the case of spherical geometry, can be calculated with Equation 3 using modified limits of integration. We consider removal of the outer surface of a spherical crystal originally of radius R, leaving a new crystal of radius N. Within the sphere of radius N, alpha particles are lost to the region r>N. However, they can also be gained back from the volume between N and N+S. Equation 1, which describes the fractional retention at a given radius $X_o$, applies equally well when $X_o$ is greater than N as when it is less than N. Thus the effective fractional retention is the integral of Equation 3 from 0 to N+S, divided by the integral of the parent distribution from 0 to N:

$$F_T(N) = \frac{\int_0^{(N+S)} (4\pi r^2)F(r)U(r)dr}{\int_0^N (4\pi r^2)U(r)dr} \qquad (5)$$

where the new symbol $F_T(x)$ is the "effective retentivity" of a sphere of radius x. A value of unity implies complete removal of ejection effects. Note that values both smaller and larger than unity are possible for this parameter. Values greater than unity will occur when parent concentration increases with radius, producing a net import of alphas into the region with radius <N. Values smaller than unity pertain to distributions which decrease with radius, reflecting a net export of alphas from the interior to the rim. The significance of this parameter is that ages obtained after removal of the outer skin, not subject to any further ejection correction, will be in error by a factor $F_T(x)$.

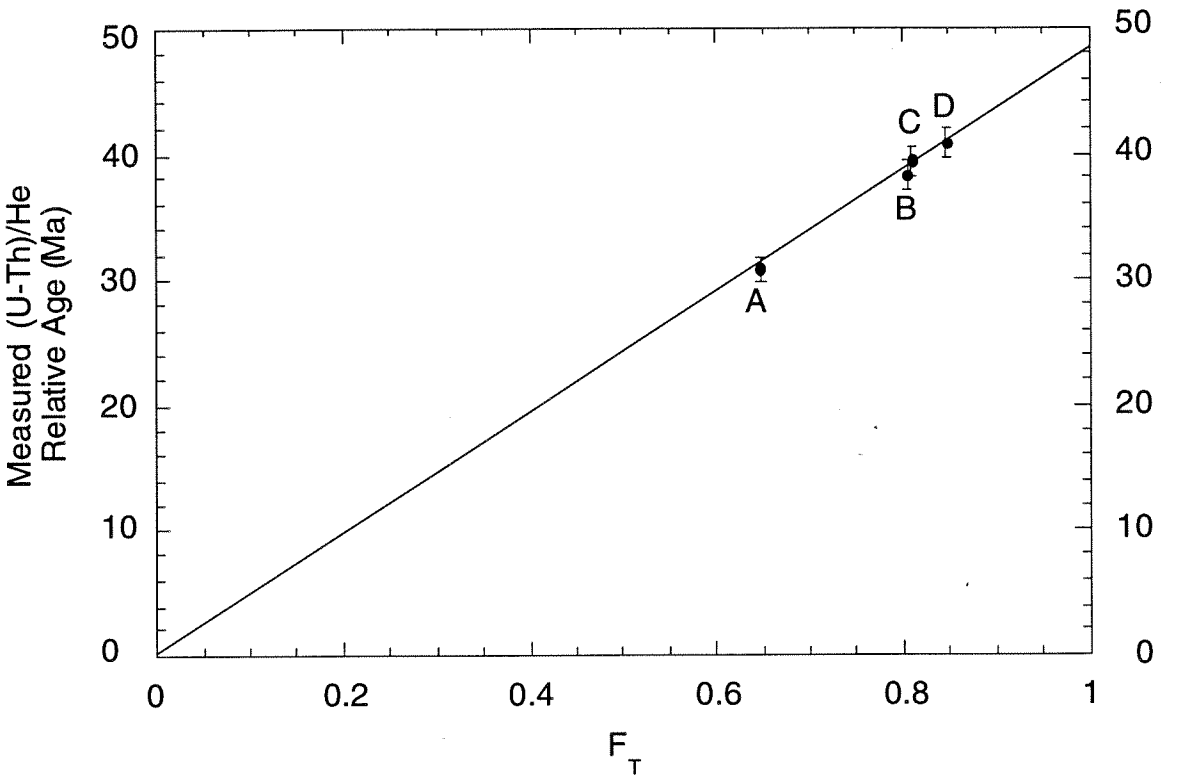


**Figure 5.**

Comparison between measured He age and computed retentivity for the four fractions. Within analytical uncertainty all 4 fractions lie on a line through the origin, consistent with a single helium age modified by alpha ejection effects as theoretically predicted.

The effects of removing the outer 20 μm of the zoned crystals previously considered are shown in Table 2, assuming a single stopping distance of 20 μm. The effective retentivities range from 0.95 to 1.18, with the most extreme value found in the distribution with the 50-fold exponential increase. In every case $F_T(80)$ is closer to unity than is $F_T$ of the original crystal, demonstrating the efficacy of the removal technique. Thus removal is a viable alternative to computing the expected retentivity, although it should be noted that uncertainties associated with zoned crystals cannot be completely eliminated by either technique.

## 1.3 Conclusions

Average alpha stopping distances on the order of 20 μm in the U and Th systems can produce substantial spatial fractionation of the parent/daughter ratio in accessory minerals likely to be used for He geochronometry. The dominant effect, alpha ejection, is roughly proportional to the surface/volume ratio of the dated grain, and if not corrected for will lead to anomalously low ages. The effects of alpha ejection are apparent even in grains of several hundred microns in minimum dimension, but they become extremely significant below about 60 microns. In our experience apatite, zircon, and titanite are commonly in the size range where ejection effects are significant, so long-stopping distances will likely limit the ultimate precision of helium ages. By careful characterization of dated grains, we have shown that it is possible to correct for ejection effects to better than a few percent even in very small grains

provided that the distribution of parent nuclides is either homogeneous or is known. These computations are also relevant for considering the consequences of trace U and Th rich phases included within dated grains (for example zircon inclusions in apatite). For inclusions smaller than about 10 μm, most alpha particles will be emitted into the host grain. In such cases the He retentivity characteristics of the inclusion are thus irrelevant for He thermochronometry.

These results provide impetus for the development of single-crystal He-dating techniques in which a single large grain from the population to be dated is carefully characterized with respect to geometry and possibly with respect to parent nuclide distribution via ion probe.

*Acknowledgments*

This work was funded by the National Science Foundation. We thank P. Damon and an anonymous reviewer for helpful comments on the manuscript.

## 1.4 References Cited

Gilleti B. J. and Kulp J. L. (1955) Radon leakage from radioactive minerals. *Am. Mineral.*, 40, 481-496.

Lippolt H. J., Leitz M., Wernicke R. S., and Hagedorn B. (1994) (U+Th)/He dating of apatite: experience with samples from different geochemical environments. *Chem. Geol.*, 112, 179-191.

Lippolt H. J. and Weigel E. (1988) 4He diffusion in 40Ar retentive minerals. *Geochim. et Cosmochim. Acta*, 52, 1449-1458.

Wolf R. A., Farley K. A. and Silver L.T. (1996) Helium diffusion and low temperature thermochronometry of apatite. *Geochim. et Cosmochim. Acta*, 60, 4231-4240.

Zeitler P. K., Herczig A. L., McDougall I., and Honda M. (1987) U-Th-He dating of apatite: a potential thermochronometer. *Geochim. et Cosmochim. Acta*, 51, 2865-2868.

Ziegler J. F. (1977) Helium: Stopping powers and ranges in all elemental matter. Pergamon.

# Chapter 2

## Helium Diffusion and Low Temperature Thermochronometry of Apatite

R.A. Wolf
K.A. Farley
L.T. Silver

(This chapter was reprinted from *Geochimica et Cosmochimica Acta* (1996), 60, 4231-4240; references have been updated and the caption for Figure 1 has been modified)

**Abstract -** To investigate the potential of the (U-Th)/He system for low temperature thermochronometry, we have studied helium diffusion and have measured helium ages on Durango fluorapatite and on apatites from a gabbro and two tonalites from the Peninsular Ranges Batholith. Diffusivity at moderate to very low temperatures (as low as 80°C) was measured to high analytical precision using long duration incremental outgassing experiments. All four apatites displayed remarkably similar helium diffusion behavior. Helium loss apparently occurs via volume diffusion from sub-grain domains (<60mm) which are nearly identical in size in all samples. At temperatures below 290°C diffusivity obeys a highly linear Arrhenius relationship with an implied activation energy of about 36 kcal/mol. Above this temperature diffusivity deviates from linearity toward lower activation energies. This transition does not arise from multiple diffusion domains, but rather from a reversible change in the physical mechanism of helium diffusion. For thermochronometric purposes the high

temperature diffusion behavior is largely irrelevant because essentially no helium is retained over geologic time at temperatures above 290°C. Using the results from the low temperature regime, all samples yield helium closure temperatures in the range 75±7°C. This value is independent of chemical composition and grain size of the apatites, suggesting that a single closure temperature may apply to a wide range of samples. The (U-Th)/He ages of these apatites (17-120 Ma) range from a small fraction to nearly 100% of the crystallization age of their host rocks, and are consistent with a low temperature thermochronometric interpretation. These results strongly support previous suggestions that (U-Th)/He dating of apatite can provide high precision chronometry of very low temperature geological events.

## 2.1 Introduction

The production of $^4$He from U and Th series decay in rocks and minerals was first proposed as a geochronometer by Rutherford (1905), and over the last century the reliability of (U-Th)/He dating has been investigated by many workers (Strutt, 1908, 1909; Hurley, 1954; Damon and Green, 1963; Fanale and Kulp, 1962; Fanale and Schaeffer, 1965; Turekian et al., 1970; Bender, 1973; Ferreira et al., 1975; Graham et al., 1987). While in some cases meaningful ages were apparently obtained, the technique has generally been considered unreliable. In most cases the helium ages were younger than expected, an observation attributed to diffusive loss of helium possibly associated with radiation damage, or the ejection of high energy alpha particles from the phase

being dated (Hurley, 1954). Zeitler et al. (1987) recently revived interest in the method by proposing that low helium ages might actually be geologically significant and related to cooling through very low temperatures. This idea was supported by helium diffusion measurements on gem quality Durango fluorapatite which indicated a closure temperature of just 100±30°C, a value recently confirmed on several additional apatites (Lippolt et al., 1994). In combination with the high analytical precision available for the technique, this uniquely low closure temperature raises the possibility that helium dating of apatite may provide a valuable new thermochronometer.

The goal of the present study was to better characterize the rate and mechanism of helium diffusion from apatite and to assess the sensitivity of diffusion to variations in apatite chemical composition and grain size. Specifically, we measured He ages on four different apatite samples and performed long-duration, low temperature stepped heating experiments to accurately determine helium diffusivity within a few degrees of the closure temperature. These experiments provide a strong foundation for apatite helium thermochronometry and indicate that the method can yield geologic insight to the cooling of apatites through the 75°C isotherm. This work complements our related investigations of the consequences of high energy alpha decay on helium ages (Farley et al., 1996) and an application of the helium method to dating the denudation of the Peninsular Ranges Batholith (Wolf et al., 1997).

## 2.2 Samples and Methods

### *2.2.1 Apatite Samples*

We have investigated helium diffusivity from four apatite samples, three plutonic specimens, and, for comparison with previous work, Durango fluorapatite. These samples vary in geologic history, chemical composition, and grain size. Durango apatite (Young et al., 1969) occurs in pyrothermal or volcanogenic deposits associated with Oligocene alkaline volcanic rocks in northwestern Mexico (McDowell and Keizer, 1977; Lyons 1988), and has been extensively investigated by the fission track community (e.g., Naeser and Fleischer, 1975). We studied fragments from the core of a large (2.5 cm long x 1 cm wide), inclusion free euhedral single crystal obtained from the Caltech mineral collection. The fragments were generally conchoidally fractured and were sieved to 160-180 mm in maximum dimension. We believe this sample is very similar in composition and grain size to that studied by Zeitler et al. (1987).

The plutonic apatites are from the Cretaceous Peninsular Ranges Batholith of Southern California and are part of a detailed study of U-Th-Pb geochronology of the batholith (Silver and Hill, 1986, and in preparation). Crystallization ages of these rocks based on U/Pb zircon analyses range from ~120 Ma in the west to ~90 Ma in the east (Silver et al., 1978; Silver and Hill, 1988). From the western portion of the batholith we analyzed an apatite from the San Marcos Gabbro ("SM") near Pala, California. This sample consists of anhedral to subhedral grains 100 to 130 mm in maximum dimension. In addition we analyzed two apatite samples from the San Jacinto intrusive

| Sample | CaO (%) | $P_2O_5$ (%) | F (%) | Cl (%) | OH (%)** | F/Cl |
|---|---|---|---|---|---|---|
| Durango | 53.7 | 40.5 | 3.39 | 0.43 | 0.00 | 7.9 |
| Durango* | 54.0 | 40.4 | 3.57 | 0.43 | 0.00 | 8.3 |
| San Marcos | 53.7 | 40.5 | 1.15 | 2.37 | 0.06 | 0.49 |
| Camplackey | 54.9 | 41.6 | 3.04 | 0.01 | 0.04 | 304 |
| Camplackey* | 54.1 | 41.0 | 3.24 | 0.01 | 0.02 | 324 |
| Palm Springs | 55.2 | 41.4 | 3.14 | 0.10 | 0.03 | 31.4 |

* Sample analyzed after helium extraction at 750°C

** by mass difference using the stoichiometric equation for apatite

**Table 1.**

Major and trace element data from electron microprobe analyses.

| Treatment | U (ppm) | Th (ppm) |
|---|---|---|
| unoutgassed | 10.54 ± .16 | 21.86 ± .33 |
| outgassed @700°C | 10.45 ± .16 | 21.72 ± .33 |
| outgassed @1100°C | 10.61 ± .16 | 20.98 ± .31 |

**Table 2.**

Uranium and thorium concentration data for heated and unheated apatite samples from the Pacoima Canyon pegmatite, California.

complex (Hill, 1984, 1988) on the northeastern margin of the batholith. The first is from a tonalite at 2070 meters elevation on the north face of Mt. San Jacinto ("CL") and consists of euhedral crystals 100-120 mm in prism diameter (length/diameter=2.5). The second is from a mylonitized tonalite at 150 meters elevation on the eastern edge of the batholith near Palm Springs ("PS"). The mylonite zone (Sharp,1966; 1979) is thought to be late Cretaceous in age (Dokka, 1984; Simpson, 1984; Goodwin and Renne, 1991). These apatites are also euhedral hexagonal prisms, but are smaller, 50 to 70 mm in diameter and with L/D~2.7. Apatites PS and CL are from our investigation of the relationship between elevation and helium age on San Jacinto (Wolf et al., 1997).

The plutonic apatites were separated from their host using a combination of heavy liquid and magnetic separations, followed by handpicking. Prior to analysis, the samples were carefully inspected for mineral contaminants such as zircon and sphene. Because these contaminants can have orders of magnitude more U and Th (and hence He) than apatite, their presence in even trace quantities can compromise He concentration determinations. It should be noted that these contaminants are particularly problematic for helium dating. The dissolution technique commonly used prior to U and Th analysis of apatite (nitric acid) will not dissolve most silicates and oxides, so mineral contamination will only act as a dilutant of the apatite. In contrast contaminants will contribute all of their helium during thermal outgassing, thus leading to "parentless" helium and anomalously old ages.

The chemical compositions of the apatite samples are listed in Table 1.

All four have little if any hydroxyl component, but the F and Cl abundances vary substantially, with SM having much more Cl than the other samples.

*2.2.2 Experimental Methods: Helium Extraction*

After mineral purification, the separates were split with a sample splitter into aliquots for diffusion studies and for measurement of total He and U and Th concentrations (for determination of helium ages). For the helium age determinations ~10 mg of apatite was loaded into a sintered steel capsule and outgassed at 1050°C in a resistively-heated double walled vacuum furnace. Repeat extraction at higher temperatures demonstrated conclusively that total helium outgassing is achieved in 20 minutes at this temperature. Initially U and Th determinations were made on a separate aliquot. Although each of the aliquots we analyzed consisted of hundreds to thousands of grains, we were concerned that heterogeneity might exist between the splits analyzed for parent and daughter. In later experiments we retrieved the apatites after heating and analyzed the outgassed grains themselves. Several experiments on apatite from the Pacoima Canyon Pegmatite of Southern California demonstrate that heating to 1050°C does not alter the U or Th abundance beyond 2-sigma analytical uncertainty (Table 2). Other than a color change, the apatites appear unaffected by protracted heating to this temperature, and thus are easily retrieved from the furnace.

For diffusion measurements, ~30 mg of apatite was loaded into a copper capsule and dropped into a stainless steel tube resistively heated from the

outside. After evacuation, the tube was double-valved from the vacuum line to prevent contamination via cross-seat leaks. Neither the sample nor the tube were baked prior to the diffusion run. The apatites were held at a constant temperature for a particular time (up to several weeks), after which the evolved helium was expanded into the gas purification line. Without reducing the temperature, the residual helium in the furnace was pumped by a turbomolecular pump for two minutes, then the furnace was isolated and raised to the next temperature step. For an initial reconnaissance we measured the temperature only with a thermocouple mounted on the external wall of the furnace, but it became clear that this design suffered from both a thermal lag and a steady-state offset relative to the temperature of the grains. In later experiments, we attached a second thermocouple directly to the copper capsule, within a few mm of the apatites (copper was used to promote thermal equilibrium between the grains and the thermocouple). With this modified design the temperature uncertainties at any step are $\pm 1$ to $\pm 4$°C and represent the total range of temperatures recorded by the thermocouple over the entire duration of the step (i.e., they include any initial overshoot of the setpoint).

Outgassing began at temperatures as low as 80°C, increasing in increments of 20-25°C below about 250°C. Above 250°C the increments ranged from 30-70°C, with the last step before total outgassing in the range 550-600°C. The duration of the steps ranged from more than two weeks to less than an hour and was governed both by the need to generate enough He for accurate quantification and the need to minimize the fraction of time during which the

grains were being ramped to the desired temperature. We assume that the step begins when the setpoint is actually achieved, rather than when the ramp is initiated. (At low temperatures the ramp time is as much as 40 minutes out of a total step duration of ~3000 minutes, although this drops to just a few minutes above 300°C). For the total outgassing step, the grains are held at 730°C for several hours. After the final step, the grains undergo reextraction at 750°C to ensure that all of the helium has been liberated. No appreciable helium has ever been measured during a reextraction step. Furthermore, a single sample was once heated to 1200°C after the 750°C reextraction, and no additional helium was recovered. Because we retrieve the grains from the furnace for post-outgassing chemical analysis, we do not take samples to their melting point (~1600°C). Nevertheless the lack of helium release at both 750°C and 1200°C demonstrates that extraction is quantitative at temperatures well below the melting point. Within expected uncertainties the total helium extracted during the diffusion runs was identical to the helium yield from the single extraction step used for helium age determinations.

Diffusion coefficients were calculated from the time and fraction of helium released at each step using the solution to the spherical diffusion equation presented by Fechtig and Kalbitzer (1966). Stated uncertainties on diffusion coefficients account for the effects of both uncertainties in step duration and in helium yield.

*2.2.3 Experimental Methods: Helium, Uranium, and Thorium Measurements*

After extraction, helium is purified by sequential exposure to a charcoal trap held at liquid nitrogen temperature and a pair of SAES getters. A split of the purified gas (mostly He and Ne) is admitted into a quadrupole mass spectrometer to determine whether the sample needs to be split prior to analysis. This step ensures that all analyses are made within a relatively restricted range of helium partial pressure. After splitting, the gas is adsorbed on a charcoal trap held at 16°K. The trap is then heated to 34°K, effecting complete separation of Ne from He. The He is then admitted into a MAP 215-50 mass spectrometer. The entire gas handling system is automated.

Helium concentrations are determined by peak height comparison with a working standard (the "MM" helium standard distributed by H. Craig). In the peak height range used for most apatite measurements, the reproducibility of standards is better than 0.2% in any given day. The amount of helium delivered by this standard (about 3.8 picomol) is periodically calibrated for tank depletion using a primary pure He standard which itself was calibrated with a thermally stabilized capacitance manometer corrected for thermal transpiration effects. The amount of helium delivered by the primary standard is known to an accuracy of better than 0.5%. As a consequence of this calibration technique, we do not suffer from uncertainties related to the absolute concentration of helium in the atmosphere as we would if we calibrated against an aliquot of air. The major source of uncertainty in this method is the linearity of the peak height response. We have calibrated for this effect by analyzing multiple aliquots of the

standard. By splitting the samples so that they are similar in size to the standard, we believe this effect is limited to a contribution of no more than 1.5% to our uncertainty. We thus believe our concentrations are precise and accurate at about the 2% level. In addition to the $^4$He peak height, we also measure $^3$He by peak jumping to a pulse-counting channeltron detector. The 215-50 has an electrostatic filter and a resolution of 600 on this detector; $^3$He is completely separated from isobaric interferences such as HD. Uncertainty in the mass discrimination factor at very low $^3$He/$^4$He ratios coupled with the counting statistics on the small $^3$He beams leads us to assign a conservative estimate of ±25% to the reported helium isotope ratios. The $^3$He abundances were, in general, too small to reliably quantify the diffusion characteristics of this isotope.

Blanks on the furnace used for diffusion experiments ranged from 3.1 to 5.8 femtomol over the course of these experiments and are inconsequential for all but the lowest temperature steps. These blanks were found to be largely insensitive to temperature and increase only slightly with the duration of the step. Hot blanks on the double-walled furnace used for total age determinations were slightly lower, ranging from 1 to 3.2 femtomol. Blanks were run before each experiment and have been subtracted from the tabulated results. Although not well determined, the isotopic ratio of the blank is approximately that of atmospheric helium.

For U and Th measurements, apatite was dissolved in nitric acid. After purification using standard column chromatography, U and Th were measured by isotope dilution thermal ionization mass spectrometry. The estimated

uncertainty on these measurements is 1%, giving us a combined uncertainty on He ages of about 3%.

## 2.3 Results

### *2.3.1 Helium Ages*

From the measured U, Th, and He concentrations and by assuming secular equilibrium among all intermediate nuclides, we have computed He ages for the four samples in Table 3. Also indicated are ages corrected for alpha emission (Farley et al., 1996) computed from the measured size of the grains within each sample. Note that the Durango sample requires no emission correction because the dated aliquot was from deep within the interior of a large crystal.

The helium age of the Durango crystal (34 Ma) is close to the helium age suggested by Zeitler et al. (1987), but is slightly higher than the K/Ar ages of the volcanics with which the apatite is associated (29-32 Ma, McDowell and Keizer, 1977). Further study is needed to determine whether this difference is significant. The oldest helium age, 120 Ma on sample SM, is very close to the oldest crystallization ages reported for the western part of the PRB (Silver et al., 1978), indicating very high helium retentivity in this sample. The two San Jacinto samples yield lower helium ages of 48 Ma (CL) and 17 Ma (PS). We show elsewhere (Wolf et al., 1997) that not only these but other apatites from the San Jacinto Mountains have helium ages strongly correlated with elevation of the sample sites.

| Sample | $^4He$ (nmol/g) | $^3He/^4He$ ($x10^{-9}$) | U (ppm) | Th (ppm) | He Age (Ma) Raw | He Age (Ma) Corrected** |
|---|---|---|---|---|---|---|
| CL* | 5.80 | 11 | 21.10 | 21.38 | 40.7 | 48 |
| SM | 8.88 | 2.3 | 10.17 | 23.56 | 103 | 120 |
| PS* | 2.30 | 5.1 | 34.56 | 20.56 | 10.8 | 17.1 |
| Durango | 8.65 | 1.4 | 8.98 | 161.3 | 33.9 | 33.9 |

* U and Th determined on same aliquot analyzed for helium

** Corrected for alpha emission using the procedure of Farley et al. (1996a)

**Table 3.**

U, Th, and He concentrations and helium ages.

All of the samples have $^3He/^4He$ ratios of $< 2x10^{-8}$ (Table 3). Such low ratios are consistent with radiogenic production (Andrews, 1985) and preclude significant atmospheric helium ($^3He/^4He=1.4x10^{-6}$) and/or mantle-derived helium (from fluid inclusions, $^3He/^4He$ ~$1x10^{-5}$ (e.g., Craig and Lupton, 1981)). We conclude that no correction for "excess" helium from these sources is required. However, these data do not rule out the possibility of trapped crustal (radiogenic) helium.

*2.3.2 Diffusion Experiments*

Results of the incremental outgassing experiments are listed in Table 4. The first set of experiments was performed with a monotonically increasing temperature schedule, from as low as 80°C to as high as 600°C, at which point helium was essentially exhausted from the samples. The resulting diffusivity profiles are shown on an Arrhenius plot in Figure 1. The four samples display remarkably similar diffusion behavior across the entire temperature range investigated. The profiles are characterized by a strongly linear segment from 80 to ~290°C; above 290°C the diffusivity increase tails off. This behavior has been noted previously (Zeitler et al., 1987; Lippolt et al., 1994) and is apparently a general characteristic of helium loss from apatite. For comparison we have also plotted one of the diffusion runs on Durango apatite from Zietler et al. (1987). Above about 350°C the profiles are in excellent agreement, but below this temperature we obtain systematically higher diffusion coefficients. At present we have no explanation for this discrepancy, although we believe our

**Figure 1.**

Arrhenius plots of helium diffusion from apatite. Diffusivity at each temperature is determined from the fraction of gas released at each increment using the formulation by Fechtig and Kalbitzer (1966). Top Panel: monotonic and cycled runs on Durango apatite, along with results from Zeitler et al. (1987) for comparison. The first step is indicated to show heating schedule for the cycled runs. Bottom Panel: all monotonic runs. CL1 and CL2 have large temperature uncertainties because they lacked the internal thermocouple. The three lowest temperature steps from CL2 are excluded because of very large uncertainties in the temperature at those steps.

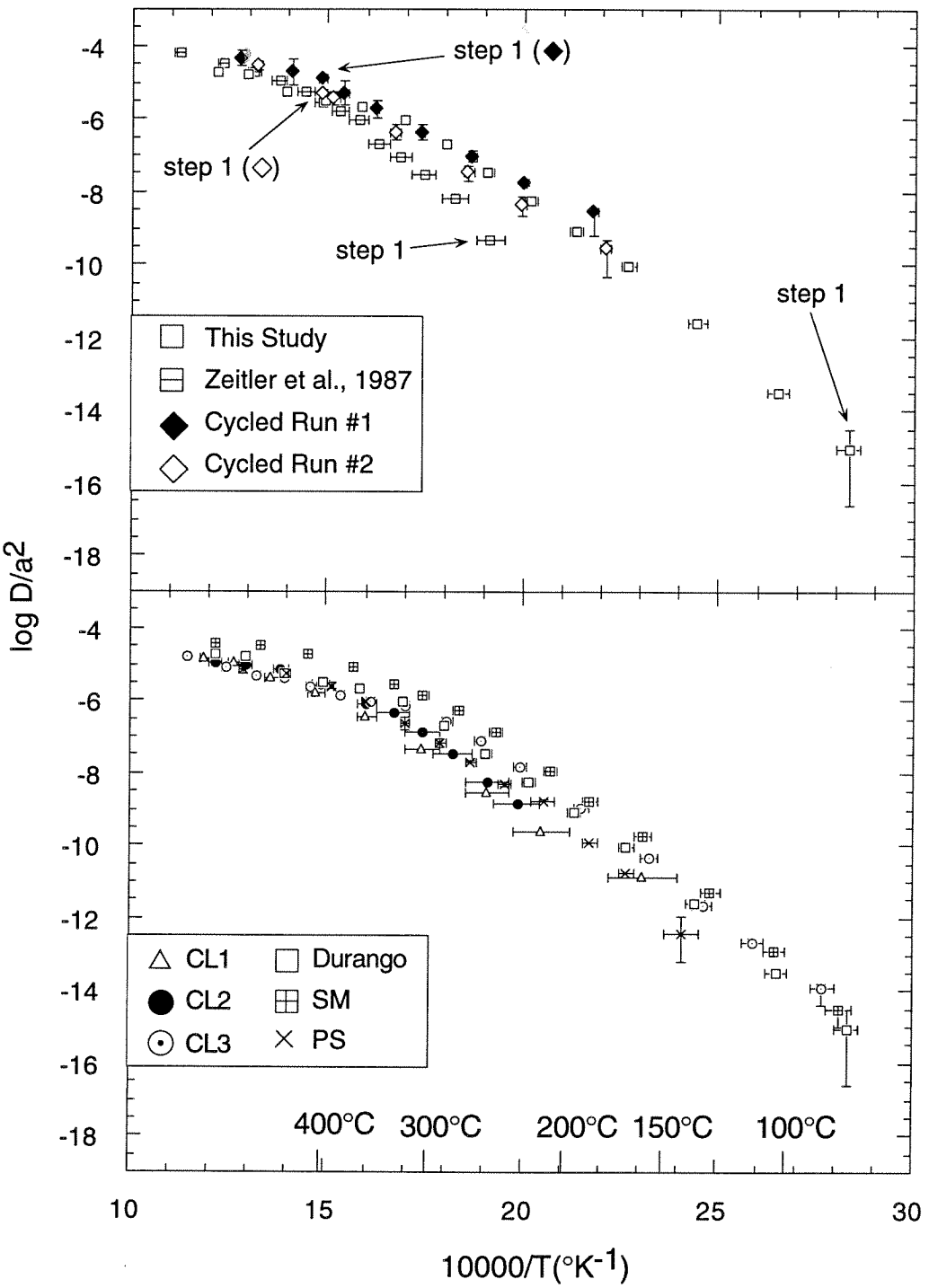
step 1 (◆)
step 1 (◇)
step 1
step 1
This Study
Zeitler et al., 1987
Cycled Run #1
Cycled Run #2
CL1
CL2
CL3
Durango
SM
PS
400°C
300°C
200°C
150°C
100°C
log D/a2
10000/T(°K-1)

results are more likely to be correct as our experiments were performed on a system designed specifically for He analyses and high precision temperature determinations at low temperatures. The striking similarity among all of our diffusion profiles is surprising given the range in grain size and chemical composition of the samples.

Previous workers have shown that argon diffusion can be very sensitive to the heating schedule used in the outgassing experiment (Lovera et al., 1989, 1991). To test for a similar effect in helium loss from apatite we analyzed two additional aliquots of the Durango sample. Both were initially heated to ~400°C (well into the region where diffusion deviates from the linear Arrhenius relationship), then rapidly cooled to lower temperatures. The outgassing then followed roughly the same schedule used in the monotonic experiments. The results of these "cycled" runs are listed in Table 5. In the first cycled run the grains were held at 400°C for 150 minutes, removing 80% of the total helium. In the second run 29% of the helium was released in 47 minutes at 388°C. As shown in Figure 1, the cycled runs yield diffusion profiles which are identical within error to that produced by the monotonically increasing temperature schedule.

To calculate diffusion coefficients we have implicitly assumed volume diffusion and spherical geometry. We have tested the validity of this assumption by performing isothermal outgassing experiments on two of our samples, Durango at 300°C and CL at 250°C. After repeatedly milking helium from the sample at the temperature of interest, it was heated to 750°C to obtain complete

| T°C | Duration (min.) | $^4$He (pmol/g) | $^4$He Released (%) | log D/a$^2$ |
|---|---|---|---|---|
| **Camp Lackey (CL1)** | | | | |
| 160 | 1373 | 21.3 | 0.35 | -10.89 |
| 215 | 1420 | 73.2 | 1.21 | -9.62 |
| 250 | 729 | 130 | 2.16 | -8.64 |
| 300 | 654 | 610 | 10.1 | -7.37 |
| 350 | 355 | 992 | 16.5 | -6.44 |
| 405 | 173 | 1018 | 16.9 | -5.79 |
| 462 | 106 | 913 | 15.1 | -5.37 |
| 517 | 40 | 553 | 9.18 | -4.97 |
| 567 | 74 | 794 | 13.2 | -4.86 |
| Final Step | | 686 | 15.3 | |
| Total Concentration | | 5791 | | |
| **Camp Lackey (CL2)** | | | | |
| 170 | 1570 | 5.80 | 0.10 | -13.00 |
| 190 | 1450 | 7.53 | 0.13 | -11.39 |
| 210 | 1390 | 14.0 | 0.23 | -10.78 |
| 230 | 1782 | 223 | 3.73 | -8.85 |
| 250 | 1105 | 211 | 3.53 | -8.26 |
| 275 | 623 | 358 | 5.97 | -7.49 |
| 300 | 135 | 203 | 3.39 | -6.89 |
| 325 | 652 | 1556 | 26.0 | -6.32 |
| 350 | 168 | 365 | 6.10 | -6.10 |
| 400 | 139 | 743 | 12.4 | -5.57 |
| 450 | 70 | 627 | 10.5 | -5.16 |
| 500 | 128 | 829 | 13.9 | -5.06 |
| 550 | 51 | 223 | 3.73 | -4.99 |
| Final Step | | 338 | 10.4 | |
| Total Concentration | | 5704 | | |

| T°C | Duration (min.) | $^4$He (pmol/g) | $^4$He Released (%) | log D/a$^2$ |
|---|---|---|---|---|
| **Camp Lackey (CL3)** | | | | |
| 88 | 5755 | 1.31 | 0.022 | -13.92 |
| 113 | 1721 | 2.05 | 0.034 | -12.65 |
| 133 | 1100 | 5.31 | 0.088 | -11.63 |
| 157 | 1461 | 33.5 | 0.55 | -10.33 |
| 192 | 1409 | 155 | 2.57 | -8.98 |
| 228 | 1511 | 552 | 9.14 | -7.86 |
| 255 | 1238 | 853 | 14.1 | -7.11 |
| 280 | 264 | 363 | 6.01 | -6.57 |
| 314 | 410 | 966 | 16.0 | -6.15 |
| 346 | 847 | 1343 | 22.3 | -6.02 |
| 377 | 328 | 415 | 6.88 | -5.87 |
| 413 | 184 | 314 | 5.20 | -5.60 |
| 446 | 155 | 294 | 4.88 | -5.41 |
| 483 | 138 | 235 | 3.89 | -5.30 |
| 533 | 117 | 201 | 3.33 | -5.09 |
| 600 | 62 | 114 | 1.89 | -4.81 |
| Final Step | | 188 | 3.11 | |
| Total Concentration | | 6035 | | |

**Table 4.**

Results of monotonic diffusion runs.

| T°C | Duration (min.) | $^4$He (pmol/g) | $^4$He Released (%) | log D/a$^2$ |
|---|---|---|---|---|
| **Durango** | | | | |
| 80 | 2780 | 0.38 | 0.004 | -15.06 |
| 104 | 5886 | 2.65 | 0.03 | -13.52 |
| 136 | 1490 | 11.1 | 0.13 | -11.59 |
| 168 | 1223 | 62.2 | 0.73 | -10.03 |
| 196 | 1230 | 156 | 1.83 | -9.10 |
| 223 | 2801 | 664 | 7.77 | -8.25 |
| 251 | 1541 | 884 | 10.3 | -7.45 |
| 282 | 499 | 843 | 9.87 | -6.72 |
| 317 | 2196 | 4449 | 52.1 | -6.04 |
| 357 | 213 | 307 | 3.59 | -5.71 |
| 397 | 1265 | 1033 | 12.1 | -5.53 |
| 445 | 281 | 77.4 | 0.91 | -5.27 |
| 500 | 107 | 34.1 | 0.40 | -4.78 |
| 548 | 372 | 21.2 | 0.25 | -4.73 |
| Final Step | | 9.52 | 0.008 | |
| Total Concentration | | 8554 | | |
| **Palm Springs** | | | | |
| 142 | 421 | 0.76 | 0.033 | -12.44 |
| 168 | 9502 | 24.1 | 1.03 | -10.76 |
| 187 | 1357 | 10.4 | 0.44 | -9.92 |
| 214 | 706 | 41.3 | 1.76 | -8.76 |
| 238 | 698 | 57.3 | 2.44 | -8.34 |
| 262 | 708 | 128 | 5.46 | -7.69 |
| 285 | 227 | 82.9 | 3.54 | -7.18 |
| 314 | 156 | 136 | 5.80 | -6.65 |
| 352 | 84 | 195 | 8.31 | -6.05 |
| 388 | 112 | 411 | 17.5 | -5.60 |
| 442 | 132 | 528 | 22.5 | -5.24 |
| 505 | 107 | 267 | 11.4 | -5.17 |
| Final Step | | 463 | 19.8 | |
| Total Concentration | | 2346 | | |

| T°C | Duration (min.) | $^4$He (pmol/g) | $^4$He Released (%) | log D/a$^2$ |
|---|---|---|---|---|
| **San Marcos** | | | | |
| 82.5 | 28245 | 2.18 | 0.025 | -14.51 |
| 105 | 2890 | 2.83 | 0.03 | -12.88 |
| 130 | 1497 | 15.8 | 0.18 | -11.29 |
| 160 | 1453 | 98.0 | 1.11 | -9.75 |
| 187 | 290 | 78.5 | 0.89 | -8.78 |
| 210 | 171 | 168 | 1.91 | -7.96 |
| 244 | 959 | 1993 | 22.7 | -6.90 |
| 271 | 529 | 1571 | 17.9 | -6.29 |
| 299 | 879 | 2760 | 31.4 | -5.86 |
| 324 | 163 | 479 | 5.45 | -5.56 |
| 365 | 152 | 792 | 9.00 | -5.10 |
| 416 | 76 | 437 | 4.97 | -4.72 |
| 479 | 71 | 284 | 3.23 | -4.46 |
| 550 | 58 | 74.1 | 0.84 | -4.43 |
| Final Step | | 40.0 | 0.45 | |
| Total Concentration | | 8795 | | |

**Table 4.** (continued)

extraction. The results of these experiments are listed in Table 6 and plotted in Figure 2 along with the predicted release from a sphere using the diffusion coefficient which best fits the experimental data. The observed and predicted curves are in excellent agreement and demonstrate that volume diffusion from a sphere can adequately describe diffusion from both of these apatites, despite the differences in their external morphology (large shards from the large euhedral single crystal of Durango and small euhedral crystals of CL). The fit to a volume diffusion model also argues against any significant "trapped helium," in contrast to some previous observations (Lippolt et al., 1994).

## 2.4 Disscussion

### *2.4.1 Helium Ages and the Helium Closure Temperature of Apatite*

As indicated by their reasonably high helium ages, the four apatites we investigated have retained a substantial fraction of their radiogenic helium over geologic time. In the case of Durango, this fraction is nearly unity, suggesting that little or no helium is lost from quickly-cooled volcanic samples. For the plutonic apatites, sample SM has a helium age very similar to the inferred crystallization age, but samples from the San Jacinto Mountains (SM and PS) have ages much lower than the crystallization ages of their host rocks. It is important to establish whether these low helium ages result from a protracted cooling history or some other phenomenon which has caused helium loss. Because we know little of the low temperature history of the PRB, we must rely on the laboratory diffusion measurements to investigate this phenomenon.

| T°C | time (min.) | ($^4$He) pmol/g | % ($^4$He) at each step | log D/a$^2$ |
|---|---|---|---|---|
| **Durango (Cycled, #1)** | | | | |
| 400 | 150 | 6854 | 80.0 | -4.90 |
| 186 | 705 | 1.96 | 0.023 | -8.55 |
| 227 | 191 | 3.48 | 0.041 | -7.75 |
| 262 | 103 | 9.49 | 0.11 | -7.05 |
| 302 | 83 | 34.9 | 0.41 | -6.38 |
| 343 | 69 | 124 | 1.45 | -5.73 |
| 375 | 55 | 230 | 2.69 | -5.31 |
| 438 | 53 | 581 | 6.79 | -4.73 |
| 510 | 81 | 638 | 7.45 | -4.35 |
| Final Step | | 84.9 | 0.99 | |
| Total Concentration | | 8564 | | |
| **Durango (Cycled, #2)** | | | | |
| 388 | 47 | 2475 | 28.8 | -5.44 |
| 180 | 923 | 1.89 | 0.022 | -9.58 |
| 228 | 457 | 14.4 | 0.17 | -8.40 |
| 265 | 797 | 190 | 2.22 | -7.49 |
| 325 | 333 | 810 | 9.43 | -6.38 |
| 400 | 102 | 1586 | 18.5 | -5.34 |
| 485 | 101 | 2853 | 33.2 | -4.55 |
| Final Step | | 658 | 7.66 | |
| Total Concentration | | 8589 | | |

**Table 5.**

Results of "cycled" diffusion runs on Durango apatite.

Previous workers (Zeitler et al., 1987; Lippolt et al., 1994) have estimated a helium closure temperature for apatite by using only the low temperature linear portion of the Arrhenius plot, implicitly assuming that the high temperature behavior is largely irrelevant in the natural setting. We will for the moment adopt this assumption, which we justify below. The diffusion parameters implied by the low temperature linear regime for the six monotonic experiments are shown in Table 7. The cutoff point of the linear regime was arbitrarily assumed to be the data point at which the linear correlation coefficient ($r^2$) dropped below 0.998. As shown in Table 7, this procedure left 7 or 8 data points in all cases (except CL1 and CL2, which were the poorly determined reconnaissance runs). Excluding CL1 and CL2, the activation energies implied by the linear segments are nearly identical within error, averaging 36.3 ± 1.6 kcal/mol, and with an average frequency factor of 7.82 ± 1.2 $sec^{-1}$. Assuming a cooling rate of 10°/Ma, the helium closure temperatures (Dodson, 1973) derived from these diffusion parameters range from 67 to 82°C and average 74 ± 5°C. As a consequence of the strong linearity of the Arrhenius plots and the high precision of the temperature measurements, the uncertainty on individual determinations of the closure temperature is typically < 5°C. Furthermore, because we have measured diffusion coefficients within just a few degrees of the closure temperature, there is little likelihood that dramatic changes in diffusion behavior exist at temperatures below which measurements were made in the laboratory. Our closure temperatures have a lower estimated uncertainty and are at the

extreme low end of the range suggested by earlier workers (Zeitler et al., 1987; Lippolt et al., 1994). This discrepancy may arise because we have at least 7 diffusion coefficient determinations in the linear regime (below the transition temperature of 290°) for all of our high quality runs; in contrast previous workers have made only a few measurements below this critical temperature.

The closure temperatures we have measured are analytically identical and so are not correlated with grain size or shape, chemical composition, or radiation exposure history. Insensitivity to grain size variations of a factor of three (between 60 mm in PS and 180 mm in Durango) require that the diffusion domain ("a" in $D/a^2$) is smaller than the grain itself (<60 mm in diameter), and is roughly equivalent in size in all of our samples. A sub-grain diffusion domain is also suggested by the insensitivity of the diffusion profile to sample shape, from angular shards in Durango, to subhedral grains in SM, to fully euhedral crystals in CL.

The samples span a large range in anion composition, and in our experience they encompass most of the compositions found in igneous rocks. The Cl content varies from below detection to > 1.1%, and F from 2.3 to 3.6%, with no detectable change in diffusion behavior. Unlike fission track annealing, the helium thermochronometer in apatite is largely insensitive to anion composition, at least over the range we have investigated.

It has been suggested that radiation damage may accelerate diffusive helium loss from some minerals, presumably by destruction of the crystal structure (Hurley, 1954; Damon and Kulp, 1957). The radiation dose received

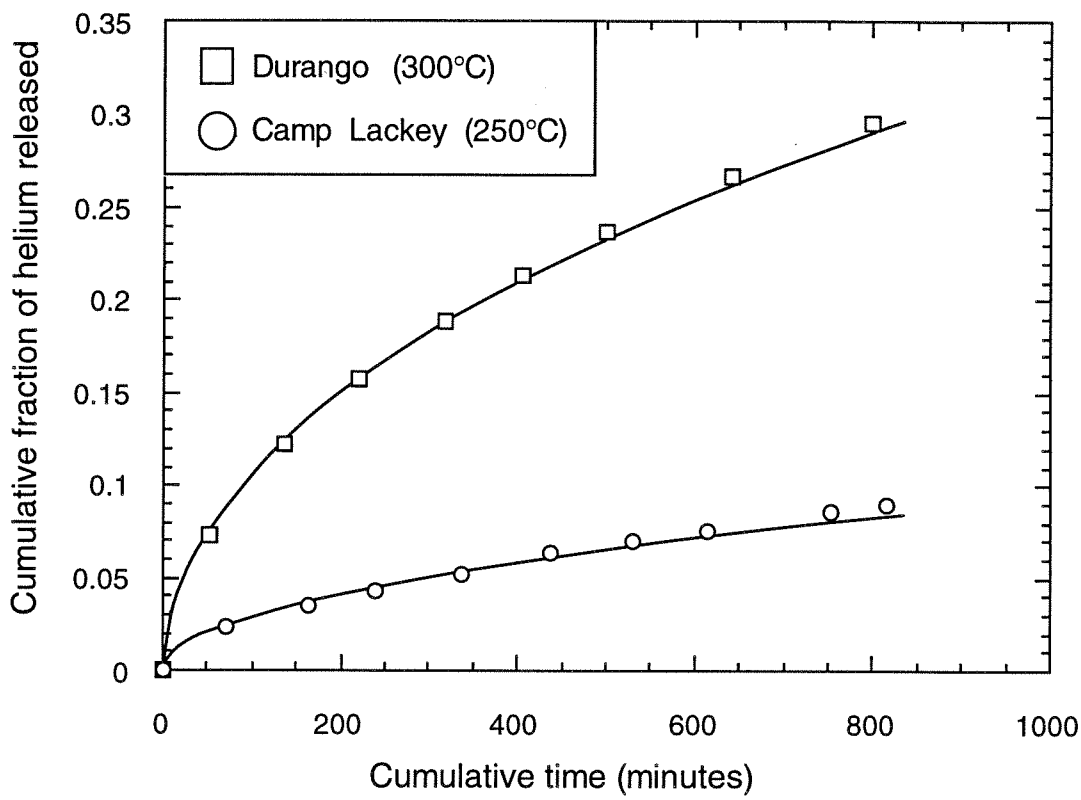


**Figure 2.**

Results of isothermal outgassing experiments (symbols) compared with the best fit to diffusion from a sphere (curve). Volume diffusion from a sphere fits both runs extremely well and justifies the assumption of a spherical diffusion geometry.

by apatite will be dominated by in-situ production, so it can be estimated from the U and Th contents and ages of our samples. Assuming a crystallization age of 100 Ma for the PRB samples, the total alpha dosages that the samples haveexperienced range from 5.2 x $10^{15}$ to 13 x $10^{15}$ alphas/g. There is no obvious indication of metamictization of these samples, nor are we aware of any work documenting the dosage at which such damage becomes detectable in apatite. For comparison, these alpha dosages are far lower than those at which zircons lose helium as a consequence of damage (Damon and Kulp, 1957) and also are lower than the dosage at which zircons begin to experience observable metamictization (Woodhead et al., 1991). Nevertheless, our samples have all experienced similar total radiation fluxes (within a factor of 3), so we cannot completely rule out damage as a control on helium diffusion from apatite.

*2.4.2 High Temperature Helium Diffusion Behavior*

The deviation from linear Arrhenius behavior at high temperature indicates a change in the mechanism of diffusion which begins at about 290°C. This change may signal the presence of multiple diffusion sites within apatite, or, alternatively, a structural or chemical transformation of the crystals. It is critical for thermochronometric applications to evaluate how this deviation from linearity affects the closure temperature. We consider two specific mechanisms for the transition: 1) there are multiple diffusion domains within the apatites, which vary in characteristic length, activation energy, or both; and 2) physical

| Cumulative Time (min) | $^4He$ (pmol/g) | Cumulative $^4He$ (%) |
|---|---|---|
| **CL** (250°C) | | |
| 70 | 133 | 2.33 |
| 162 | 66.3 | 3.49 |
| 240 | 44.2 | 4.27 |
| 337 | 56.0 | 5.25 |
| 437 | 64.4 | 6.38 |
| 531 | 39.6 | 7.07 |
| 614 | 30.9 | 7.62 |
| 753 | 52.8 | 8.54 |
| 814 | 22.3 | 8.93 |
| **Durango** (300°C) | | |
| 51 | 578 | 7.27 |
| 136 | 396 | 12.3 |
| 220 | 284 | 15.9 |
| 217 | 250 | 19.0 |
| 404 | 192 | 21.4 |
| 500 | 185 | 23.8 |
| 642 | 241 | 26.8 |
| 800 | 233 | 29.7 |

**Table 6.**

Results of isothermal outgassing experiments.

and/or chemical transformations occur, such as defect annealing, changes in crystal structure, or loss of volatile components.

Lovera and coworkers (1989, 1991) have developed a model for Ar diffusion from feldspars which calls upon domains with different diffusion properties to account for deviations from simple linear behavior on an Arrhenius plot. In these models the low temperature regime we observe in Figure 1 would be attributed to a single diffusion domain carrying up to 80% of the total helium (the maximum gas fraction we observed in the linear regime). The deviation at higher temperatures would be attributed to the increasing significance of a more He-retentive domain (or domains) which are only apparent after helium has been extracted from the least retentive (lowest temperature) domain. An important prediction of such multiple domain models is that samples which are heated to high enough temperatures to reveal the second domain will, upon cooling, no longer lie on the original low temperature diffusion array. Instead they will have lower diffusivities resulting from the depletion of gas from the least retentive domain. As shown in Figure 1, our thermally cycled samples, which were initially heated well into the region in which non-linear behavior pertains, plot on precisely the same low temperature array as the uncycled samples. This effectively precludes a multi-domain model. The absence of exsolution lamellae and/or twinning in apatite (unlike feldspar) may account for this distinction.

A second interpretation of the deviation from linearity at high temperatures is that there are physical and/or chemical changes occurring as

the apatite is heated. Structural decomposition such as the loss of a volatile component during vacuum heating can be expected to dramatically modify diffusion behavior. To investigate this possibility we analyzed the volatile content of two of our samples before and after an incremental outgassing run (Table 1). We observed no loss of F or Cl, nor any change in any other constituent we measured. While we could not measure other volatiles (OH, $CO_3$), detailed investigations of apatite have recently shown that both of these anions are retained to temperatures in excess of 1000°C (S. Nadeau, personal communication). We conclude that devolatilization is an unlikely explanation for our results. The cycling experiments also argue against such a mechanism as they demonstrate that the change in diffusion behavior is completely reversible.

We are aware of no literature indicating changes in the crystal structure of apatite over the temperature range we have investigated, but subtle changes in atomic arrangement which modify helium diffusion cannot be ruled out. Alternatively, changes in the mechanism of helium diffusion at ~290°C may be associated with the onset of diffusion of ions of the apatite structure. In this regard it is interesting that the annealing of fission tracks (a process thought to involve diffusion of at least some of the constituents of apatite) increases rapidly near this temperature. For example, laboratory studies in the range 1-10 hours show a rapid increase in the rate of fission track shortening at roughly 300°C (Crowley et al., 1991; Green et al., 1986). The deviation from linearity which we observe cannot be a direct consequence of structural annealing (radiation damage or other microstructural defects) because our cycled runs reveal

| Sample | n* | log $D_0/a^2$ ($sec^{-1}$) | $E_a$ (kcal/mol) | $T_C$** (°C) |
|---|---|---|---|---|
| CL1 | 5 | 3.8±0.5 | 29.4±2.9 | 67±7 |
| CL2 | 5 | 7.2±2.2 | 36.3±5.1 | 82±18 |
| CL3 | 8 | 7.7±0.8 | 35.7±1.7 | 70±5 |
| Durango | 7 | 7.7±0.5 | 36.2±1.0 | 75±2 |
| SM | 8 | 9.4±0.6 | 38.6±1.1 | 71±3 |
| PS | 8 | 6.5±0.8 | 34.9±1.8 | 81±5 |

*number of points in linear regime

** assumes a cooling rate of 10°C/Ma

**Table 7.**

Diffusion parameters for low temperature linear regime.

reversibility in the rate of helium diffusivity. However, the increase could be produced, for example, by diffusion of He assisted by mobility of lattice vacancies.

We tentatively conclude that subtle changes in crystal structure or in the mobility of the structural atoms of the apatite crystal are responsible for the change in He diffusivity at ~290°C. If so, the fraction of gas which is removed in the linear regime is governed only by the cumulative time the sample is held below 290°. Furthermore, it should be possible to remove 100% of the helium in the linear regime. Because He diffusion at temperatures over 290°C is very rapid in a geologic sense, a cooling apatite will retain no memory of the high temperature diffusion mechanism, and so it is of no significance to low temperature thermochronometry.

*2.4.3 Geochronometric Implications*

A helium closure temperature of just 75°C is far lower than that reported for any other dating technique, and has important implications for the use of the system for geochronological applications. The closure temperature is so low that it is important to consider how much helium will be lost at ambient temperatures on the Earth's surface. For an isothermal system, the helium concentration in a grain reflects the balance between helium production and diffusive loss and can be computed directly (Trull et al., 1991). Solutions for this case are shown in Figure 3 for a variety of temperatures using the diffusion data from the Durango sample. Even over periods of up to 100 Ma, retention of

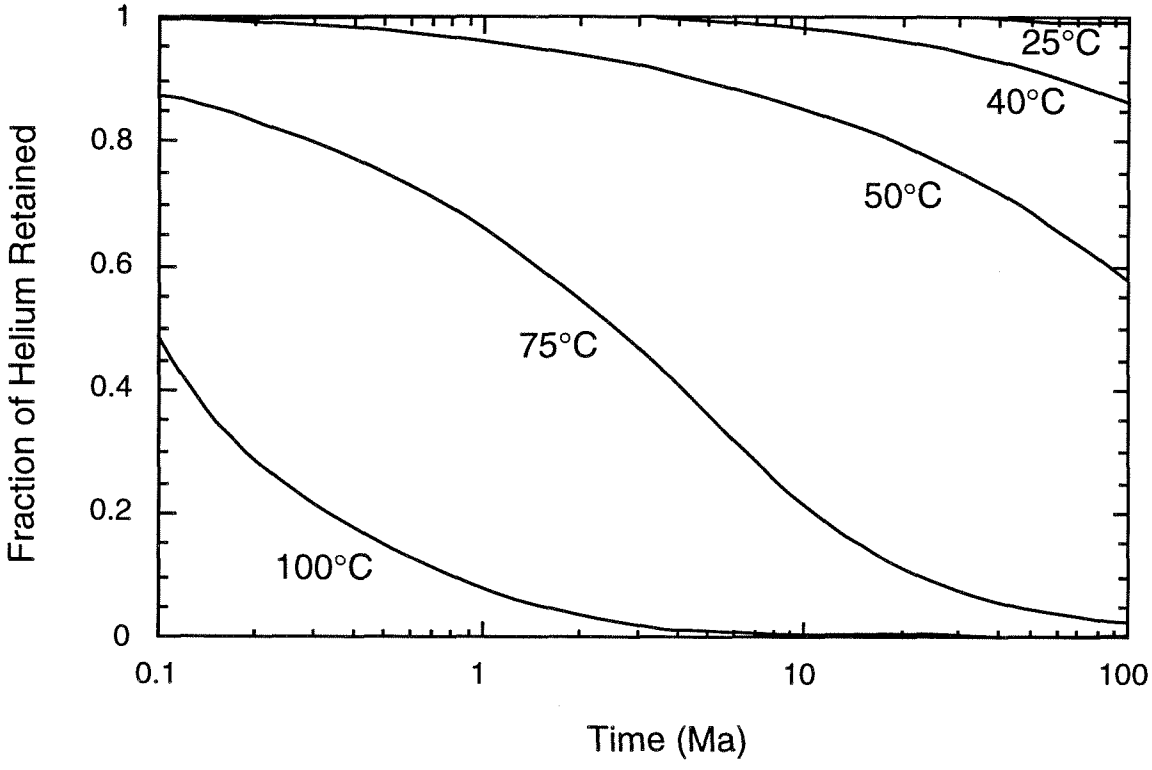


**Figure 3.**

Fraction of helium retained in an isothermal apatite as a function of temperature and time, using the diffusion data measured (or extrapolated from) Durango apatite. This plot demonstrates that retentivity at Earth's surface temperatures is very high, but drops rapidly at only slightly higher temperatures.

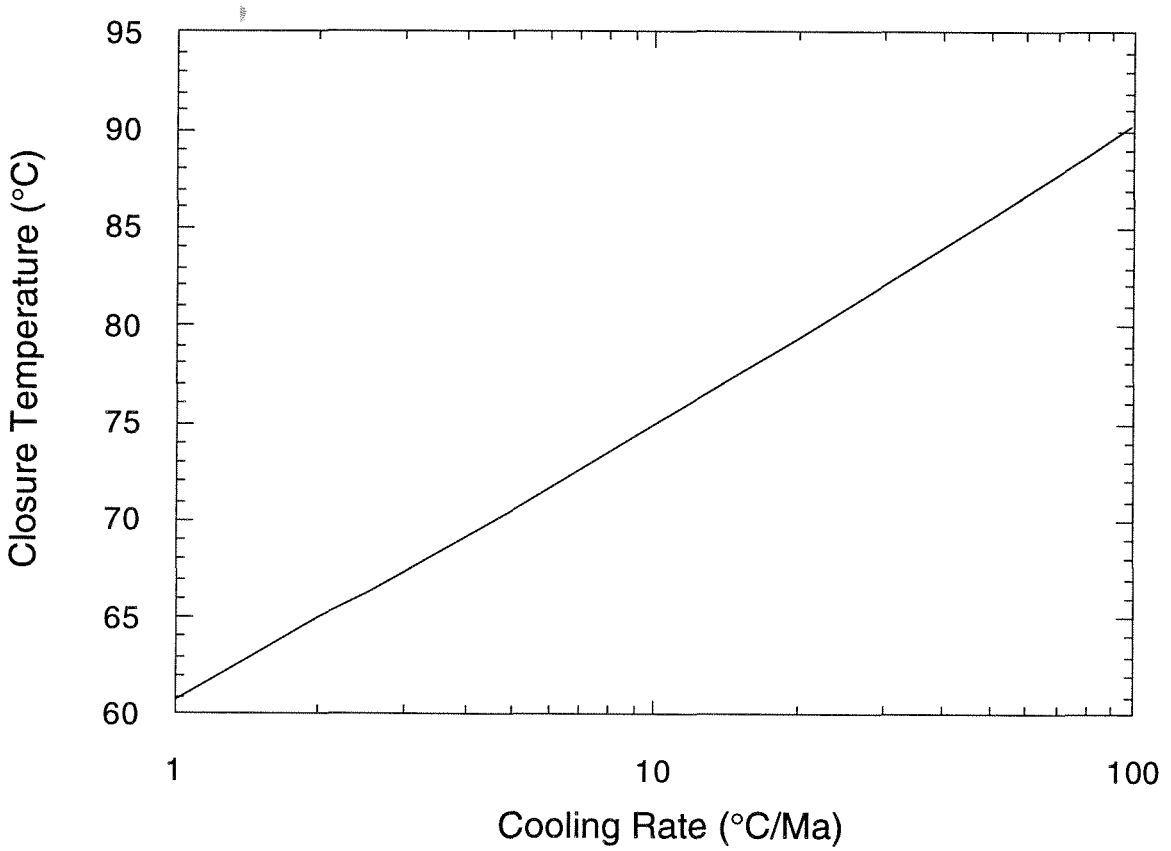


**Figure 4.**

Closure temperature as a function of cooling rate for Durango apatite, using the formulas given by Dodson, 1973.

helium is nearly quantitative at 25°C. However, at temperatures as low as 45°C, measured helium ages will be low by almost 40% over this same period. As pointed out by Trull et al. (1991), the relevant temperature for these calculations is not simply the mean annual temperature, but some estimate of the maximum temperatures experienced by the sample, because diffusivity increases exponentially with temperature. The closure temperatures we compute are about as low as can be used without having to resort to corrections for diffusive loss at ambient temperatures.

It is also important to recognize that the calculated closure temperature is sensitive to the choice of cooling rate (Figure 4). This is a particularly important aspect of helium thermochronometry because low temperature cooling rates are in general more variable and often much slower than high temperature cooling rates. As a consequence the period during which partial retention occurs is likely to be more variable from place to place and generally longer than assumed for other chronometers. In the case of very slow cooling or high ambient temperatures, it may prove necessary to numerically model the entire solution to the time-dependent He-ingrowth/diffusive loss equation rather than use the simple closure temperature concept.

## 2.5 Conclusions

Our experiments indicate that He geochronometry of apatite is a viable tool for studies of low temperature geological events, and provide a strong basis for interpretation of helium cooling ages. Samples which have experienced

quick cooling yield helium ages very similar to those given by other techniques, while potentially slowly-cooled plutonic samples have helium ages which range from nearly the crystallization age to small fractions of that age. Helium diffusion from apatite can be described by a single thermally-activated mechanism over most of its release, indicating a closure temperature of about 75±5°C. Although an additional mechanism(s) of diffusion appears above 290°C, this mechanism is largely irrelevant for low temperature thermochronometry. We have detected no sensitivity of the closure temperature to grain size or chemical composition in specimens which span a fairly large range of the spectrum observed in igneous apatites. Thus it appears that a single closure temperature may be valid for most apatites.

Although the closure temperature for apatite is narrowly defined by our results, interpretation of helium ages must consider the implications of partial diffusive loss of helium at temperatures close to that of the Earth's surface as well as the sensitivity of the system to cooling rate. Nonetheless, we believe that apatite thermochronometry can yield new insight into structural and tectonic problems occurring in the uppermost crust.

*Acknowledgments*

This work was supported by the National Science Foundation. We thank M. Harrison and M. Grove for helpful suggestions and P. Damon and an anonymous reviewer for their comments on the manuscript.

## 2.6 References Cited

Andrews J. N. (1985) The isotopic composition of radiogenic helium and its use to study groundwater movement in confined aquifers. *Chem. Geol.*, 49, 339-351.

Bender M. (1973) Helium-Uranium dating of corals. *Geochim. Cosmochim. Acta*, 37, 1229-1247.

Craig H. and Lupton J. E. (1981) Helium-3 and mantle volatiles in the ocean and the oceanic crust. In *The Sea*, Vol. 7 (ed. C. Emiliani), 391-428. J. Wiley and Sons.

Crowley K., Cameron M., and Schaefer R. (1991) Experimental studies of annealing of etched fission tracks in fluorapatite. *Geochim. Cosmochim. Acta*, 55, 1449-1465.

Damon P. E. and Green W. D. (1963) Investigations of the helium age dating method by stable isotope dilution technique. In Radioactive Dating, IAEA, 55-71.

Damon P.E. and Kulp, J.L. (1957) Determination of radiogenic helium in zircon by stable isotope dilution technique, *Trans. Am Geophys. Union*, 38, 945-953.

Dodson M. H. (1973) Closure temperatures in cooling geological and petrological systems. *Contrib. Mineral. Petrol.*, 40, 259-274.

Dokka R. (1984) Fission track geochronologic evidence for late Cretaceous mylonitization and early Paleocene uplift of the northern Peninsular Ranges, California. *Geophys. Res. Let.*,11, 46-49.

Fanale F. P. and Kulp J. L. (1962) The helium method and the age of the Cornwall, Pennsylvania magnetite ore. *Econ. Geol.* 57, 735-746.

Fanale F. P. and Schaeffer O. A. (1965) Helium-uranium ratios for Pleistocene and tertiary fossil aragonites. *Science*, 149, 312-317.

Farley K., Wolf R., and Silver L. (1996) The effects of long alpha-stopping distances on (U-Th)/He dates. *Geochim. Cosmochim. Acta*, 60, 4223-4230.

Fechtig H. and Kalbitzer S. (1966) The diffusion of argon in potassium bearing solids. In Potassium-Argon Dating (ed. O. A. Schaeffer and J. Zahringer), 68-106. Springer.

Ferreira M., Macedo R., Reynolds J., Riley J., and Rowe M. (1975) Rare gas dating. II. Attempted U-He dating of young volcanic rocks from the Madiera Archipelago. *Earth Planet. Sci. Let.*, 25, 142-150.

Goodwin L.B. and Renne P.R. (1991) Effects of progressive mylonitization on Ar retention in biotites from the Santa Rosa Mylonite Zone, California, and thermochronologic implications. *Contrib. Mineral. and Petrol.*, 108, 283-297.

Graham D. W., Jenkins W. J., Kurz M. D., and Batiza R. (1987) Helium isotope disequilibrium and geochronology of glassy submarine basalts. *Nature*, 326, 384-386.

Green P., Duddy I., Gleadow A., Tingate P., and Laslett G. (1986) Thermal annealing of fission tracks in apatite: 1. A qualitative description. *Chem. Geol.*, 59, 237-253.

Hill R. (1984) Petrology and petrogenesis of batholithic rocks, San Jacinto Mountains, southern California. Ph.D., California Institute of Technology.

Hill R. (1988) San Jacinto intrusive complex. 1. Geology and mineral chemistry, and a model for intermittent recharge of tonalitic magma chambers. *J. Geophys. Res.*, 93, 10325-10348.

Hurley P. M. (1954) The helium age method and the distribution and migration of helium in rocks. In Nuclear Geology (ed. H. Faul), 301-329. Wiley.

Lippolt H. J., Leitz M., Wernicke R. S., and Hagedorn B. (1994) (U+Th)/He dating of apatite: experience with samples from different geochemical environments. *Chem. Geol.*, 112, 179-191.

Lovera O., Richter F., and Harrison T. (1989) The 40Ar/39Ar thermochronometry for slowly cooled samples having a distribution of domain sizes. *J. Geophys. Res.*, 94, 17917-17935.

Lovera O., Richter F., and Harrison T. (1991) Diffusion domains determined by 39Ar released during step heating. *J. Geophys. Res.* 96, 2057-2069.

Lyons J.I. (1988) Volcanogenic iron oxides, Cerro de Mercado and vicinity, Durango, Mexico. *Econ. Geol.*, 83, 1886-1906.

McDowell F. and Keizer R. (1977) Timing of mid-Tertiary volcanism of the Sierra Madre Occidental between Durango City and Mazatlan, Mexico. *Geological Society of America, Bulletin*, 88, 1479-1487.

Naeser C. and Fleischer R. (1975) Age of the apatite at Cerro de Mercado, Mexico: a problem for fission track annealing records. *Geophys. Res. Lett.*, 2, 67-70.

Rutherford E. (1905) Present problems in radioactivity. *Popular Science*, May, 1-34.

Sharp R. V. (1966) Ancient mylonite zone and fault displacements in the Peninsular Ranges of southern California. *Geological Society of America Special Paper*, 101, 333.

Sharp R.V. (1979) Some characteristics of the Eastern Peninsular Ranges Mylonite Zone. *U.S.G.S. Open-File Report 79-1239*, 258-267.

Silver L. and Hill R. (1986) U-Th-Pb micro discordance in young zircons: a case study in the San Jacinto Mountains. *EOS, Trans. Am. Geophys. Union,* 67, 399-400.

Silver L., Taylor H., and Chappell B. (1979) Some petrological, geochemical and geochronological investigations of the Peninsular Ranges Batholith near the international border of the USA and Mexico. In *Mesozoic Crystalline Rocks* (ed. P. Abbot and V. Todd). Geological Society of America Guidebook, Annual Meeting, San Diego.

Simpson C. (1984) Borrego Springs - Santa Rosa mylonite zone: a late Cretaceous west-directed thrust in southern California. *Geology*, 12, 8-11.

Strutt R. (1908) The accumulation of helium in geologic time. *Roy. Soc. London Proceedings*, 81A, 272-277.

Strutt R. (1909) The leakage of helium from radioactive minerals. *Roy. Soc. London Proceedings*, 82A, 166-169.

Trull T. W., Kurz M. D., and Jenkins W. J. (1991) Diffusion of cosmogenic 3He in

olivine and quartz: implications for surface exposure dating. *Earth Planet. Sci. Lett.*, 103, 241-256.

Turekian K., Kharkar D., Funkhouser J., and Schaeffer O. (1970) An evaluation of the U-He method of dating bone. *Earth Planet. Sci. Lett.*, 7, 420-424.

Woodhead J. A., Rossman G. R., and Silver L. T. (1991) The metamictization of zircon: radiation dose-dependent structural characteristics. *Am. Mineral.*, 76, 74-82.

Young E., Myers A., Munson E., and Conklin N. (1969) Mineralogy and geochemistry of fluorapatite from Cerro de Mercado, Durango, Mexico. *United States Geological Survey, Professional Paper 650-D*, D84-D93.

Zeitler P. K., Herczig A. L., McDougall I., and Honda M. (1987) U-Th-He dating of apatite: a potential thermochronometer. *Geochim. Cosmochim. Acta*, 51, 2865-2868.

# Chapter 3

## A Sensitivity Analysis of the Apatite (U-Th)/He Thermochronometer

R.A. Wolf
K.A. Farley
D.M. Kass

**Abstract** - In general, crustal rocks may reside for long periods at temperatures where helium in apatite is neither quantitatively retained nor lost by diffusion (i.e., partial helium retention occurs). To better characterize the response of apatite helium ages to thermal history and partial helium retention, we solved the full radiogenic helium production/diffusion equation. Because of partial helium retention, apatite helium ages are very sensitive to temperature in the range ~45-80°C in a thermally static environment. This range of temperatures defines the helium partial retention zone and is ~35°C cooler than the analogous fission track partial annealing zone, suggesting that the apatite (U-Th)/He system may record more recent thermal histories than the apatite fission track method. We also explore the response of apatite helium ages to more complex thermal histories to (1) investigate helium age/sample elevation profiles for arbitrary cooling histories, (2) to determine whether apatite (U-Th)/He thermochronometry can help refine fission track length derived cooling models and (3) to assess the effects of ambient surface temperatures on helium

ages. The number of possible thermal histories produced by fission track length derived thermal models can be refined by rejecting thermal histories whose model helium ages are inconsistent with measured values. Although helium diffuses rapidly at low temperatures, modeling suggests that helium ages are unaffected by Earth surface temperatures and natural fires. Helium ages from samples which spend long durations in the helium partial retention zone are sensitive to the measured range of diffusion parameters as well as temperature, and therefore, high precision diffusion experiments may be required for some future studies.

## 3.1 Introduction

Apatite (U-Th)/He thermochronometry provides a tool for interpreting low temperature histories of the upper crust (i.e., <100°C) (Zeitler et al., 1987; Lippolt et al., 1994; Wolf et al., 1996; Wolf et al., 1997). For high temperature thermochronometers such as the $^{40}Ar/^{39}Ar$ method, the closure temperature concept (Dodson, 1973), in which cooling is assumed to be constant with time, has proven useful. However, at the low temperatures relevant to apatite (U-Th)/He thermochronometry, cooling histories will, in general, not be so simple, reflecting the complex tectonic and erosional processes which expose rocks on the Earth's surface. Such rocks may experience varying amounts of time at temperatures where helium is only partially retained. Therefore, it is necessary to develop a more sophisticated approach to interpret apatite (U-Th)/He ages. We have solved the full radiogenic helium production/diffusion equation. This

allows us to investigate the response of helium ages to any prescribed thermal history.

### 3.2 Helium Production and Diffusion: General Overview

Our model of helium production and diffusion in apatite assumes that helium is produced only by the radioactive decay of uniformly distributed uranium and thorium and that helium is lost only by diffusion. We assume a spherical diffusion geometry, consistent with laboratory measurements of helium diffusion from apatite (Wolf et al., 1996). We neglect helium loss by alpha emission (Farley et al., 1996a) because the diffusion domain size is apparently much smaller than the physical grain size (Wolf et al., 1996). Thus, the helium concentration gradients produced by alpha emission over the entire crystal are insignificant for modeling diffusion from the individual domains. The helium age equation is:

$$^4He(t) = 8\,^{238}U(t)\,[\exp(\lambda_{238}t) - 1] + 7\,^{235}U(t)\,[\exp(\lambda_{235}t) - 1] + 6\,^{232}Th(t)\,[\exp(\lambda_{232}t) - 1] \quad (1)$$

where $^4He(t)$ is the amount of helium measured at time t. U(t) and Th(t) are the amounts of uranium and thorium measured at time t, and $\lambda$'s are the decay constants for the parent nuclides. As a consequence of radiogenic production and diffusive loss, the concentration of helium as a function of radial position r within the spherical diffusion domain of radius, a, is:

$$\left[\frac{\partial\, {}^4He_v(r,t)}{\partial t}\right] = D(t)\left[\frac{\partial^2\, {}^4He_v(r,t)}{\partial r^2} + \frac{2}{r}\frac{\partial\, {}^4He_v(r,t)}{\partial r}\right] + 8\,\lambda_{238}{}^{238}U_v(t) + 7\,\lambda_{235}{}^{235}U_v(t) + 6\,\lambda_{232}{}^{232}Th_v(t) \quad (2)$$

where in this equation, $He_v(r,t)$, $U_v(t)$, and $Th_v(t)$ represent the concentrations of helium, uranium, and thorium at time t, per unit volume. D(t) is the time dependent diffusion coefficient. The equation for D(t) is:

$$D(t) = D_0 \exp\left[\frac{-E_a}{R\,T(t)}\right] \quad (3)$$

where $D_0$ is the diffusivity at infinite temperature, $E_a$ is the activation energy, R is the gas constant, and T(t) is an arbitrary thermal history. $E_a$ and $D_0/a^2$ are derived from laboratory incremental outgassing experiments (Wolf et al., 1996). Since the diffusion domain radius, a, is not deconvolved from D(t) in laboratory experiments, equations (2) and (3) are normalized by $a^2$. We assume a present day $^{238}U/^{235}U$ ratio of 137.88 and a Th/U ratio of 1. It makes little difference if we choose a different Th/U ratio because their decay constants and alpha yields are similar. We assume $^4He = 0$ at the surface of the sphere. For most cases, we assume the initial condition $^4He(t=0) = 0$, but we also consider the effects of a finite and uniform initial helium concentration (i.e., $^4He(t=0) > 0$).

### 3.3 Isothermal Diffusion: An Analytical Solution

Initially, we investigate the simplest case of production and diffusion in a crystal, an isothermal history. Isothermal diffusion implies a constant diffusion coefficient, for which there is an analytical solution to equation (2). To simplify, we also assume that the rate of helium production is constant because the parent abundances vary only slightly with time. For instance, in 200 Ma, $\exp(\lambda_{238}t)$-1 differs from $\lambda_{238}t$ by 1.5%, and thorium by even less ($^{235}U$ varies by much more but its contribution is insignificant). Therefore, equation (1) can be rewritten as:

$$^4He(t) = 8\,^{238}U\,\lambda_{238}t + 7\,^{235}U\,\lambda_{235}t + 6\,^{232}Th\,\lambda_{232}t = P\,t \qquad (4)$$

$$P = [8\,\lambda_{238}\,^{238}U + 7\,\lambda_{235}\,^{235}U + 6\,\lambda_{232}\,^{232}Th]$$

where P is the constant production rate. The general solution to equation (2), assuming an initial homogeneously distributed concentration of helium, $^4He^*(t=0)$, is:

$$\frac{^4He}{P} = t' = \frac{a^2}{D}\left[\frac{1}{15} - \sum_{n=1}^{\infty}\frac{6}{\pi^4 n^4}\exp\left(-n^2\pi^2\frac{D}{a^2}t\right)\right] + t''\sum_{n=1}^{\infty}\frac{6}{\pi^2 n^2}\exp\left(-n^2\pi^2\frac{D}{a^2}t\right) \qquad (5)$$

where $t'$ is the helium age, t is the time over which isothermal diffusion and production occur, and $t''$ is the provenance helium age ($t'' = {}^4He^*(t=0)/P$). If we assume no initial helium, then the solution reduces to:

$$\frac{^4He}{P} = t' = \frac{a^2}{D}\left[\frac{1}{15} - \sum_{n=1}^{\infty}\frac{6}{\pi^4 n^4}\exp(-n^2\pi^2\frac{D}{a^2}t)\right] \quad (6)$$

which was previously presented by Trull et al. (1991) based on a mathematical solution for argon diffusion from a sphere (Fechtig and Kalbitzer, 1966).

For equations (5) and (6), the exponential term disappears for large values of $[(D/a^2)t]$, and a steady state between helium production and loss is achieved, with an apparent helium age of $(15D/a^2)^{-1}$. In this instance, helium age no longer increases with time, and chronometric information is no longer recorded. Figure 1a illustrates the transition from complete retention to the steady state between production and diffusion at different temperatures for samples with no initial helium.

For studies involving sedimentary apatites which may have a provenance helium age, it is useful to know how long it takes for apatites to equilibrate their helium concentration to new temperatures. Figure 1b illustrates the transition from a provenance age of 100 Ma to the steady state. For instance, at 100°C the provenance helium has effectively been erased in ~1 Ma, but at 60°C, it takes ~200 Ma.

**Figure 1.**

Evolution of helium age as a function of time for apatites held isothermally at several different temperatures. Unlabeled curves represent 25°C and 35°C. In (a), apatites have no initial helium. In (b), apatites start with a 100 Ma helium age and a uniform helium distribution. The curves demonstrate the steady state helium age and the time required to achieve it as a function of temperature. We used the Durango apatite diffusion coefficients, $E_a$ = 36.2 kcal/mol and log $D_0/a^2$ = 7.7 $sec^{-1}$ (Wolf et al., 1996).

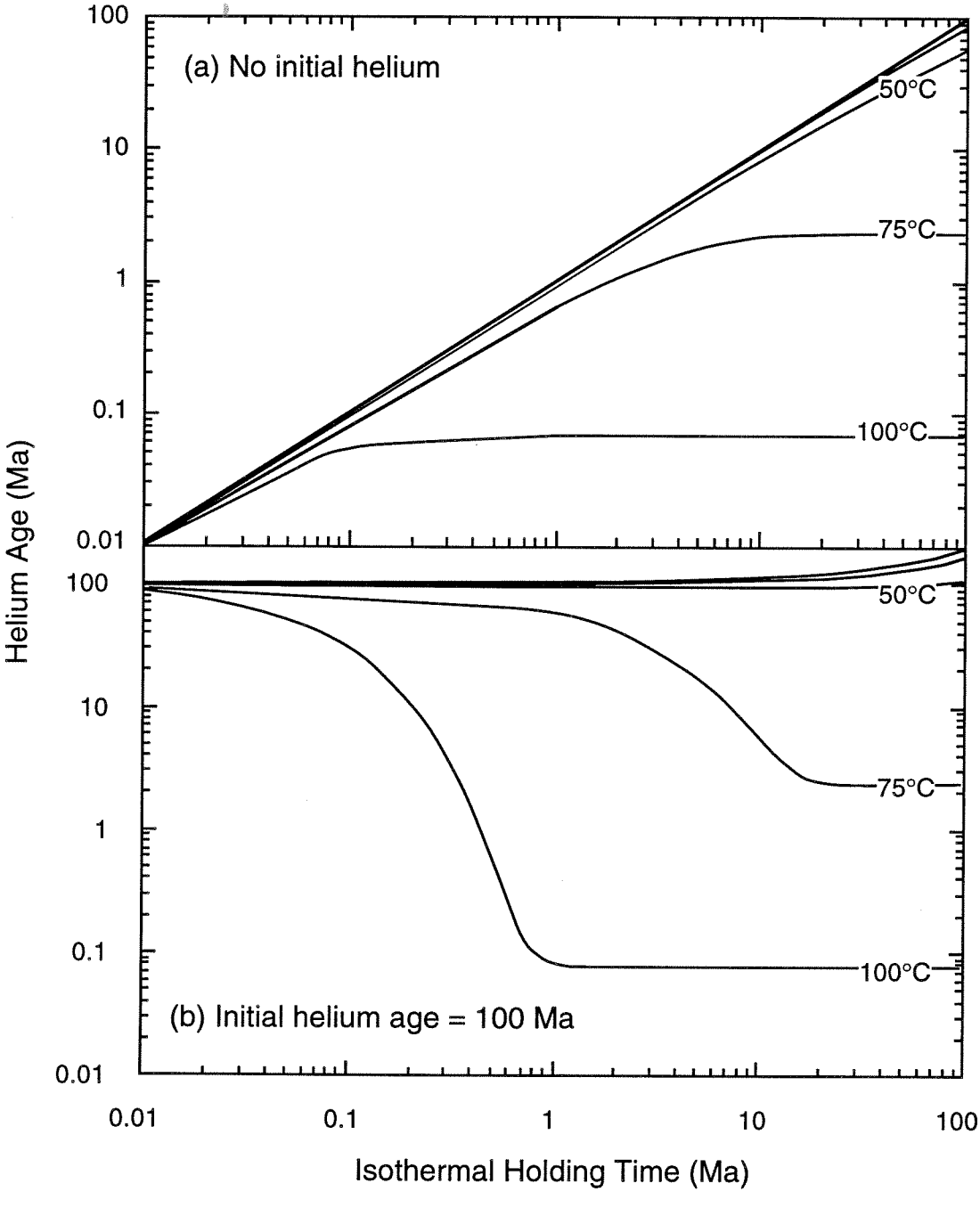
(a) No initial helium
50°C
75°C
100°C
(b) Initial helium age = 100 Ma
50°C
75°C
100°C
Helium Age (Ma)
Isothermal Holding Time (Ma)
100
10
1
0.1
0.01
0.01
0.1
1
10
100

As time increases, the higher order terms in n become less significant. Therefore, the characteristic time constant for the approach to equilibrium, t*, is given by the longest time constant, n = 1, and $t^* = (a^2/D)/\pi^2$. The characteristic time constant decreases as temperature increases (Figure 2). In 5t*, the approach to equilibrium is largely complete. At the ambient temperatures for most of the surface of the Earth, ~25°C, retention is nearly quantitative, and a steady state is not achieved over geologic time. By using 5t* as the time necessary to achieve the steady state, we can approximate the time necessary to effectively eradicate provenance helium in sedimentary apatites in a static thermal environment.

Figure 1 illustrates how helium ages change with time at different temperatures, but does not clearly demonstrate how helium ages differ at various temperatures for a constant holding time t. Such a view would be useful for considering helium age variations with depth in the crust. If we illustrate a slice in time at, say, 50 Ma from Figure 1, for various temperatures, we observe a zone of temperatures where helium age changes very rapidly with temperature (Figure 3). We refer to this zone as the helium partial retention zone, HePRZ, and use it as an analog to the fission track partial annealing zone, FTPAZ (Wagner et al., 1989; Fitzgerald and Gleadow, 1990). We operationally define the HePRZ to be the range of temperatures where helium age falls from 90% to 10% of the holding time t (i.e., $0.1 \leq t'/t \leq 0.9$). Figure 3 illustrates how sensitive helium age is to temperature in the HePRZ. For a holding time of 50 Ma, the HePRZ resides between ~40°C and ~70°C. In the

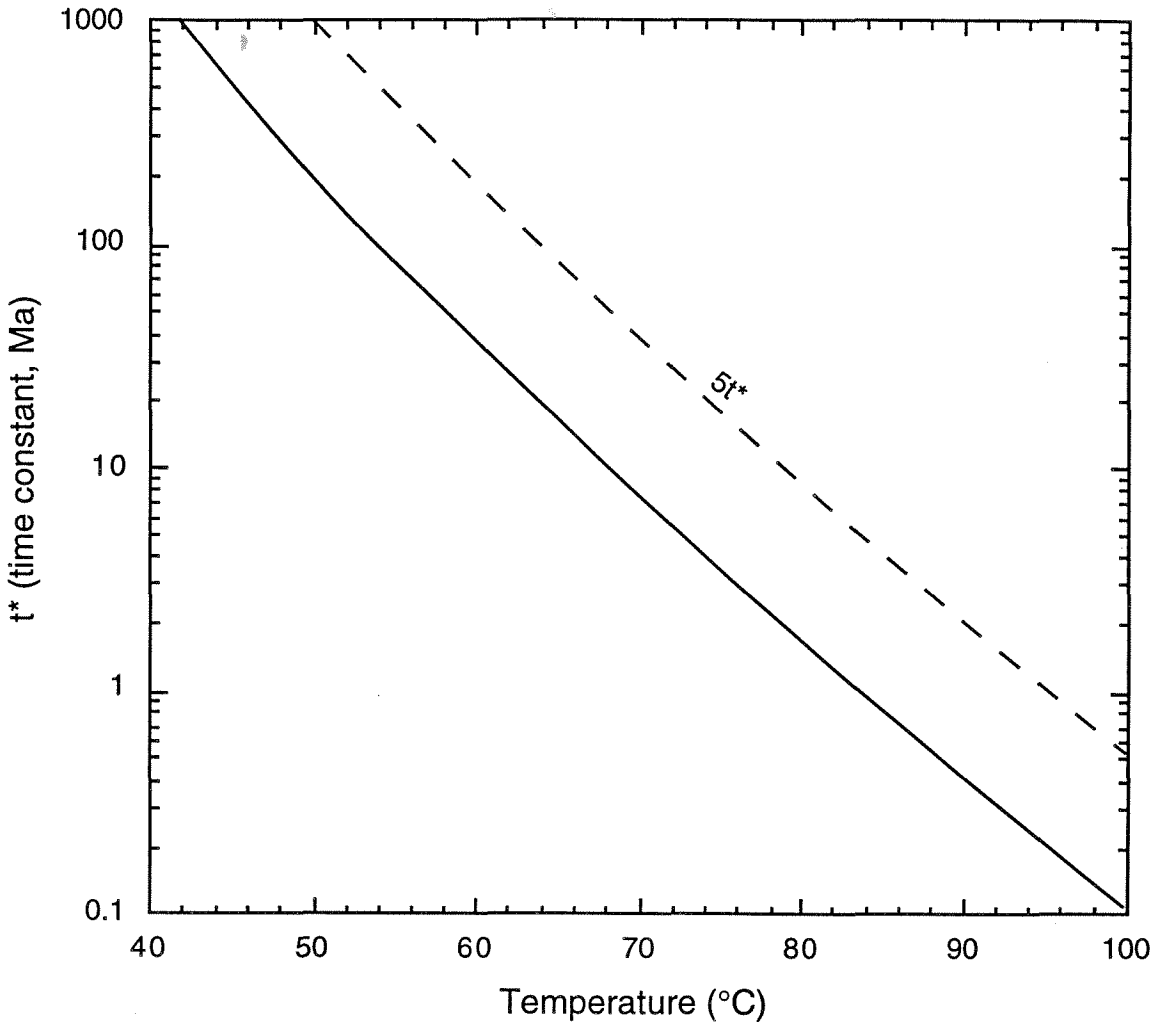


**Figure 2.**

Characteristic time constant, t*, for isothermal helium diffusion (solid line). The approximate time necessary to reach the steady state as a function of temperature in an isothermal setting is ~5t* (dashed line). This plot illustrates how fast helium ages equilibrate to a new thermal environment. Calculations are based on Durango apatite diffusion coefficients, $E_a$ = 36.2 kcal/mol and log $D_0/a^2$ = 7.7 $sec^{-1}$ (Wolf et al., 1996).

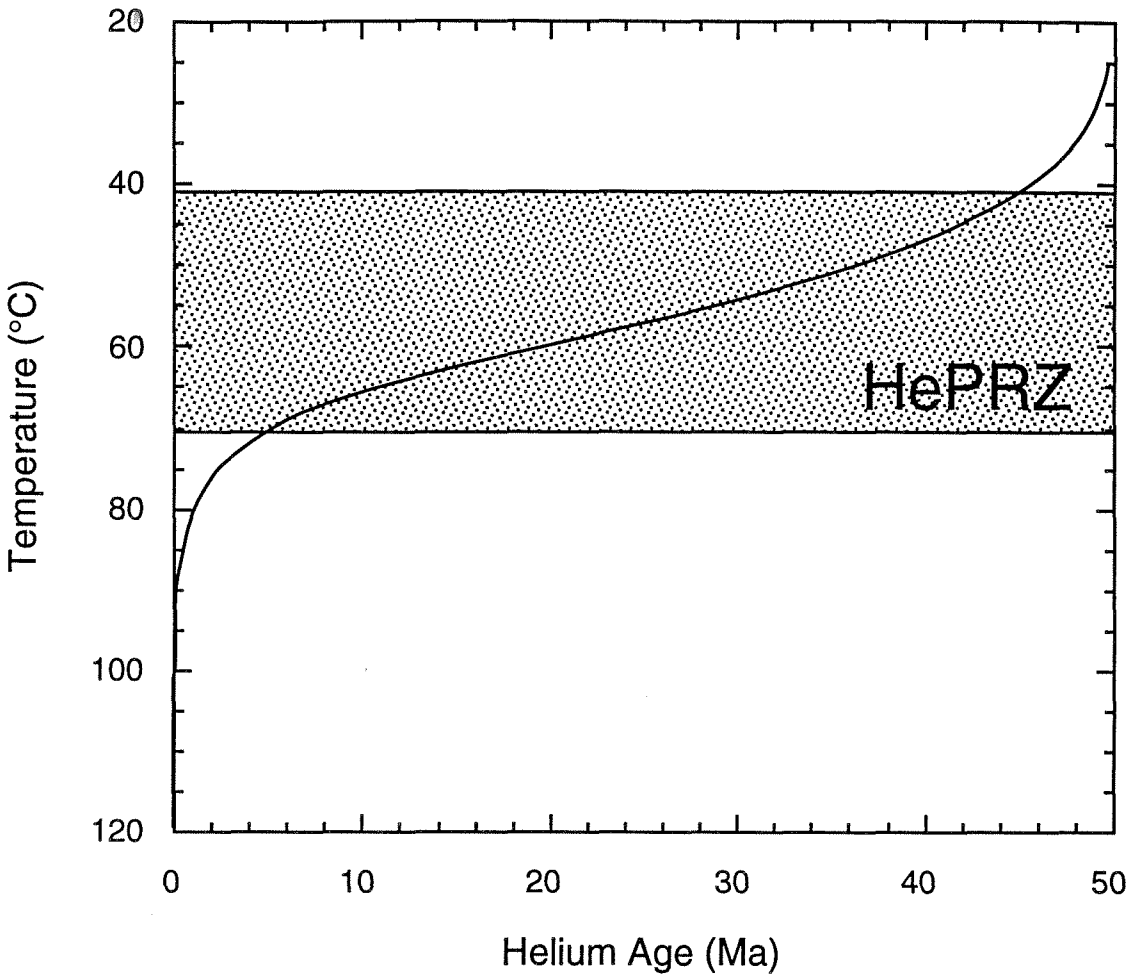


**Figure 3.**

Model calculation of helium ages as a function of temperature held isothermally at different temperatures for 50 million years. This is analogous to a slice in Figure 1a taken at a holding time of 50 million years. Shaded region encompasses the helium partial retention zone. Model calculations assume no initial helium and use Durango apatite diffusion coefficients, $E_a$ = 36.2 kcal/mol and log $D_0/a^2$ = 7.7 $sec^{-1}$ (Wolf et al., 1996).

most sensitive region of the HePRZ, helium age differs by almost 10% for a difference in temperature of <3°C.

One consequence of defining the HePRZ in this way is that the temperature range of the HePRZ is holding time dependent. This effect can be seen most clearly when the fractional helium age ($t'/t$) is plotted against holding time (figure 4). At sufficiently low temperatures, helium is quantitatively retained, so $t'/t = 1$ and plots horizontally in Figure 4. However, at higher temperatures, helium is only partially retained, so $t'$ does not increase as fast as t, and the fractional helium age decreases with holding time. The 10% and 90% limits we have chosen to define the HePRZ are indicated in a shaded region in Figure 4.

Figure 5 shows the change in the range of temperatures for the HePRZ with time. The contours in Figure 5 represent the fractional helium age, $t'/t$. The shaded area represents the HePRZ as defined above. Whereas the HePRZ lies between ~40°C and ~70°C for a holding time of 50 Ma, it lies between ~50°C and ~83°C for a holding time of 10 Ma and between ~38°C and ~67°C for a holding time of 100 Ma. Because the range of temperatures which define the HePRZ changes with the holding time, we must describe the HePRZ in terms of a finite holding time. On the right axis of Figure 5, depth is plotted for a 20°C/km geothermal gradient. This indicates that the HePRZ resides at ~2±1 km over geologic time, and suggests that apatite helium thermochronometry records processes occurring in this depth range.

To determine the sensitivity of the HePRZ to differences in diffusivity characteristics of various apatites, we used the range of diffusion coefficients

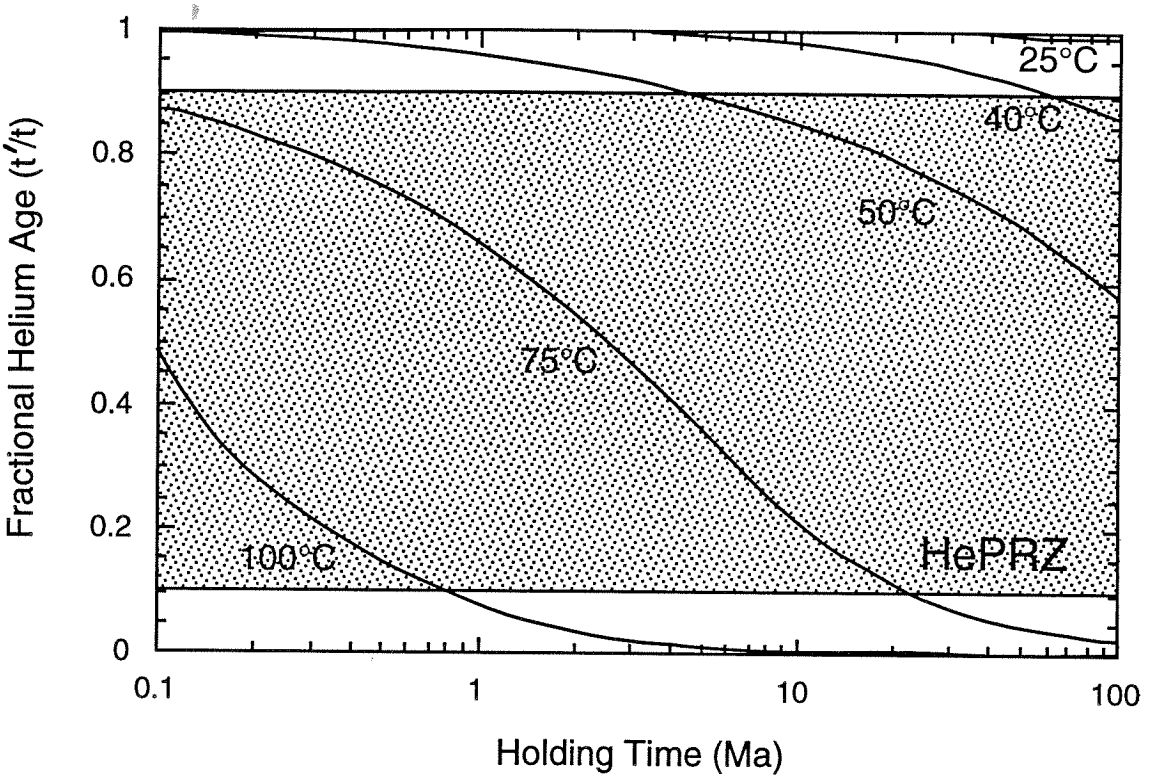


**Figure 4.**

Fractional helium age ($t'/t$) as a function of holding time. Isothermal contours assume no initial helium. The HePRZ is shown in the shaded region. A consequence of the definition of the HePRZ is that its temperature range is time dependent. Model calculations assume no initial helium and use Durango apatite diffusion coefficients, $E_a$ = 36.2 kcal/mol and log $D_0/a^2$ = 7.7 $sec^{-1}$ (Wolf et al., 1996).

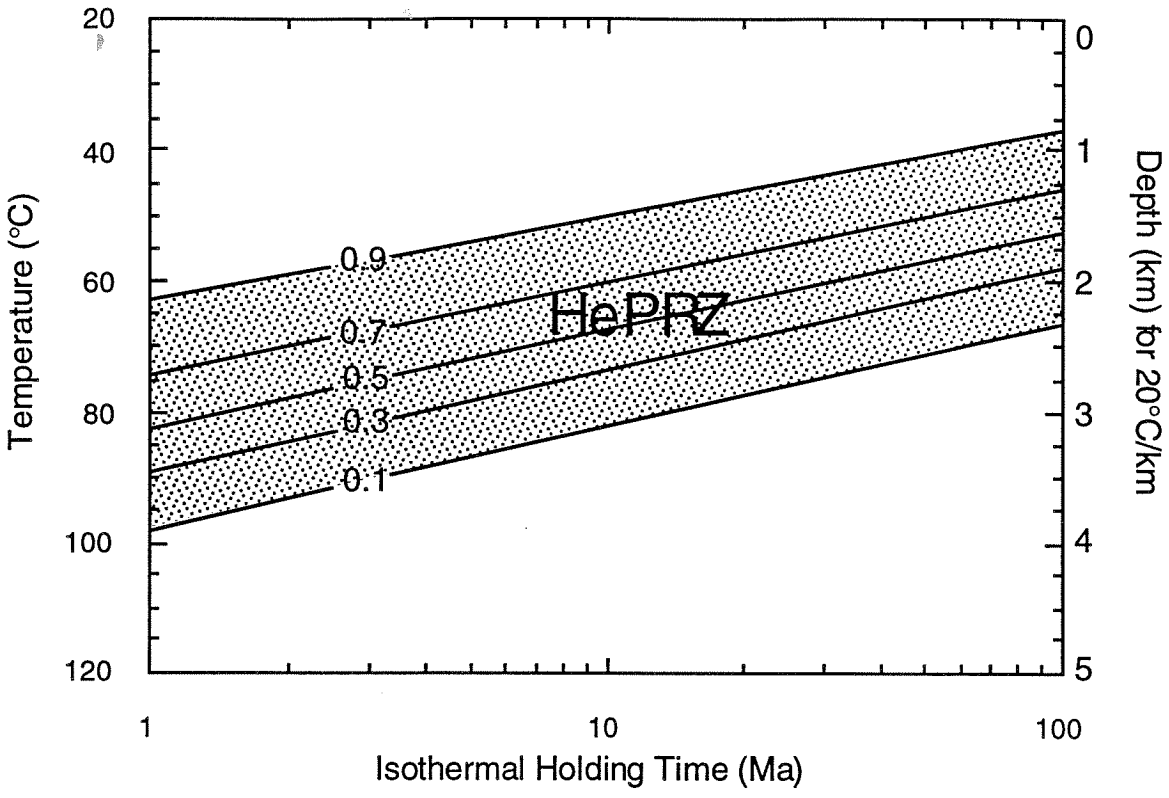


**Figure 5.**

The helium partial retention zone (operationally defined as the zone in which the helium ages range from 10% to 90% of the holding time) for isothermal apatites as a function of holding time. Defined in this way, the HePRZ is ~35°C wide (~2±1 km in the crust under typical geothermal gradients), and its exact position depends on the isothermal holding time. Contours are for t'/t. Calculations are based on Durango apatite diffusion coefficients, $E_a$ = 36.2 kcal/mol and log $D_0/a^2$ = 7.7 $sec^{-1}$ (Wolf et al., 1996).

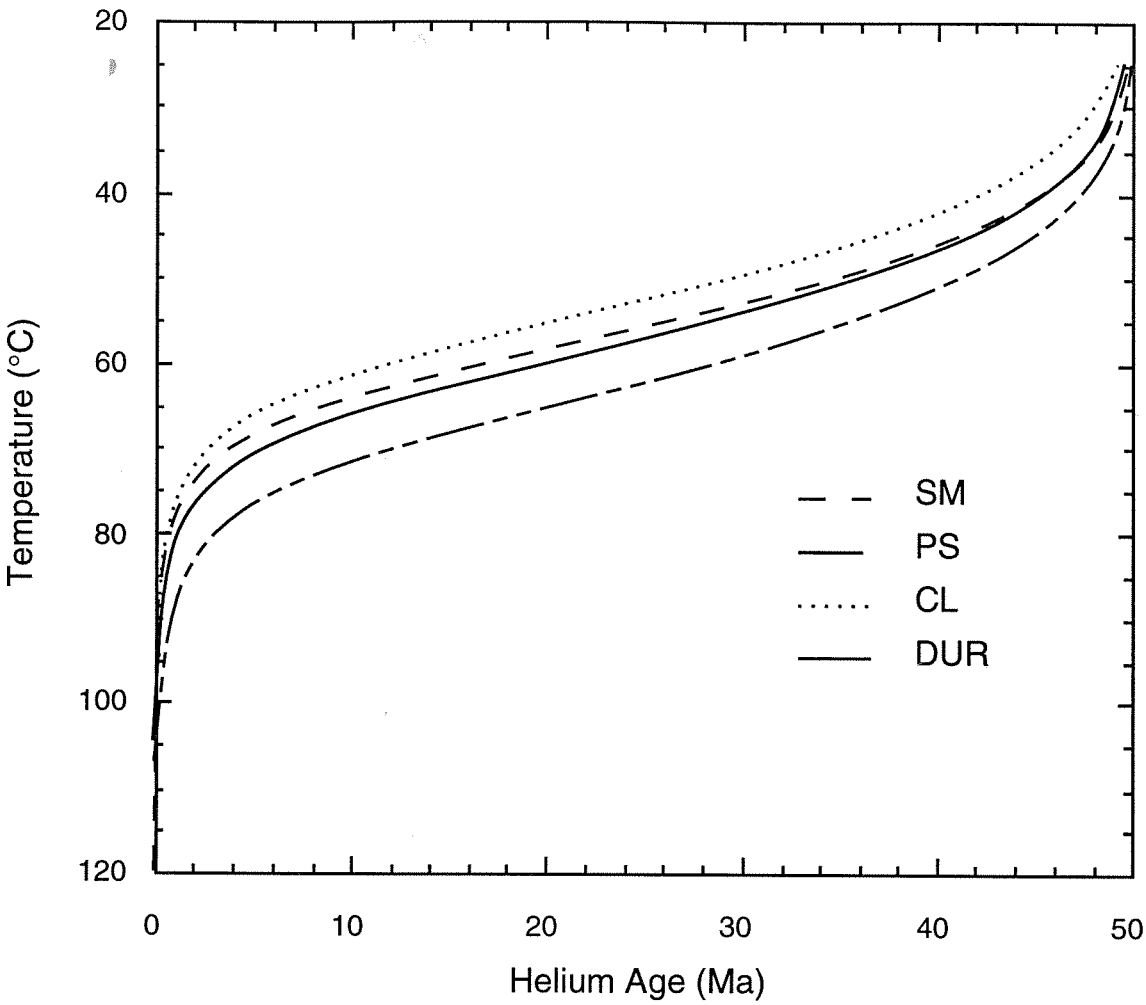


**Figure 6.**

Plot of the HePRZ for the measured range of diffusion parameters (SM = San Marcos gabbro; CL = Camp Lackey tonalite; PS = Palm Springs mylonitic tonalite; Durango pyrothermal apatite; Wolf et al., 1996). Within the HePRZ helium ages are sensitive to the measured range of diffusion parameters, further emphasizing the importance of high precision incremental outgasing experiments.

measured by Wolf et al. (1996) and calculated the HePRZ as in Figure 3 (Figure 6). These diffusivity experiments were conducted on apatites which vary with respect to chemical composition and grain size and yield a narrow range of closure temperatures, 75±5°C (assuming a cooling rate of 10°C/Ma). Despite the nearly identical values for their closure temperature, the relative position of the HePRZ curves for each of the four diffusion coefficients are different. At ~52°C, the difference in helium age between samples is as much as ~20 Ma. There is no correlation between the observed differences in the calculated helium partial retention zones and the chemical or physical make-up of the apatites. Because helium age is quite sensitive to differences in diffusion parameters within the HePRZ, some critical applications of (U-Th)/He thermochronometry may require especially high precision diffusion coefficient measurements.

### 3.4 Complex Thermal Histories: A Numerical Solution

When the temperature is not constant, the diffusion coefficient varies with time, and the diffusion equation no longer has a general analytical solution. In this case, it is necessary to use a numerical solution to equation (2). We used the Crank-Nicolson method to solve this equation for arbitrary thermal histories (Crank and Nicolson, 1947; Crank, 1975).

The solution to equation (2) is the concentration of helium atoms per unit volume at any time t. By inserting the integrated helium concentration into equation (1), we find the sensitivity of helium age to thermal history and

diffusivity. To test the sensitivity of helium age to thermal history, we vary T(t) for only one set of diffusion parameters, $E_a$ and $D_0/a^2$. To determine the sensitivity of helium age to diffusion parameters, we vary the parameters for only one thermal history.

To relate the helium partial retention zone and the fission track partial annealing zone, we compared model helium ages to model fission track ages (Green et al., 1989) for the Otway Basin, a sedimentary basin off the coast of Australia (Figure 7). We chose the Otway Basin because it is one of the best known examples of the fission track partial annealing zone in a natural setting, and it is also a good natural approximation to an isothermal setting. Furthermore, Green et al. (1989) modeled apatite fission track ages as a function of temperature based on laboratory annealing experiments and demonstrated reasonable agreement with measured fission track ages (Gleadow et al., 1981, 1983) from several boreholes in the Otway Basin. Because the Otway Basin has not had an isothermal history, it was necessary to model helium ages using the numerical solution to equation (2). The thermal history for the basin is derived from geologic constraints which suggest that the volcanogenic sediments in the basin were deposited soon after crystallization in the early Cretaceous (~120 Ma). The basin subsided slowly as a function of continuous deposition until the Miocene when it reached its present depth of burial (thermal history from reference well Port Cambell-4, Green et al., 1989). Therefore, from Cretaceous to Miocene time, the rocks were slowly heated (~0.3°C/Ma) during subsidence. In addition to plotting the HePRZ modeled for

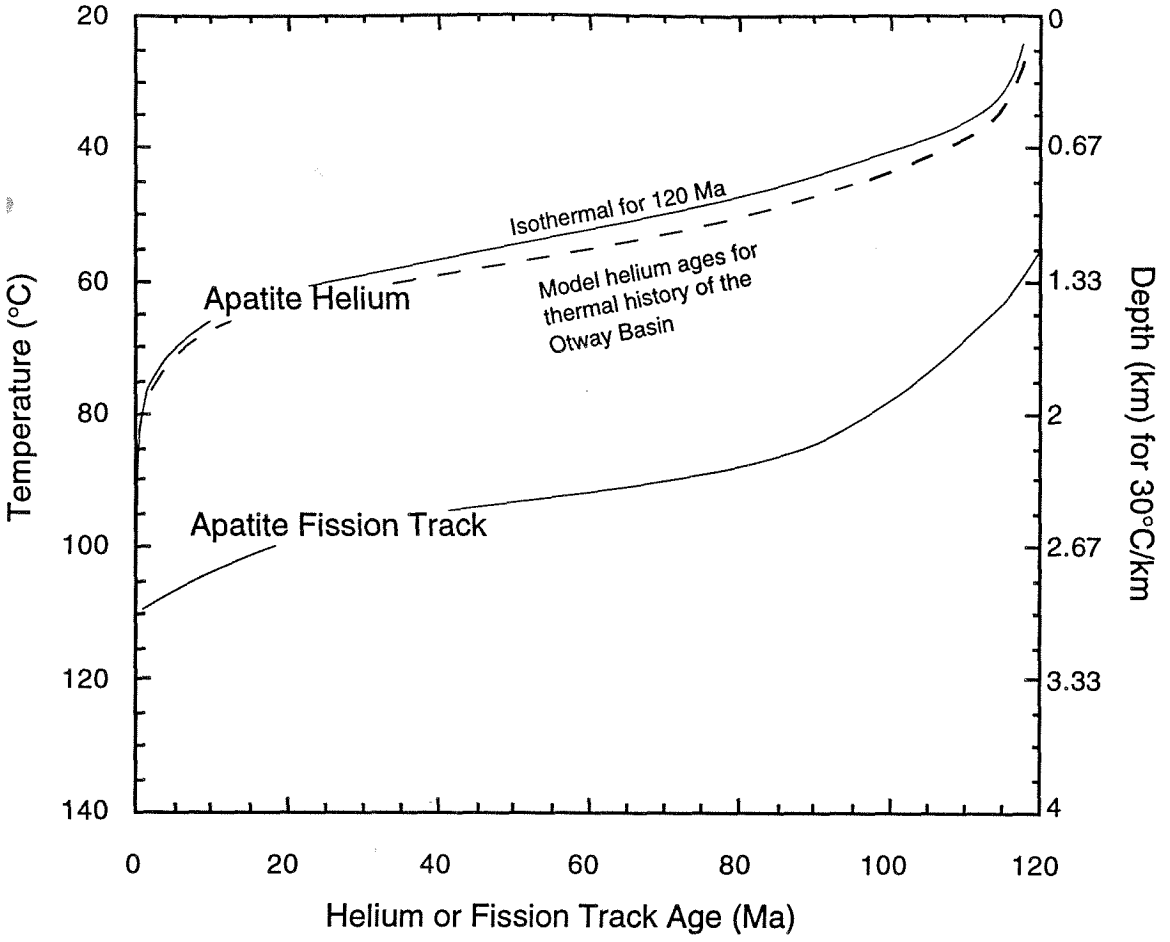


**Figure 7.**

Comparison of our model of the HePRZ with a model of the FTPAZ (Green et al., 1989) for apatites in the Otway Basin. We model the HePRZ for two separate histories. The first is isothermal for 120 Ma (solid line). The second is calculated for the thermal history of the Otway Basin (reference well, Port Cambell-4, Green et al., 1989) (dashed line). The HePRZ calculated for both thermal histories are similar because there is only a subtle difference between the static thermal history and the thermal history of the Otway Basin proposed by Green et al. (1989). There is no overlap between the HePRZ and the FTPAZ and they are separated by ~35°C at their centers. Calculations are based on Durango apatite diffusion coefficients, $E_a$ = 36.2 kcal/mol and log $D_0/a^2$ = 7.7 $sec^{-1}$ (Wolf et al., 1996).

the Otway Basin thermal history, we also depict the HePRZ modeled for a 120 Ma isothermal history (Figure 7). The subtle difference between the two curves reflects the fact that the heating of Otway Basin sediments during subsidence was extremely slow and was followed by an isothermal period since the Miocene.

The model HePRZ in the Otway Basin resides at between ~40°C and ~65°C. If we describe the model fission track partial annealing zone in an analogous fashion to the HePRZ, it resides between ~70°C and ~105°C. Thus, the HePRZ and the FTPAZ do not overlap. The helium ages decline to 0 Ma just as the fission track ages begin to decrease (Figure 7). At 50% retention, the HePRZ is separated from the FTPAZ by ~35°C. In typical geothermal gradients of ~15-35°C/km, the model predicts that the HePRZ should be centered ~2±1 km shallower than the FTPAZ. Thus, we predict that helium ages will always be less than or equal to fission track ages. In cases where rocks have been quickly cooled, such as volcanic samples or samples which have experienced rapid tectonic exhumation, it is possible to have identical helium and fission track ages. Because there is no overlap between the HePRZ and the FTPAZ, we predict that in some cases (situations including as much as ~2 km of exhumation), helium ages could be almost completely reset in samples which do not exhibit the effects of fission track age reduction.

To determine the sensitivity of helium ages to more dynamic thermal histories, we have chosen three illustrative cases which span a broad range of typical geologic histories, and modeled the change in helium age with time

**Figure 8.**

A model for the change in helium age with time as a function of thermal history for three plausible goelogic histories. Each of the thermal histories begins at 100°C and ends at 20°C, but the helium ages at the end of the holding time vary by more than a factor of 2, demonstrating the sensitivity of the apatite (U-Th)/He method to thermal histories below ~100°C. Calculations are based on Durango apatite diffusion coefficients, $E_a$ = 36.2 kcal/mol and log $D_0/a^2$ = 7.7 $sec^{-1}$ (Wolf et al., 1996).

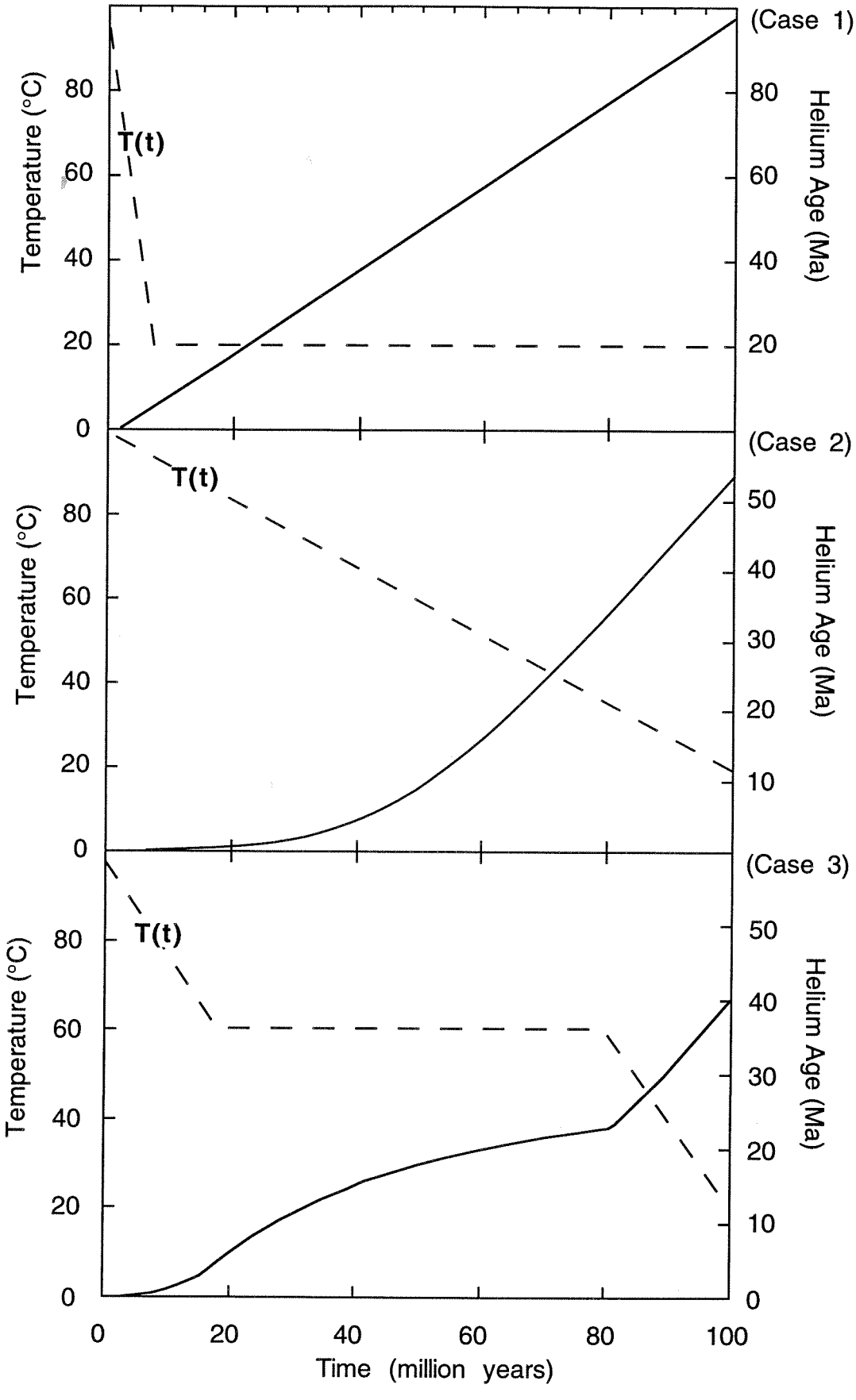
(Case 1)
Temperature (°C)
Helium Age (Ma)
T(t)
0
20
40
60
80
(Case 2)
Temperature (°C)
Helium Age (Ma)
T(t)
0
10
20
30
40
50
(Case 3)
Temperature (°C)
Helium Age (Ma)
T(t)
0
20
40
60
80
100
Time (million years)

(Figure 8). We arbitrarily select a 100 Ma duration simply to illustrate how helium ages change over long timescales. Case 1 is fast cooling followed by an isothermal period, indicative of rapid exhumation followed by thermal quiescence. This is what we might expect from a metamorphic core complex or a pluton which was brought to the surface 90 million years ago and has sat essentially in the same position in a constant geothermal gradient since then. Case 2 is very slow monotonic cooling that might be associated with typical continental erosion rates. This thermal history is equivalent to scenarios covered by Dodson's (1973) formulation of the closure temperature. The thermal history is calculated assuming 0.04 mm/yr of erosional removal in a 20°C/km geothermal gradient which corresponds to a cooling rate of 0.8°C/Ma. This would give a closure temperature of 60°C using Dodson's (1973) formulation. Case 3 involves cooling followed by an isothermal period at 60°C which is then followed by cooling. Thermal histories like case 3 involving two periods of cooling separated by a long isothermal period have often been proposed from fission-track-length models (Corrigan, 1991; Lutz and Omar, 1991).

Helium ages corresponding to the three thermal histories are plotted as a function of time in Figure 8. Even though the histories start at 100°C and end 100 million years later at 20°C in each case, the resulting helium ages differ by more than a factor of 2, demonstrating the sensitivity of the system to cooling histories below 100°C. Cases 1 and 2 from Figure 8 involve cooling which is adequately described by Dodson's (1973) formulation. The last case involves a

more complex thermal history where the sample spends most of its history in the HePRZ (at 60°C). In this case, the closure temperature inadequately characterizes the helium age. Case 3 also demonstrates the extreme sensitivity of helium ages to temperature in the HePRZ. If the isothermal period in case three occurs at 58°C instead of 60°C, the sample retains 12% more helium.

The rate of change of helium age with depth in a static setting is shown in Figure 3. However, if we vary the thermal history, the helium age profile with depth changes considerably. We calculated how helium age varies with depth using the three thermal histories from Figure 8 plus an additional thermal history (Figure 9). The additional thermal history involves cooling which may come from the rapid erosion of a steep mountain and is presented to compare how helium ages from a vertical profile change as a function of erosion rate. The thermal history is calculated assuming 0.1 mm/yr of erosional removal in a 20°C/km geothermal gradient which corresponds to a cooling rate of 2°C/Ma (this yields a closure temperature of 64°C). We selected this additional thermal history because it demonstrates how helium age changes with depth if we increase the erosion rate from case 2 in Figure 8. For clarity the thermal histories have all been replotted, and the sample at 0 km depth in each case relates to the thermal history shown in Figure 9a. Each of the curves assumes a geothermal gradient of 20°C/km.

The quickly cooled sample which endures 90 million years of thermal quiescence looks like the isothermal HePRZ shown in Figure 3. The remaining thermal histories yield distinctly different curves which exhibit simple monotonic

**Figure 9.**

(a) A plot of the thermal histories described in Figure 8 plus an additional thermal history calculated for an erosion rate of 0.1 mm/yr in a 20°C/km geothermal gradient. Lines correspond to those in (b). (b) Helium age/depth profile at the end of 100 million years for each of the thermal histories described in Figure 8. The samples at 0 km correspond to the thermal histories shown above. Forward modelling of this type may help refine the number of plausible thermal histories for helium ages measured on vertical sampling profiles.

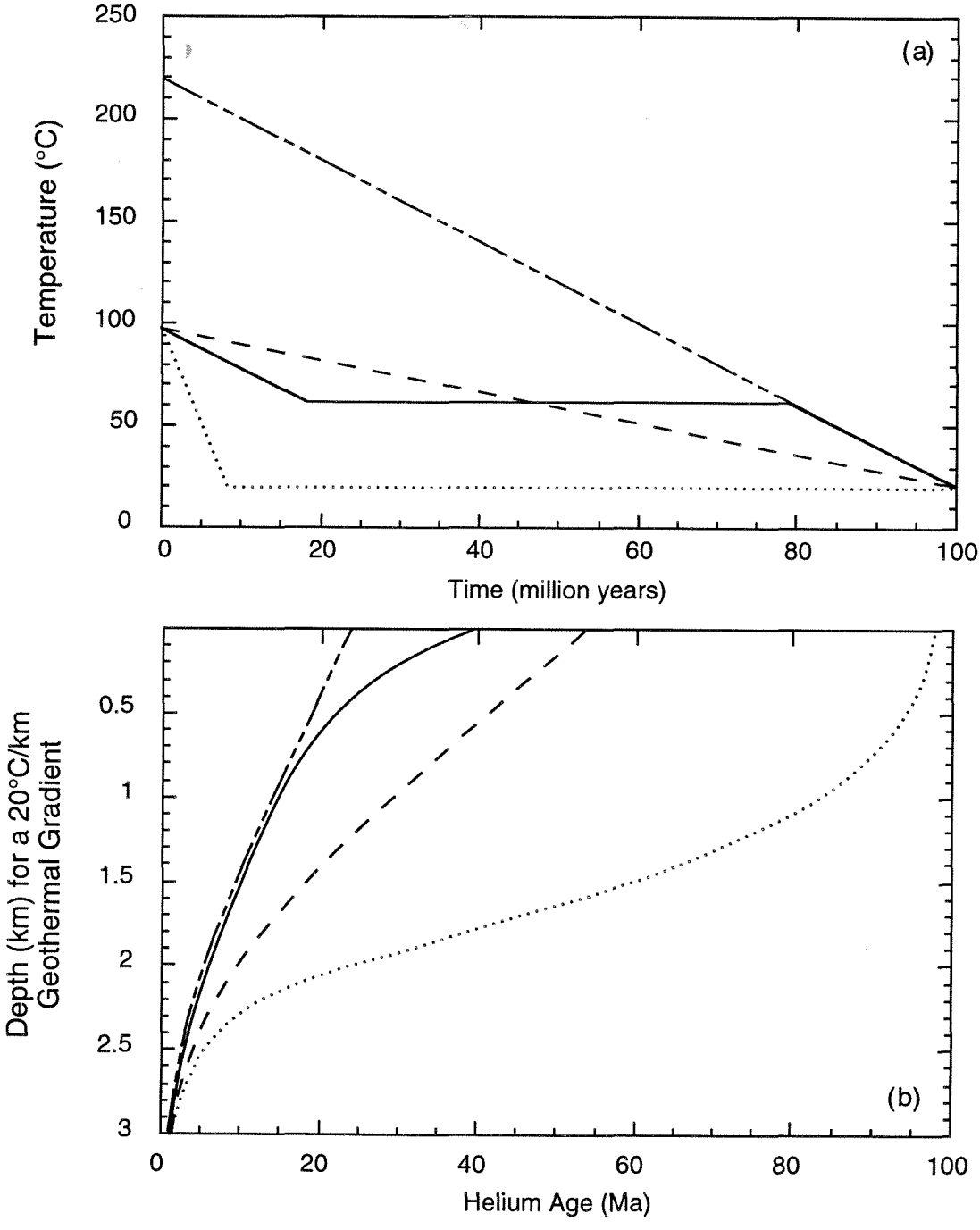
250
200
150
100
50
0
Temperature (°C)
(a)
0
20
40
60
80
100
Time (million years)
0.5
1
1.5
2
2.5
3
Depth (km) for a 20°C/km
Geothermal Gradient
(b)
0
20
40
60
80
100
Helium Age (Ma)

decreases in helium age with sample depth similar to the correlations observed in the San Jacinto and Sierra Nevada Mountains, California (Wolf et al., 1997; House et al., submitted). Comparison of forward models like the ones in Figure 9 to observed variations in helium age with sample elevation enable us to constrain allowable thermal histories. The two erosional histories yield distinctly different depth profiles indicating that helium ages may be useful for determining the rate of erosional exhumation of mountain blocks.

The sensitivity of helium ages to thermal history may also allow us to refine fission track length derived cooling models (Farley et al., 1996b), which yield a family of possible thermal histories from the fission track length distribution in a single sample (Corrigan, 1991; Lutz and Omar, 1991). Because helium ages are sensitive to the lowest temperatures accessible by the fission track method, fission track and helium age measurements can be used as complementary data sets. An example of the family of thermal histories which might be generated by a track-length-derived thermal model is shown in Figure 10a (Lutz and Omar, 1991). Although all of these thermal histories may be allowed from the track lengths, each one yields a different model helium age (Figure 10b). Thermal histories which yield model helium ages that do not agree with measured ages may be rejected, provided the two systems are properly intercalibrated.

One complication to such use is the sensitivity of helium ages within the HePRZ to the measured range of diffusion parameters (Figure 7). To determine how the sensitivity of helium ages to the measured range of diffusion

**Figure 10.**

(a) Track length derived cooling models yield a family of possible cooling paths for a single sample. This depicts a family of synthetic thermal histories which might be observed in a fission track length derived cooling model (Corrigan, 1991; Lutz and Omar, 1991). We have taken a number of thermal histories which lie inside the realm of possible histories allowed by track lengths in one model from Lutz and Omar (1991). (b) Plots of the change in helium age with time for the cooling models shown above. At the end, the spread of helium ages is nearly 100% and illustrates how cooling histories which are allowed by the fission track data can be refined with helium ages. Thermal histories which yield model helium ages that do not agree with measured helium ages can potentially be rejected.

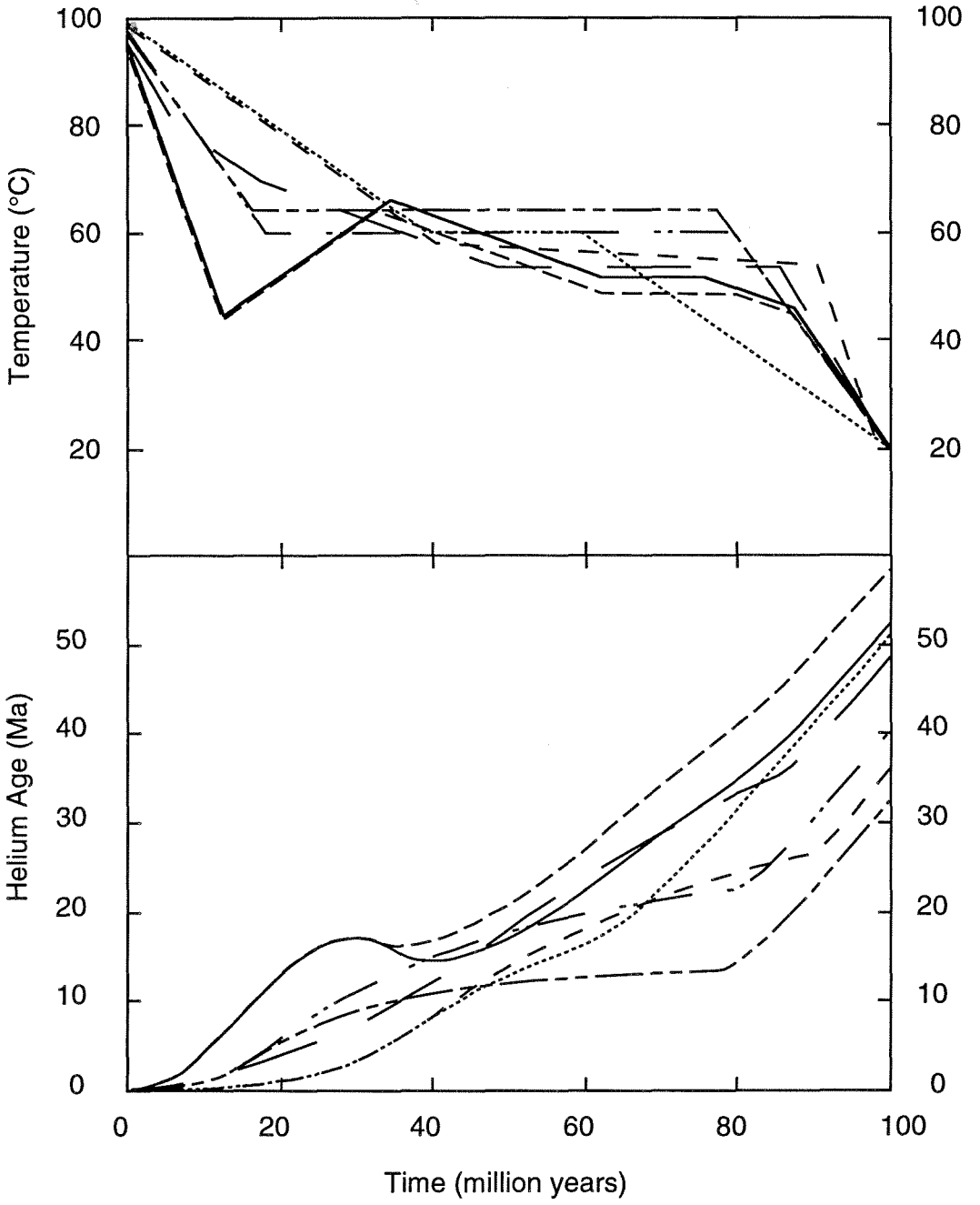
Temperature (°C)
100
80
60
40
20
Helium Age (Ma)
50
40
30
20
10
0
0
20
40
60
80
100
Time (million years)

parameters is manifested in different thermal histories, we modeled case 3 from Figure 8 for the measured range of diffusion parameters as a worst scenario. Because samples spend 60 million years in the HePRZ, this is a worst case scenario for the effect of variations in diffusivity on helium age. At the end of 100 million years, the ages for each of the diffusion coefficients differ by as much as a factor of 2 (Figure 11). Therefore, comparisons of forward models to helium ages measured on uplifted mountain blocks and the refinement of fission track length derived thermal models may require a very accurate knowledge of the diffusion coefficients of actual samples used if the thermal histories suggest long durations in the HePRZ.

### 3.5 The Effect of Ambient Temperature Variations on Helium Ages

It has been proposed that forest fires and even ambient temperature variations can cause the diffusive loss of cosmogenic helium from some mineral phases (Bierman and Gillespie, 1991; Trull et al., 1995). To assess whether apatite is susceptible to these ambient effects, we modeled the diffusive loss that occurs as a function of depth in a rock as a function of ambient conditions. We start by modeling the effects of forest fires on helium diffusion from apatite. Following previous work, we assume a fire heats a rock for 10 minutes, and the surface of the rock reaches a peak temperature of 600°C (Bierman and Gillespie, 1991). Assuming a plane source of heat and heat flow in one direction, we can calculate temperature as a function of depth in the rock (Carslaw and Jaegar, 1959). We assume a thermal diffusivity typical of granite

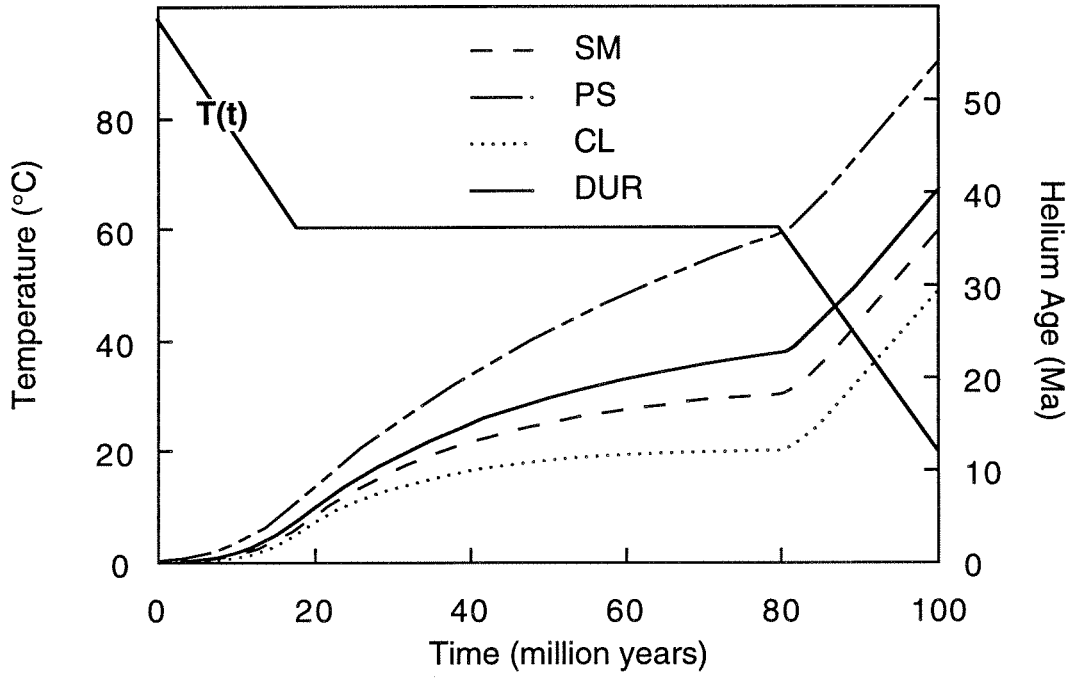


**Figure 11.**

Plot of the change in helium age for the case 3 thermal history (Figure 8) using the measured range of diffusion parameters (SM = San Marcos gabbro; CL = Camp Lackey tonalite; PS = Palm Springs mylonitic tonalite; Durango pyrothermal apatite; Wolf et al., 1996). Samples which spend long durations in the HePRZ are quite sensitive to the measured range of diffusion parameters as also illustrated in Figure 6. This thermal history is a worst case because it requires that samples spend 80 million years in the HePRZ.

of 0.01 $cm^2/s$ (Germak et al., 1982). After 10 minutes the fire stops heating the rock, and the temperature profile with depth in the rock is at a maximum (Figure 12). For ease of calculation, we assume the extreme case of the rock enduring the maximum temperature profile for the entire 10 minute period, and we calculate how the helium age changes as a function of depth in the rock based on this thermal profile (Figure 12). The region affected by the fire is only ~1.5 cm thick. Since granite tends to spall after a fire exposing fresh surfaces, and sampling usually involves chipping away the outer weathered rind, it is unlikely that apatite helium ages will be modified by the effects of a fire. Since fires might burn for more than 10 minutes, we also modeled a fire which heats the rock for 1 hour (Figure 12). In 1 hour only the outer ~4.5 cm is affected by the fire; even in this extreme case, we do not expect apatites to be significantly affected by fire.

To assess whether variations in Earth surface temperatures can affect apatite helium ages, we chose to model the effects of ambient temperatures measured in Death Valley, California (Climatological Data, 1995). The case of Death Valley represents a worst case scenario because it routinely records some of the highest air temperatures on the Earth. To model these effects, we ignore the direct solar heating of the rock surface and focus only on the ambient temperature. Figure 13 shows the diurnal variation in temperature measured for each day in Death Valley in 1995. A model which computes the helium age as it changes over the course of a day is impractical, so we start by analyzing more extreme cases.

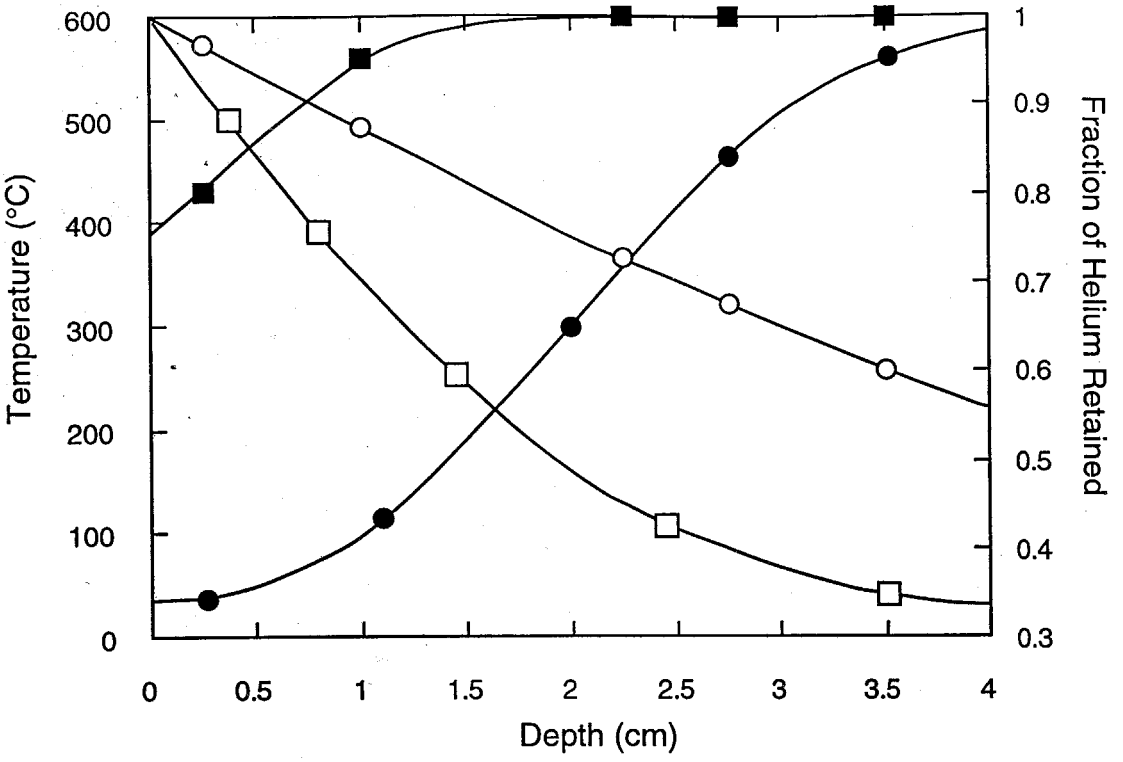


**Figure 12.**

Plot of the effect of two forest fires which heat a block of granite to 600°C for different durations. Boxes represent a forest fire which heats the rock for 10 minutes, and circles represent a forest fire which heats the rock for 1 hour. Filled symbols show the fractional helium age as a function of depth in the rock. Open symbols represent temperature with depth in the rock. Model calculations use Durango apatite diffusion data (Wolf et al., 1996).

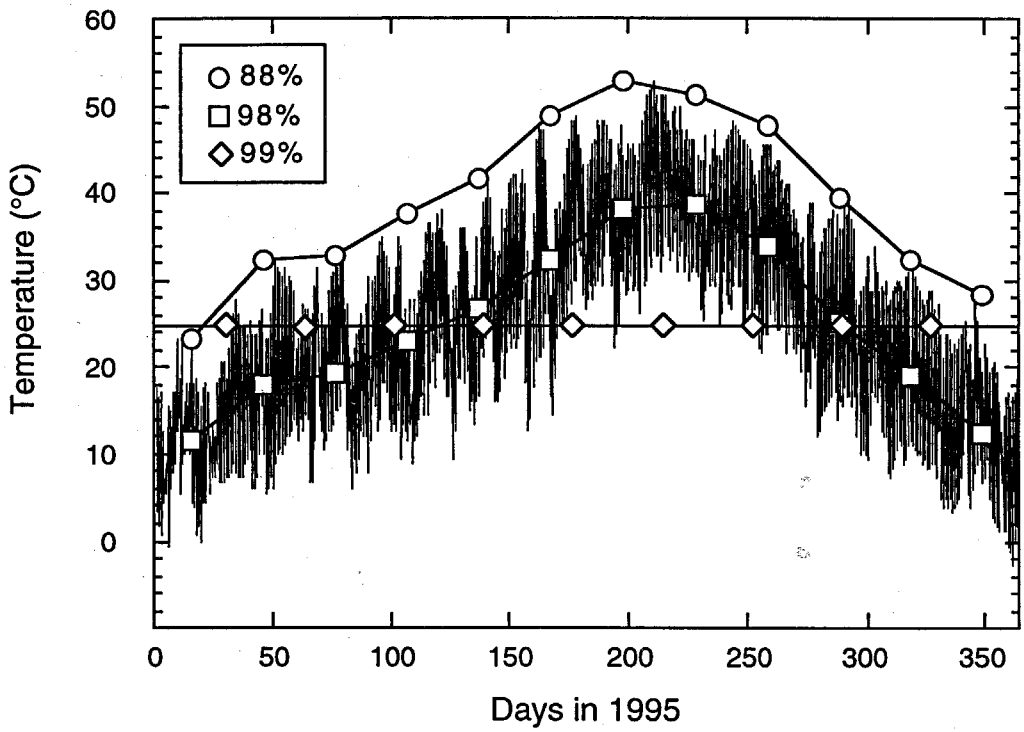


**Figure 13.**

Plot of the diurnal variation in temperature for Death Valley in 1995. Open boxes are the average value of the daily temperature variations and the open circles are the maximum temperatures measured for each month. Diamonds represent the mean annual temperature. Box in the upper left corner represents the fraction of helium retained in 50 million years. Model calculations assume no initial helium and use Durango apatite diffusion coefficients, $E_a$ = 36.2 kcal/mol and log $D_0/a^2$ = 7.7 $sec^{-1}$ (Wolf et al., 1996).

The peak temperature measured in 1995 was ~50°C. If a sample with no initial helium is held at 50°C for 50 million years, for example, the helium age reaches only 72% of the true age. This sets an upper limit for helium loss at ambient temperatures. A more realistic limit is obtained from the maximum temperature envelope over the course of a year (open circles in Figure 13). For ease of calculation, we used the highest temperature measured in each month. With this temperature history, a sample retains 88% of its helium over 50 million years. This maximum envelope is again an overestimate because only the samples at the surface of the rock endure the maximum daily temperature variation. The temperature difference between the daily high and low, $\Delta T$, is damped exponentially with depth in the rock (Carslaw and Jaegar, 1959). The equation for the decrease in $\Delta T$ with depth, z, is: $\Delta T = \exp(-z(\omega/2\kappa)^{1/2})$, where $\kappa$ is the thermal diffusivity and $2\pi/\omega$ is the period of the oscillation. For example, the average $\Delta T$ in Death Valley is ~40°C, and by 30 cm depth, a sample effectively endures only the mean temperature for each day. For ease of calculation, we use the average temperature measured each month to approximate the average daily temperature endured by a sample at 30 cm depth (open boxes in Figure 13). In this scenario, the sample retains 98% of its helium over 50 million years, and the helium age is essentially unaffected by the ambient temperatures. Finally, the annual cycle is damped out at ~10 m depth. Thus, at ~10 m depth, a sample endures the mean annual temperature of ~25°C. In this case, samples retain 99% of the helium in 50 million years.

We have shown that in the worst case, a sample retains 72% of its helium in 50 million years, and that samples just 30 cm beneath the surface retain 98% of their helium in this time. Of course a typical sample will not spend all of its history at the surface enduring the full effects of the diurnal temperature fluctuation. In general, erosion will expose fresh rock in a short time. If we assume a typical erosion rate of .03 mm/yr, a sample at 30 cm depth will reach the surface in 1 million years. This means that the sample withstands <1 million years of the full effects of diurnal temperature variations. If any reasonable amount of erosion occurs, samples spend only a short portion of their history enduring the effects of surface temperature variations, and only in geologic environments which sustain little or no erosion will helium ages be partially affected by ambient thermal fluctuations.

## 3.6 Conclusions

We solved the equation for the diffusion and production of helium in apatite to create a more thorough understanding of the sensitivity of the system to thermal history and the measured range of diffusion parameters. The analytical solution to this equation for isothermal diffusion illustrates the sensitivity of helium ages to temperature in the helium partial retention zone, analogous to the fission track partial annealing zone. Comparison of the helium partial retention zone and the fission track partial annealing zone indicates that they do not overlap, suggesting that the apatite (U-Th)/He method should record

lower temperature histories than the apatite fission track method. This is consistent with studies which have compared fission track and helium ages.

The numerical solution to the full diffusion/production equation allows us to model the sensitivity of the system to variations in thermal history, and suggests that helium ages are very sensitive to variations in temperature between ~40-90°C. By combining model helium ages with measured variations in helium age from uplifted mountain blocks, one can refine the number of plausible thermal histories for the uplifted blocks. By combining measured helium ages to model helium ages calculated from fission track-length-derived thermal models, we can further refine the number of permissible thermal histories. Cooling histories involving long residence times in the helium partial retention zone yield significantly different helium ages when we use the range of diffusion parameters obtained (Wolf et al., 1996), and therefore, seemingly small uncertainties in diffusivity can propagate into large variations in modeled helium age. In the future, high precision diffusion coefficient measurements may be necessary on samples whose helium ages are the result of long residence times in the HePRZ. Although helium diffusivity is high at low temperatures, forest fires and variations in the ambient surface temperature do not significantly affect helium ages.

## 3.7 References Cited

Bierman P. and Gillespie A. (1991) Range fires; a significant factor in exposure age determination and geomorphic surface evolution. *Geology*, 19, 641-644.

Carslaw H.S. and Jaeger J.C. (1959) Conduction of heat in solids. 2nd ed., Oxford, Clarendon Press, 510p.

Cermak V., Huckenholz H.G., Rybach L., Schmid R., Schopper J.R., Schuch M., Stoffler D., and Wohlenberg J. (1982) Numerical Data and Functional Relationships in Science and Technology: Physical Properties of Rocks. volume 1, subvolume a, New York, Springer-Verlag, 315.

Climatological Data (1995) Publication of the California Division of Mines and Geology and the National Oceanic and Atmospheric Administration, 99, no.1-13.

Corrigan J. (1991) Inversion of apatite fission track data for thermal history information. *Journal of Geophysical Research,* 96, 10347-10360.

Crank, J. and Nicolson (1947) *Proc. Camb. phil. Soc. math. phys. Sci.* 43, 50p.

Crank, J. (1975) The mathematics of diffusion. 2nd ed., Oxford, [Eng]: Clarendon Press, 414p.

Dodson, M.H. (1973) Closure temperature in cooling geochronological and petrological systems. *Contributions to Minerology and Petrology*, 40, 259-274.

Farley K.A., Wolf R.A., and Silver L.T. (1996a) The effects of long alpha stopping distances on (U-Th)/He ages. *Geochimica et Cosmochimica Acta*, 60, 4223-4230.

Farley K.A., Blythe A.E., and Wolf R.A. (1996b) Apatite helium ages: comparison with fission track ages and track length derived thermal models. *American Geophysical Union Fall Meeting, Abstract Volume*, 77, F644-F645.

Fitzgerald P.F. and Gleadow A.J.W. (1990) New approaches in fission track geochronology as a tectonic tool - examples from the Transantarctic Mountains. *Nuclear Tracks and Radiation Measurements*, 17, 351-357.

Fechtig H. and Kalbitzer S. (1966) Diffusion of argon in potassium bearing solids. in Potassium-Argon Dating, O. Schaeffer, ed., 68-106, Springer, Berlin.

Gleadow A.J.W. and Duddy I.R. (1981) A natural long-term annealing experiment for apatite. *Nuclear Tracks and Radiation Measurements*, 5, 169-174.

Gleadow A.J.W., Duddy I.R., and Lovering J.F. (1983) Fission track analysis: a new tool for the evaluation of thermal histories and hydrocarbon potential. *Australian Petroleum Exploration Association Journal*, 23, 93-102.

Green P.F., Duddy I.R., Laslett G.M., Hegarty K.A., Gleadow, A.J.W., and Lovering, J.F. (1989) Thermal annealing of fission tracks in apatite 4:

Quantitative modelling techniques and extension to geologic timescales. *Chemical Geology*, 79, 155-182.

Lutz T.M. and Omar G. (1991) An inverse method of modelling thermal histories from apatite fission track data. *Earth and Planetary Sciences Letters*, 104, 181-195.

Trull T.W., Kurz M.D., and Jenkins W.J. (1991) Diffusion of cosmogenic $^{3}He$ in olivivne and quartz - implications for surface exposure dating. *Earth and Planetary Sciences Letters*, 103, 241-256.

Trull T.W., Brown E.T., Marty B., Raisbeck G.M., and Yiou F. (1995) Cosmogenic $^{10}Be$ and $^{3}He$ accumulation in Pleistocene beach terraces in Death Valley, California, USA - implications for cosmic-ray exposure dating of young surfaces in hot climates. *Chemical Geology*, 119, 191-207.

Wagner G.A., Gleadow A.J.W., and Fitzgerald P.G. (1989) The significance of the partial annealing zone in apatite fission track analysis - projected track lenght measurements and uplift chronology of the Transantarctic Mountains. *Chemical Geology*, 79, 295-305.

Wolf R.A., Farley K.A., and Silver L.T. (1996) Helium diffusion and low temperature thermochronometry of apatite. *Geochimica et Cosmochimica Acta*, 60, 4231-4240.

Wolf R.A., Farley K.A., and Silver L.T. (1997) Assessment of (U-Th)/He thermochronometry: the low temperature history of the San Jacinto Mountains, California. *Geology*, 25, 65-68.

Zeitler P.K., Herczeg A.L., Mcdougall I., and Honda M. (1987) U-Th-He dating of apatite: a potential thermochronometer, *Geochimica et Cosmochimica Acta*. 51, 2865-2868.

# Chapter 4

## A Natural Test of Helium Retention in Apatite: (U-Th)/He Thermochronometry of the Cajon Pass Deep Drillhole, California

R.A. Wolf
L.T. Silver
K.A. Farley

**Abstract -** Helium ages measured on apatites from the Cajon Pass Deep Drillhole decrease with depth and temperature from 41.1 Ma at 526 m to 0.3 Ma at 2018 m. Helium ages decline to 0 Ma just as fission track ages begin to exhibit the effects of age reduction (Kohn et al., 1994; Kohn, personal communication), an observation consistent with models of laboratory diffusion and annealing experiments which indicate that the most rapid change in helium age occurs ~35°C cooler than the most rapid change in fission track age. The simplest interpretation of the helium ages in the drillhole is that they are in equilibrium with present-day temperatures, and laboratory diffusion data (Wolf et al., 1996a) are applicable to natural systems. However, if the current thermal profile is a transient phenomenon related to recent erosion as proposed by Lachenbruch and Sass (1992), then either (1) samples have endured a complex thermal history (including the proposed recent erosional exhumation) that happens to yield helium ages which mimic an equilibrium profile and/or (2) natural diffusivity of helium from apatite differs from laboratory results in such a

way that the thermal history predicted by Lachenbruch and Sass (1992) produces the observed helium ages. In either case, the agreement of helium ages with the present-day temperature profile, as well as their relationship to fission track ages, would be fortuitous.

## 4.1 Introduction

Modeling of laboratory diffusion data presently provides the primary temperature calibration of apatite (U-Th)/He thermochronology (Zeitler et al., 1987; Lippolt et al., 1993; Wolf et al., 1996a; Wolf et al., 1996b; Warnock et al., submitted). However, measuring helium ages in a borehole with a measured geothermal gradient and a well constrained thermal history provides an independent test of helium diffusivity in the natural environment. Helium ages show patterns in rough agreement with laboratory data in one other borehole, the KTB borehole, Germany, but uncertainties in the helium ages make the results difficult to interpret (Warnock et al., submitted).

We measured helium ages in apatites from plutonic rocks in the Cajon Pass Deep Drillhole to assess the applicability of laboratory diffusion data in nature and also to further our understanding of the low temperature history of the region. We compared helium ages in the drillhole to fission track ages from the same samples to test a model based on laboratory experiments (Wolf et al., 1996b; chapter 3, this volume) which predicts that the most rapid decrease in helium age with temperature occurs ~35°C cooler than the most rapid decrease in fission track age with temperature.

## 4.2 Geological Setting

The drillhole is located ~32 km north of San Bernardino, California, and 1 kilometer above sea level near the junction of I-15 and state route 138, approximately 3.5 kilometers from the San Andreas fault (Figure 1). The drillhole extends to ~3.5 km depth. The primary scientific purpose for the drillhole was to use the heat flow and stress measurements from a deep drillhole as an indication of shear stress on the nearby San Andreas fault (Sass et al., 1992). An exploratory oil well previously drilled near the site of the drillhole, the Arkoma well (1.7 km depth), had yielded anomalously high heat flow with respect to other heat flow measurements along the San Andreas fault (Sass et al., 1986). The Cajon Pass Drillhole supported the original observation of a high heat flow anomaly.

The geologic setting of the drillhole has been inferred from mapping and stratigraphic studies (Noble 1954; Dibblee, 1967; Woodburne and Golz, 1972; Ehlig, 1988; Reynolds, 1985; Weldon, 1986; Silver and James, 1988). The region is characterized by Miocene and younger sedimentary rocks which lie unconformably on Mesozoic and older granitic basement. The Miocene sedimentary rocks around the drillhole exhibit multiple episodes of compressional and transpressional deformation which occurred between

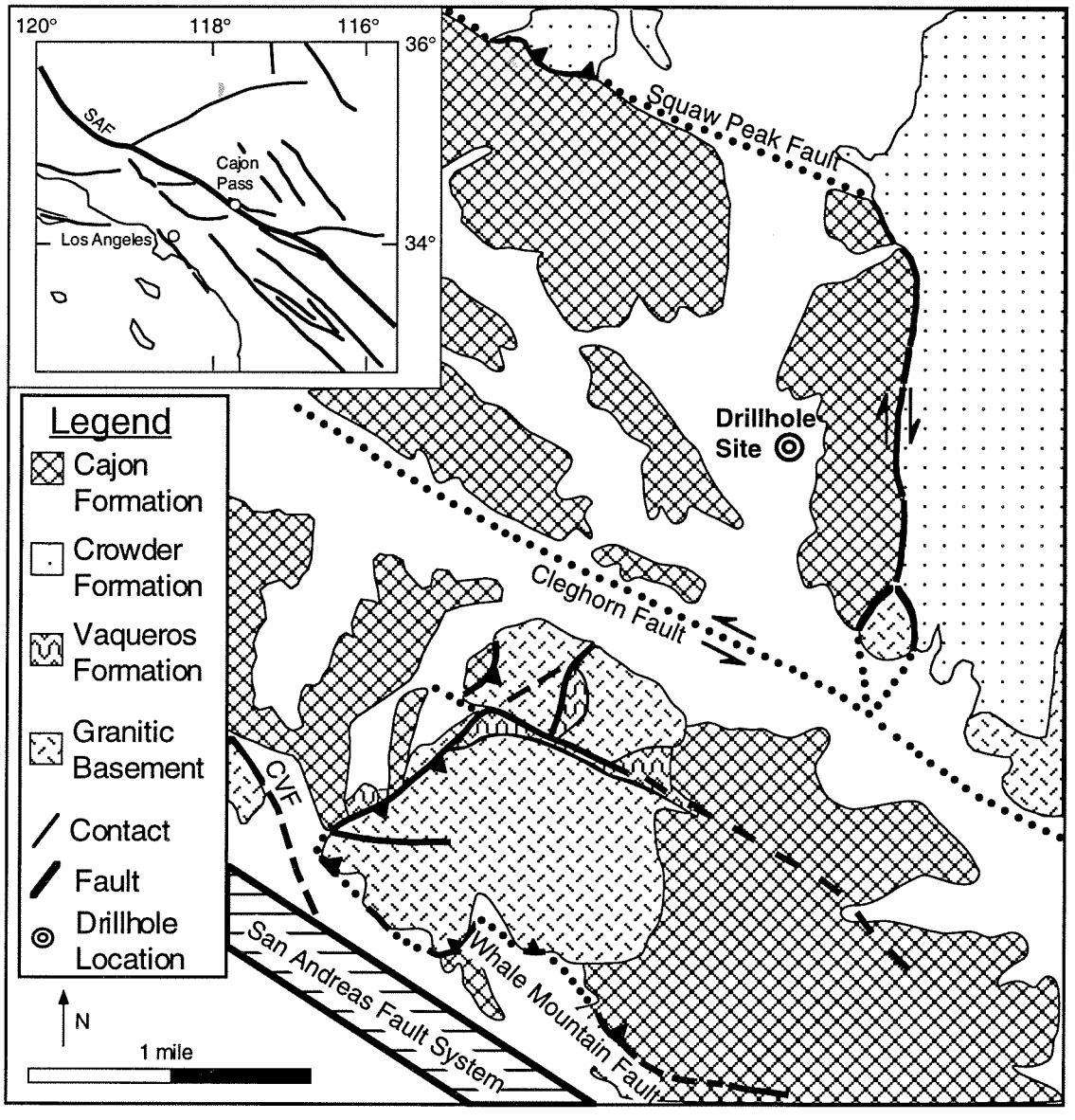


**Figure 1.**

Location and geologic maps of the Cajon Pass region. Geologic map is the result of an amalgamation of different studies (Diblee, 1967, Weldon, 1986, and Meisling and Weldon, 1989).

roughly 6.2 and 4.2 Ma (Miller and Weldon, 1992; Weldon et al., 1993). Field relations suggest vertical uplift of the Western San Bernardino Arch (which includes the drillhole site) relative to the rest of the region between 2.0 and 1.5 Ma (Meisling and Weldon, 1989; Weldon et al., 1993). The Victorville fan lies to the northeast of the drillhole site and includes detritus from the San Gabriel Mountains which are southwest of the drillhole site. The formation of Cajon Creek drainage in the last 1 Ma permitted the erosional removal of an estimated ~1-1.5 km of sediment, including the Victorville fan deposits and older sediments, from above the drillhole site (Weldon, 1986, Meisling and Weldon, 1989; Weldon et al., 1993). One interpretation of the heat flow anomaly and the geologic data is that the high heat flow is a transient phenomenon produced by the recent tectonic and erosional history (Lachenbruch and Sass, 1992; Sass et al., 1992).

Rocks from the drillhole have been characterized petrographically and chemically (Silver et al., 1988; James and Silver, 1988; Pratson et al., 1992). The first 520 m of the drillhole consist of highly folded beds of the Cajon Formation. The Cajon Formation contains non marine sandstones and conglomerates which have yielded middle to late Miocene vertebrate fossils, and are assigned an age of 18 to 13.5 Ma (Reynolds, 1985; Woodburne and Golz, 1972; Meisling and Weldon, 1989). A fault contact separates the plutonic basement rocks from the Cajon Formation at 520 m depth (Figure 2). From this contact down to ~1150 m, the core consists of weakly foliated granite and granodiorite. From ~1150 m to ~1350 m, there is an interval of interspersed

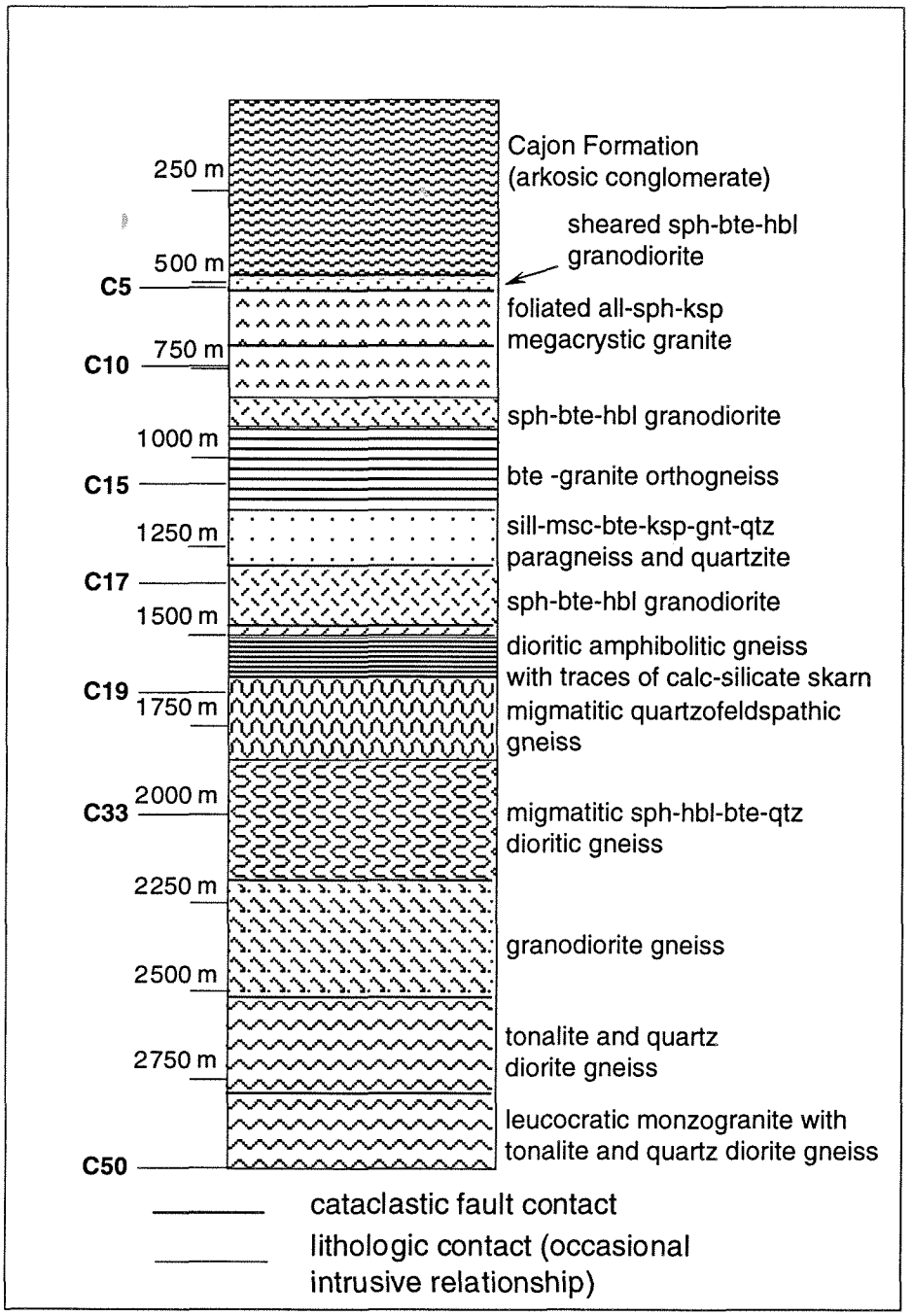


**Figure 2.**

Lithologic column for the Cajon Pass Drillhole compiled from Silver and James (1988) and Pratson et al. (1992). Sample locations are listed on the left side of the column.

quartzite and paragneiss which is separated by a fault contact from granodiorite (Silver et al., 1988; Silver and James, 1988). The remainder of the drillhole consists of gneissic dioritic to granodioritic basement broken by cataclastic fault zones with zeolite alteration.

## 4.3 (U-Th)/He Age Results

Helium ages were measured on apatites from seven granitic samples in the drillhole from the shallowest basement found at 526 m down to 3019 m following procedures described by Wolf (this volume, chapter 6) and House et al. (submitted) (Table 1). Apatite helium ages decrease monotonically from 41.1 Ma at 526 m depth to 0.3 Ma at 2018 m depth (Table 1). The sample at 3019 m depth retained no detectable helium, and the sample at 2018 m depth yielded an amount of helium just above the detection limit. The most rapid decline in helium age occurs between ~750 m and ~1500 m depth, corresponding to present-day temperatures of ~45°C to ~75°C (Figure 3).

## 4.4 Discussion

The observed decrease in helium age with depth in the Cajon Pass borehole is not obviously related to proximity to recognized faults or hydrothermal/zeolite alteration. The sample (C5) located closest to one of the more significant cataclastic faults in the drillhole retains the most helium of any of the samples. Therefore, it appears unlikely that frictional heating or fluid flow along these faults has locally affected the helium ages. At 1885 m, there is a

| Sample | Rock Type | Depth (m) | Temperature (°C) | (U-Th)/He Age (Ma) | $F_T$ | He nmol/g | U ppm | Th ppm |
|---|---|---|---|---|---|---|---|---|
| C5 | granodiorite | 526 | 38 | 41.1 ± 2.5 | 0.82 | 3.29 | 14.00 | 16.89 |
| C10 | granite | 745 | 44 | 34.7 ± 2.1 | 0.78 | 4.70 | 27.15 | 19.86 |
| C15 | granite | 1149 | 58 | 25.4 ± 1.0 | 0.81 | 2.83 | 22.72 | 10.87 |
| C17 | tonalite | 1353 | 65 | 6.0 ± 0.5 | 0.77 | 0.18 | 5.57 | 8.81 |
| C19 | granodiorite | 1656 | 76 | 5.7 ± 2.4 | 0.82 | 0.82 | 25.87 | 20.16 |
| C33 | diorite | 2018 | 90 | 0.3 ± 0.3 | 0.79 | 0.06 | 38.97 | 25.97 |
| C50 | granodiorite | 3019 | 126 | 0.0 ± 0.0 | 0.75 | 0.00 | 33.24 | 37.69 |

**Table 1.**

Helium ages represent the mean age for replicate analyses (C50 represents a single analysis). Uranium, thorium, and helium were measured on the same apatite aliquots consisting of 10 to 20 crystals (~200 μg total mass), selected on the basis of grain size and morphology. Each grain was measured using an optical micrometer, and alpha emission correction factors, $F_T$, were calculated as described by Farley et al. (1996a). Helium was analyzed by peak height comparison to a pure helium standard of known amount. Most helium concentrations were measured using a quadrupole mass spectrometer which has a 1σ external reproducibility of ±4% at the level of ~0.1 pmol of helium (this volume, chapter 6). C19, C33, and one replicate from C17 were analyzed using a sector mass spectrometer which has higher sensitivity than the quadrupole mass spectrometer (Wolf et al., 1996a, Wolf et al., 1997). Uranium and thorium were measured on an ICP-MS which has an external reproducibility of 2% (House et al., submitted). Concentrations are based on mass estimates from grain size measurements. Estimated 1σ uncertainties reflect the combined analytical uncertainty and the reproducibility of replicate analyses.

major retrograde transition from laumontite to stilbite zeolitization indicating a change in the grade of hydrothermal alteration (James and Silver, 1988), and the helium ages decrease consistently with depth across this zone.

The change in helium age with temperature closely resembles model simulations of the helium partial retention zone, HePRZ (Wolf et al., 1996b; chapter 3, this volume). In the drillhole, helium ages fall to ~50% of their maximum value at ~1200 m depth and ~60°C. We modeled the equilibrium HePRZ calculated for the present-day down-hole temperatures using the range of diffusion parameters we have measured in apatites (shaded region, Figure 3) (Wolf et al., 1996). The model assumes that samples in the drillhole have remained at their present temperature for 46 Ma. This value was chosen because it is the median value between the oldest measured helium age and the fission track age at the top of the drillhole. We know that the projected helium age at the top of the hole must be greater than or equal to the oldest helium age we measure, 42 Ma, and less than or equal to the mean fission track age near the top of the drillhole, 52 Ma (assuming the helium closure temperature in apatite is less than the fission track annealing temperature, Wolf et al., 1996a; chapter 2, this volume). There are no igneous samples available to check this assumption because the upper 500 m of the drillhole consists of the sedimentary Cajon Formation which has a different history prior to deposition in the Miocene. The HePRZ in an isothermal environment equilibrated with the present thermal gradient overlaps the measured helium

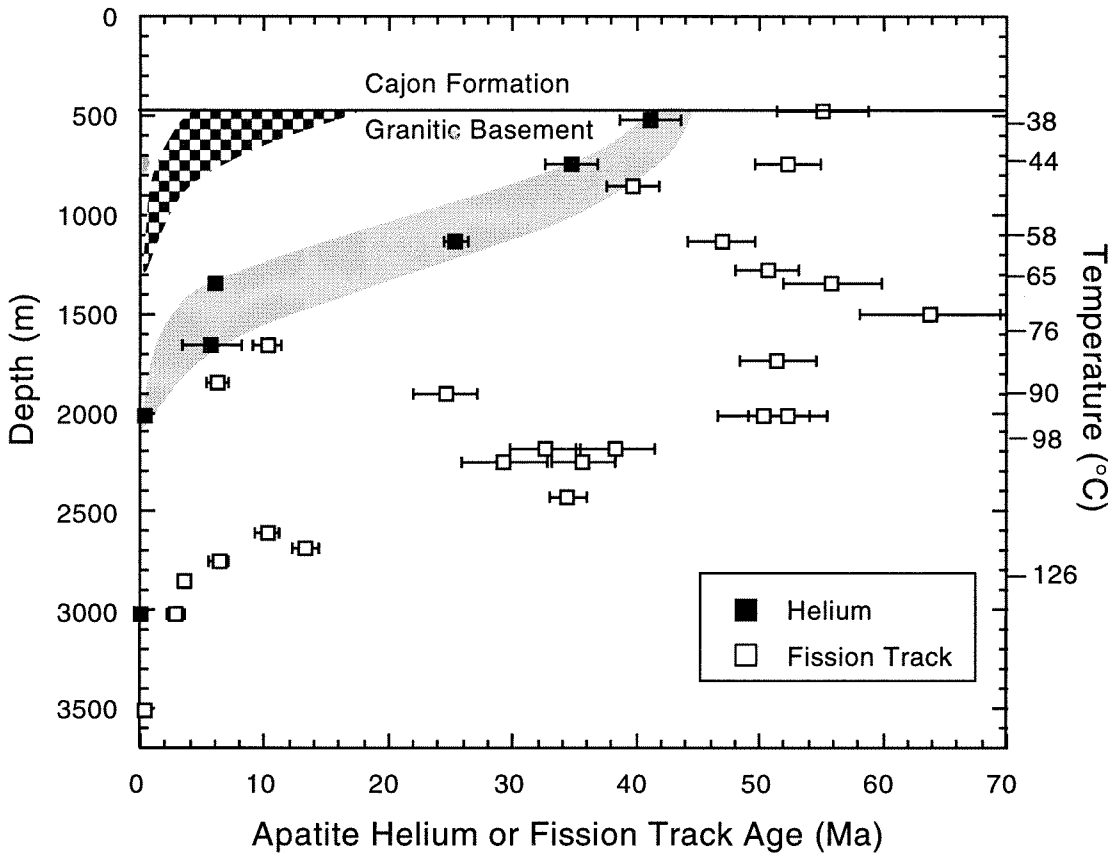


**Figure 3.**

Apatite helium ages, filled boxes, and apatite fission track, hollow boxes, plotted as a function of depth and temperature measured in the Cajon Pass Deep Drillhole. Fission track ages are from Kohn et al. (personal communication). Temperatures are plotted for the mean geothermal gradient (~35°C/km) for the drillhole. The grey shaded swath represents a model calculation of the isothermal helium partial retention zone, held for 46 Ma, using the range of measured diffusion parameters (Wolf et al., 1996a). Checkered swath represents helium ages for the thermal history shown in Figure 4.

ages (Figure 3), suggesting that a static thermal history offers one reasonable explanation of the helium age data.

The helium ages are consistent with the present geothermal gradient having been maintained for the late Cenozoic. However, the geologic data indicate that the top of the drillhole may have been buried by ~1 km of material at ~4 Ma and that ~1-1.5 km of this material was removed from above of the drillhole in the last 1 Ma (inset, Figure 4) (Weldon, 1986; Meisling and Weldon, 1989; Weldon et al., 1993). Moreover, the anomalous heat flow in the region has been interpreted as a thermal transient caused by the recent erosional exhumation of the drillhole region (Lachenbruch and Sass, 1992; Lachenbruch et al., 1995). As a test of whether the measured helium ages in the drillhole are also consistent with a thermal history created by the proposed recent sedimentation and erosion, we modeled the downhole temperatures as a function of the sedimentation and erosion rate (Figure 4) (numerical heat flow model was developed by Gary Clow and applied previously in Lachenbruch et al., 1995). We assume a thermal diffusivity for the rocks of $1.015 \times 10^{-6}$ $m^2 s^{-1}$, a thermal conductivity of 2.3 W $m^{-1} K^{-1}$, and an exponential increase in radioactive heat generation with depth starting at a value of 1.8 $\mu W m^{-3}$ (same values used by Lachenbruch et al., 1995).

The helium ages produced by the model thermal history in Figure 4, using the measured range of diffusion parameters (Wolf et al., 1996a), form the checkered swath in Figure 3, and do not overlap our measured helium ages at all. If the measured range of laboratory diffusion parameters are applicable in

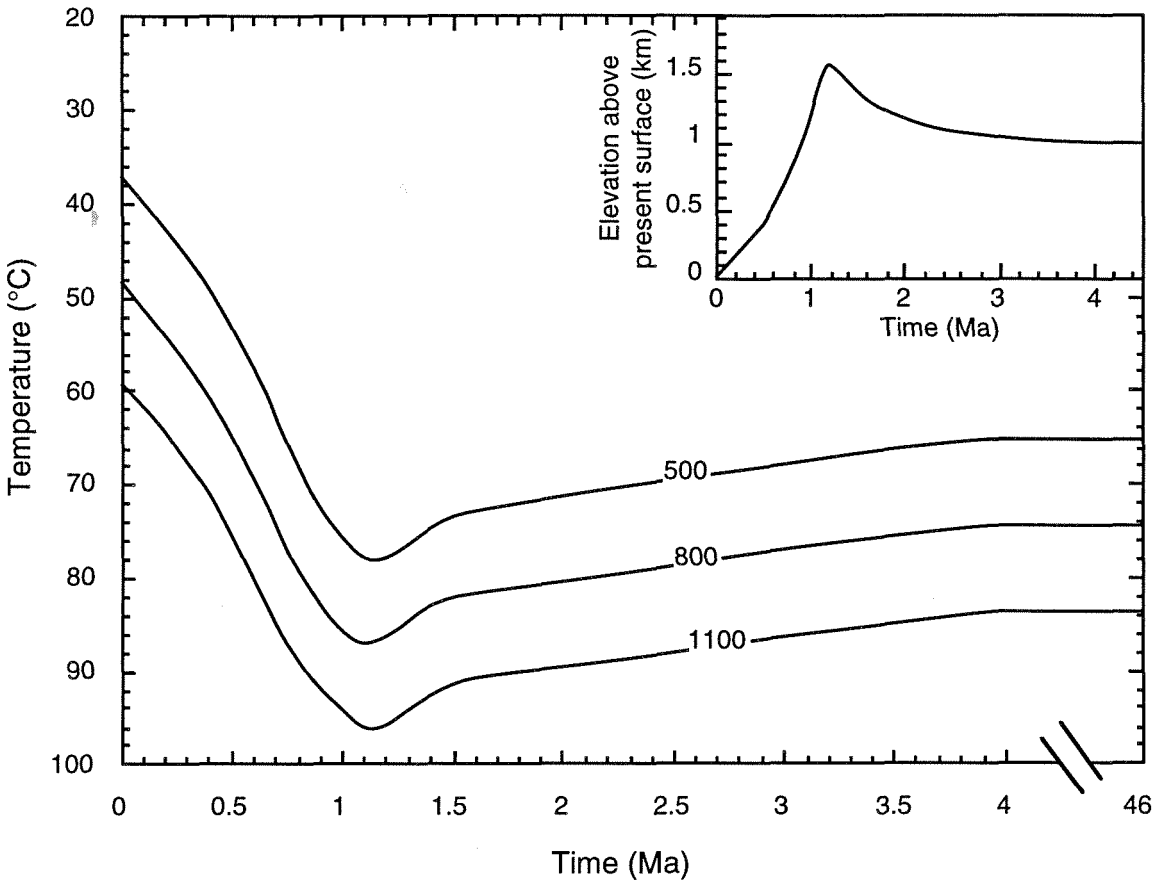


**Figure 4.**

Thermal history calculated for the recent sedimentation/erosion history of Cajon Pass. (inset) Sedimentation/erosion history derived from the work of Weldon (1986), illustrated in Lachenbruch and Sass (1992). Thermal history was calculated using a numerical model for the change in heat flow as a function or erosion and sedimetation rate (created by Gary Clow for use in Lachenbruch et al., 1995). Our thermal history assumes a static period from 46 Ma until ~4 Ma when rapid sedimentation and erosion began. The lines represent samples which are currently at 500 m, 800 m and 1100 m depth.

nature, then the measured helium ages preclude the thermal history in Figure 4. Therefore, the only way to reconcile having diffusion data which is applicable to natural systems and the recent sedimentation and erosion history is to have a more complex thermal history which happens to produce a helium age profile similar to the equilibrium profile. Samples would have to be older prior to burial than in the equilibrium scenario.

We assume that prior to the recent sedimentation and erosion history the samples were in a static thermal environment from 46 Ma to ~4 Ma. One possible alternative is that the projected age at the top of the drillhole should be >46 Ma, since the proposed geologic history has the samples buried under ~1 km of sediment prior to ~4 Ma. However, the sample which is now at 0.5 km depth was at 65°C for most of its history, and at this temperature, the steady state between helium production and loss is nearly achieved in this amount of time (chapter 3, this volume). Therefore a longer holding time will barely increase the helium ages for the modeled samples.

The helium ages indicate three alternative models for the thermal history of the drillhole. The first is that our laboratory diffusion experiments are applicable to natural systems, and the helium ages are the result of the present thermal gradient having been the thermal gradient in the drillhole for much of the Cenozoic. This suggests that the present heat flow is the same as it has been for much of the Cenozoic and, thus, is not an erosional and/or tectonic anomaly. The second interpretation allows for the recent sedimentation and erosion history but requires a more complex thermal history for the drillhole

which does not keep the present drillhole surface buried for long periods of time. In this scenario, laboratory diffusion data is applicable to natural systems, but the samples have endured a complex thermal history which fortuitously creates a helium age profile similar to the equilibrium scenario. A more complex thermal history is certainly permitted by the geologic data, and therefore, is a reasonable alternative to the thermal equilibrium interpretation. The last scenario permits laboratory measurements of diffusion parameters which are not applicable to natural systems. This scenario could involve any number of possible thermal histories depending on the real value for the diffusion parameters in nature. We cannot distinguish between the first two scenarios. However, to consider whether laboratory measurements are applicable to natural systems, we compare helium ages to fission track ages measured in the drillhole (Kohn et al., 1994; Kohn, personal communication).

Separate apatite aliquots from the same samples analyzed for helium ages were previously analyzed for fission track ages (Kohn et al., 1994; Kohn, personal communication). Except for a few notable samples between 1500 m and 2000 m depth, the fission track ages remain essentially constant (at ~55 Ma) with depth until they reach ~2050 m depth where they begin to monotonically decrease. The decrease in fission track age with increased depth and temperature below 2050 m mimics the fission track partial annealing zone, FTPAZ, observed in the Otway Basin borehole (Gleadow et al., 1981, 1983). In the Cajon Pass Drillhole, apatite helium ages are close to 0 (i.e., no helium retention) at a depth that fission track ages begin to show the effects of age

reduction (Figure 3). This agrees with laboratory observations that helium is quantitatively lost from apatite at lower temperatures than fission tracks are annealed (Wolf et al., 1996a; Green et al., 1986, 1989).

The Otway Basin is one of the best known examples of a fission track partial annealing zone observed in a borehole. In the Otway Basin, fission track ages decrease with depth in a manner similar to that predicted by laboratory annealing experiments (Green et al., 1989). If we normalize the fission track ages to compare the Cajon Pass Drillhole to the Otway Basin borehole, the normalized ages are similar, and except for a few samples in the Cajon Pass data, they essentially overlap (Figure 5). Comparison of the two data sets at 50% age reduction indicates that the two are only displaced from one another by ~5-10°C. In the Cajon Pass drillhole, the FTPAZ is centered at ~2400 m depth and ~100°C. The HePRZ and the FTPAZ are separated by ~1200 m and ~40°C (Figure 3). The fission track ages which are not consistent with the preservation of the FTPAZ may reflect faulting of blocks in from the sides or some other process such as localized hydrothermal circulation. Whatever the cause of the discrepant fission track ages, we suggest that the fission track ages in the drillhole essentially reflect a fission track partial annealing zone. If the FTPAZ has been displaced relative to the equilibrium position in the drillhole because of faulting or some other process, we suggest that these effects are localized and occur on the scale of a few hundred meters (i.e., ~5-10°C) based on the comparison with the Otway Basin data.

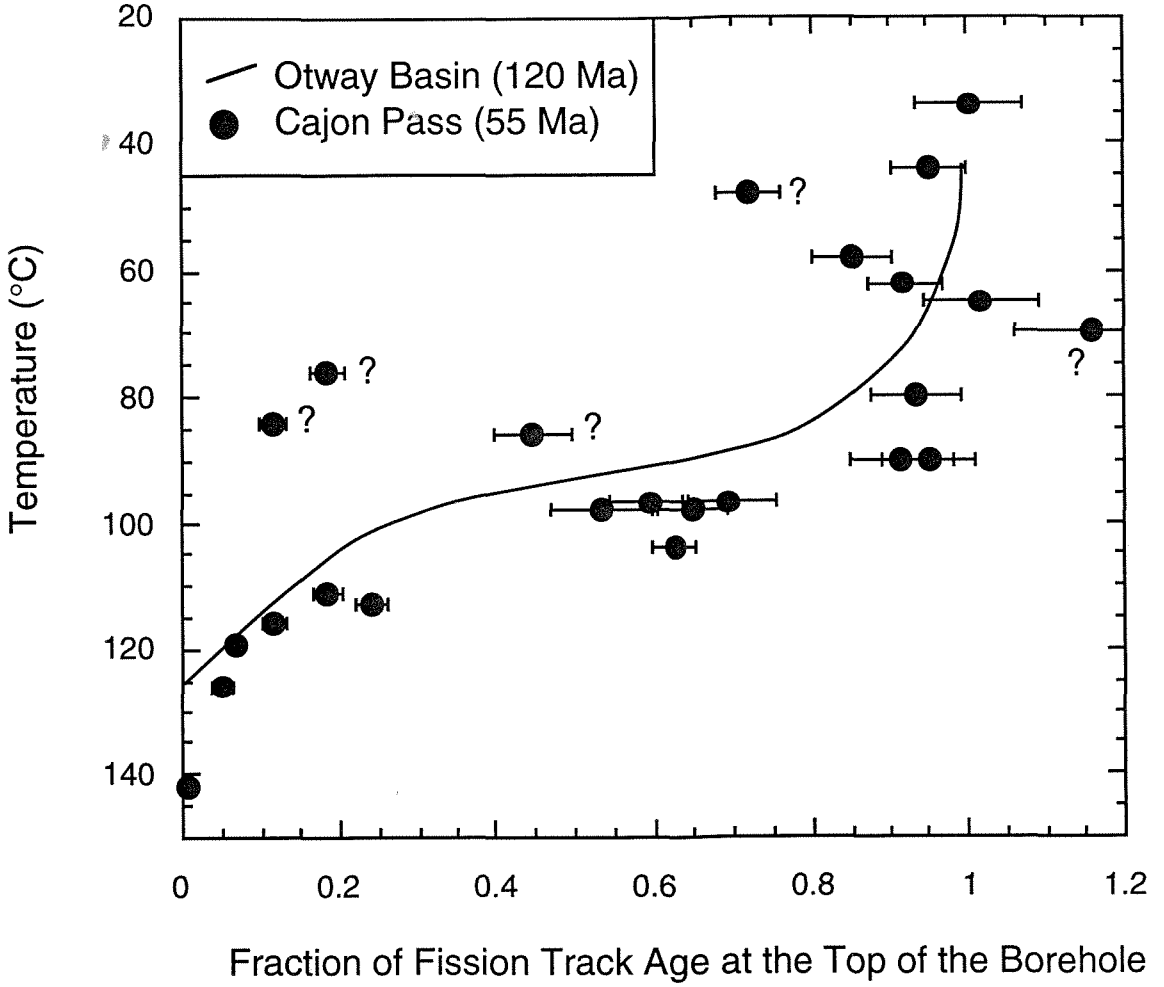


**Figure 5.**

Data points represent apatite fission track ages from Cajon Pass (Kohn et al., 1994; Kohn, personal communication). Line is interpolated through data from the Otway Basin (Gleadow et al., 1981,1983). Fission track ages in both cases are normalized by the fission track age measured at the top of the respective borehole. Steady decrease in fission track age from ~90°-140°C in Cajon Pass is similar to the fission track partial annealing zone observed in the Otway Basin suite between ~75°C and ~125°C. Samples which do not appear to mimic a partial annealing zone are shown with question marks next to filled circles.

Comparison of the HePRZ and the FTPAZ which use laboratory diffusion and annealing measurements predict a ~35°C separation between the center of the two zones (Wolf et al., 1996b; chapter 3, this volume). We assert that both the HePRZ and the FTPAZ are preserved in the Cajon Pass Drillhole, and that they are separated by ~40°C. Since models based on laboratory data are consistent with what we observe in nature in Cajon Pass, we suggest that laboratory diffusion measurements are applicable to natural systems.

## 4.5 Conclusions

Helium ages measured on samples from the Cajon Pass Drillhole appear to be in equilibrium with the present down-hole temperature profile. If this is correct, then the present down-hole temperature profile reflects the temperature profile through much of the Cenozoic. This interpretation suggests that the heat flow measured in the drillhole is not a transient feature, and further complicates the argument about whether the San Andreas is a weak fault or a strong fault in this region (Sass et al., 1986; Lachenbruch and Sass, 1992; Lachenbruch et al., 1995). If the helium ages are not the result of the equilibrium scenario, then the drillhole must have endured a more complex thermal history resulting in helium ages which fortuitously resemble the equilibrium scenario. We cannot distinguish between these two interpretations. The separation between the helium partial retention zone and the apparent fission track partial

annealing zone suggests that laboratory measurements are applicable to natural systems. However, complexities in the fission track data and the geologic history require that this comparison be repeated elsewhere.

## 4.6 References Cited

Carslaw H.S. and Jaeger J.C. (1959) Conduction of Heat in Solids. 2 ed., Oxford, Clarendon Press, 510p.

Dibblee T.W. (1967) Areal geology of the western Mojave Desert, California. *U.S.G.S. Professional Paper*, 522, 153p.

Dodson M.H. (1973) Closure temperature in cooling geochronological and petrological systems. *Contributions to Minerology and Petrology*, 40, 259-274.

Ehlig P.L. (1988) Geologic structure near the Cajon Pass scientific drillhole. *Geophysical Research Letters*, 15, 953-956.

Farley K.A., Wolf R.A., and Silver L.T. (1996a) The effects of long alpha stopping distances on (U-Th)/He ages. *Geochimica et Cosmochimica Acta*, 60, 4223-4230.

Farley K.A., Blythe A.E. and Wolf R.A. (1996b) Apatite helium ages: comparison with fission track ages and track length derived thermal models. *American Geophysical Union Fall Meeting, Abstract Volume*, 77, F644-F645.

Gleadow A.J.W. and Duddy I.R. (1981) A natural long-term annealing experiment for apatite. *Nuclear Tracks and Radiation Measurements*, 5, 169-174.

Gleadow A.J.W., Duddy I.R., and Lovering J.F. (1983) Fission track analysis: a new tool for the evaluation of thermal histories and hydrocarbon potential. *Austral. Petrol. Expl. Assoc. Journal*, 23, 93-102.

Green P., Duddy I., Gleadow A., Tingate P., and Laslett G. (1986) Thermal annealing of fission tracks in apatite: 1. A qualitative description. *Chemical Geology,* 59, 237-253.

Green P.F., Duddy I.R., Laslett G.M., Hegarty K.A., Gleadow A.J.W., and Lovering J.F. (1989) Thermal annealing of fission tracks in apatite 4: Quantitative modelling techniques and extension to geological timescales. *Chemical Geology*, 79, 155-182.

House M.A., Wernicke B.P., Farley K.A., and Dumitru T.A., Cenozoic thermal evolution of the central Sierra Nevada from (U-Th)/He thermochronometry. submitted to *Earth and Planetary Science Letters.*

James E.W., and Silver L.T. (1988) Implications of zeolites and their zonation in the Cajon Pass Deep Drillhole. *Geophysical Research Letters*, 15, 973-976.

Kohn B.P., Saltus R.W., and Gleadow A.J.W. (1994) Thermotectonic history of the Cajon Pass Deep Drillhole, southern California: an apatite fission track study. *Abstracts from the Eighth International Conference on Geochronology, Cosmochronology, and Isotope Geology, U.S. Geological Survey Circular*, 1107, 176.

Lippolt H.J., Leitz M., Wernicke R.S., and Hagedorn B. (1994) (U+T)/He dating of apatite - experience with samples from different geochemical environments. *Chemical Geology*, 112, 179-191.

Lachenbruch A.H., Sass J.H., Clow G.D., and Weldon R.J. (1995) Heat flow at Cajon Pass, California, revisited. *Journal of Geophysical Research*, 100, 2005-2012.

Lachenbruch, A.H. and Sass, J.H. (1992) Heat-flow from Cajon Pass, fault strength, and tectonic implications. *Journal of Geophysical Research*, 97, 4995-5015.

Meisling K.E. and Weldon R.J. (1989) The Late Cenozoic tectonics of the northewestern San Bernardino Mountains, southern California. *Geological Society of America Bulletin*, 101, 106-128.

Miller M.G., and Weldon R.J. (1992) A lateral ramp origin for the north trending segment of the Squaw Peak fault, Cajon Pass, California. *Journal of Geophysical Research*, 97, 5153-5165.

Noble L.F. (1954) The San Andreas fault zone from Soledad Pass to Cajon Pass, California. *Bulletin of the California Division of Mines and Geology*, 170, 32-48.

Pratson E.L., Anderson R.N., Dove RE, Lyle M, Silver L.T., James E., and Chappell B.W. (1992) Geochemical logging in the Cajon Pass Drillhole and its application to a new, oxide, igneous rock classification scheme. *Journal of Geophysical Research*, 97, 5167-5180.

Reynolds R.E. (1985) Tertiary small mammals in the Cajon Valley, San Bernardino, California. ed. by Reynolds R.E., in *Geologic Investigations along Interstate 15, Cajon Pass to Mannix Lake, California: Western*

*Association of Vertebrate Paleontologists Field Trip Guidebook*, 60th Meeting, Redlands California, San Bernardino County Museum, 49-58.

Sass J.H., Lachenbruch A.H., Moses T.H., and Morgan P. (1992) Heat Flow from a Scientific Research Well at Cajon Pass, California. *Journal of Geophysical Research*, 97, 5017-5030.

Sass J.H., Lachenbruch A.H., Galanis Jr., S.P., Munroe R.J., and Moses T.H. (1986) An analysis of thermal data from the vicinity of Cajon Pass, California. *U.S.G.S. Open File Report*, 86-468, 47p.

Silver L.T. and James E.W. (1988) Geologic setting and lithologic column of the Cajon Pass Deep Drillhole. *Geophysical Research Letters*, 15, 941-944.

Silver L.T., James E.W., and Chapple B.W. (1988) Petrological and geochemical investigations at the Cajon Pass deep drillhole. *Geophysical Research Letters*, 15, 961-964.

Wagner G.A., Gleadow A.J.W., and Fitzgerald P.G. (1989) The significance of the partial annealing zone in apatite fission track analysis - projected track length measurements and uplift chronology of the Transantarctic Mountains. *Chemical Geology*, 79, 295-305.

Warnock A.C., P.K. Zeitler R.A. Wolf and Bergman S.C. Low-Temperature Thermochronometry using the Apatite (U-Th)/He Method. submitted to*Geochimica et Cosmochimica Acta.*

Weldon R.J. (1986) The late Cenozoic geology of Cajon Pass: implications for

tectonics and sedimentation along the San Andreas fault, Ph.D. Thesis, California Institute of Technology, 400p.

Weldon R.J., Meisling K.E., and Alexander J. (1993) A speculative history of the San Andreas fault in the central Transverse Ranges, California, in The San Andreas fault system: displacement, palinspastic reconstruction, and geologic evolution. ed. by Powell, R.E., R.J. Weldon, and Matti, J.C., *Memoir of the Geological Society of America*, 178, 161-198.

Wolf R.A., Farley K.A., and Silver L.T. (1996a) Helium diffusion and low temperature thermochronometry of apatite. *Geochimica et Cosmochimica Acta*, 60, 4231-4240.

Wolf R.A., Kass D.M., and Farley K.A. (1996b) The sensitivity of the apatite (U-Th)/He system to thermal history. *American Geophysical Union Fall Meeting, Abstract Volume*, 77, F644.

Wolf R.A., Farley K.A., and Silver L.T. (1997) Assessment of (U-Th)/He thermochronometry: the low temperature history of the San Jacinto mountains, California. *Geology*, 25, 65-68.

Woodburne M.O. and Golz D.J. (1972) Stratigraphy of the Punchbowl Formation, Cajon Valley, southern California, *University of California Publ. Geol. Sci.* 92, 57p.

Zeitler P.K., Herczeg A.L., Mcdougall I., and Honda M. (1987) U-Th-He dating of apatite - a potential thermochronometer. *Geochimica et Cosmochimica Acta*, 51, 2865-2868.

# Chapter 5

## Assessment of (U-Th)/He Thermochronometry: The Low-Temperature History of the San Jacinto Mountains, California

R. A. Wolf
K. A. Farley
L. T. Silver

(This chapter was reprinted from *Geology* (1997), 25, 65-68)

**Abstract** - (U-Th)/He ages have been measured on igneous apatites from the San Jacinto Mountains, a high region at the junction of the Peninsular and Transverse Ranges, to investigate the potential of this technique for thermochronometry of slowly cooled rocks. Helium ages from 79 to 17 Ma are younger than ages obtained by other dating techniques, including apatite fission-track counting, and are consistent with laboratory experiments that indicate this system has a uniquely low closure temperature. Helium ages are strongly correlated with elevation and record the latest low-temperature thermal evolution of the range. They suggest relative tectonic quiescence in the latest Cretaceous through mid-Tertiary, and provide no evidence for rapid unroofing of the block during this period. Nor do they obviously require a large degree of uplift associated with convergence between the Transverse and Peninsular ranges in the last few million years. Helium ages document modest westward tilting of the block (~7°) and a significant vertical component of motion on the

block's bounding faults after helium retention began. This work suggests that apatite helium ages record low-temperature tectonic and thermal histories that are not apparent from other dating techniques.

## 5.1 Introduction

Thermal histories of rock masses can be deduced from the analysis of parent/daughter systems in which retention of the radiogenic daughter product is a sensitive function of temperature. Although many thermochronometers have been developed, there remains need for a high-precision dating technique sensitive to very low temperatures (<100°C), e.g., for study of mountain range exhumation and for assessment of hydrocarbon potential in sedimentary basins. Laboratory diffusion measurements indicate that the accumulation of radiogenic He from U and Th decay in apatite provides such a tool (Zeitler et al., 1987; Lippolt et al., 1994; Wolf et al., 1996). Diffusive loss of He from apatite is governed by a simple thermally activated mechanism that yields a closure temperature of 75°±5°C assuming a cooling rate of 10°C/Ma (Wolf et al., 1996). This closure temperature is apparently invariant over a broad range of apatite composition and grain size. In many rocks, apatite He ages will reflect cooling through temperatures at which radiogenic He is neither quantitatively retained nor lost. Partial He retention occurs between ~75°and ~40°C, and in a normal geothermal gradient occurs in a zone ~2 km wide centered at 2 km depth. It is analogous to the fission track partial annealing zone (Fitzgerald and Gleadow, 1990), but typically lies ~2 km shallower.

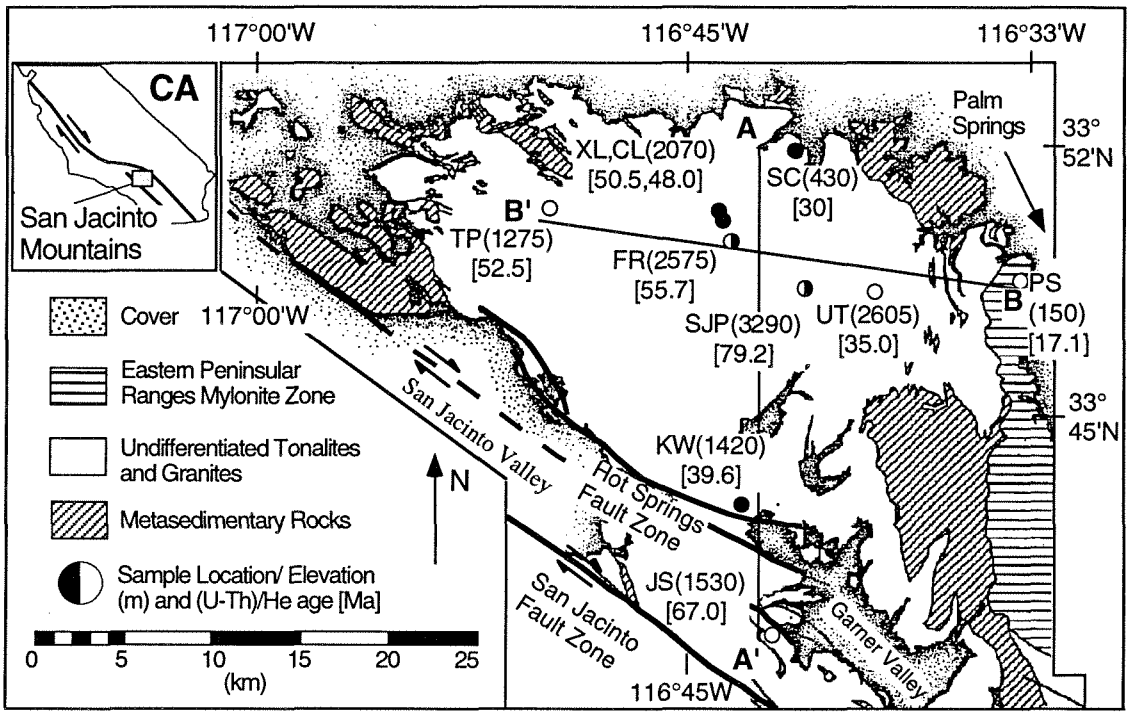


**Figure 1.**

Geologic map of the region around Mt. San Jacinto (after Hill, 1984). Filled symbols represent samples taken along a N-S transect (A-A'), open symbols along a nearly E-W transect (B-B'). Half-filled symbols are on both transects. Sample designations are indicated, as are elevations in metres (in parentheses) and He ages in Ma (in brackets). All samples lie within the San Jacinto block, except for sample JS, which lies south of the Hot Springs fault zone.

Here we report He ages of apatites collected from two high-relief transects of the San Jacinto mountains, near Palm Springs, California. Our goal was to assess whether He ages record geologically significant information in rocks that may have resided in the He partial retention zone for a long period. The San Jacinto Mountains are a fault-bounded block of Cretaceous plutonic rocks in the extreme northeastern corner of the Peninsular Ranges (Figure 1). The Banning strand of the San Andreas transform system provides the northern limit in San Gorgonio pass, and the San Jacinto family of faults provides the western and southern limits. On the east, faults beneath the alluviated Coachella Valley represent the youngest structures of the Gulf of California rift and transform system. Mount San Jacinto is the second highest peak (3292 m) in southern California, 40 km south of Mount San Gorgonio, the highest peak (3507 m). The proximity of these two elevations is plausibly attributed to crustal convergence between the Transverse and Peninsular Ranges associated with the restraining bend in the San Andreas fault system. In contrast, extensional collapse of the crust along the plate boundary east of the San Jacinto Mountains has produced the Coachella Valley, at sea level or below, and has contributed significantly to the great local relief. Much of the current topography of the San Jacinto Mountains is probably related to opening of the Gulf of Califonia, which began at ca. 5 Ma (Atwater, 1971).

Detailed field mapping (Hill, 1984, 1988) and petrology and geochemistry studies (Hill, 1988; Silver and Hill, 1986) have established that the entire San Jacinto plutonic complex has a limited range of lithologies

(tonalite and granodiorite), is structurally coherent, and was emplaced between 97 and 92 Ma. Biotite K-Ar and sphene and zircon fission track ages (Armstrong and Suppe, 1973; Smith et al. 1991; George and Dokka, 1994) indicate that most of the exposed block cooled well below 300°C by ca. 75 Ma. Apatite fission track ages of ca. 75 Ma suggest the block also cooled through ~105°C early in its history (George and Dokka, 1994).

The San Jacinto Mountains were selected for this initial study of He thermochronometry because 1) the rocks are homogenous, reducing the likelihood that He diffusion characteristics vary within the block, 2) field mapping suggests the block has behaved as a coherent body since crystallization, simplifying interpretation of ages, and 3) a large collection of high purity apatite separates was available from previous studies (Silver and Hill, 1986). An additional reason for studying these rocks is that the north and east faces of the block are steep escarpments that expose for sampling more than 3 km of relief. Investigations of apatite fission track ages from similar settings elsewhere have revealed correlations between age and elevation that are thought to record cooling associated with denudation and uplift (e.g., Wagner and Reimer, 1971; Fitzgerald et al., 1995). Apatite fission track ages from the San Jacinto Mountains are latest Cretaceous and are invariant with elevation (George and Dokka, 1994), an observation taken to indicate rapid uplift and cooling at that time. The apatite fission track ages apparently do not record the effects of convergence of the Peninsular and Transverse ranges in the last few million years. Because the zone of partial He retention is lower in temperature than that

of apatite fission track partial annealing, by studying vertical variations of He age it should be possible to more fully characterize the Late Cretaceous cooling event and potential recent activity on the San Andreas system.

## 5.2 Samples and Results

To explore He age systematics, we sampled much of the topographic and geographic extent of the range (Figure 1). All of our samples come from the tectonically coherent portion of the San Jacinto block with the exception of sample JS, which lies south of the active Hot Springs fault. Reconstruction of the precise prefaulting position of JS relative to the other samples is not possible. For ease of discussion we divide the samples into two approximately perpendicular transects. Seven lie on a well-defined north-south array (A-A' in Figure 1) and represent an ~3 km vertical transect with samples taken on both sides of the summit. Five define an intersecting nearly east-west transect (278°, B-B' in Figure 1). Two of the samples described here (CL and PS) are among the apatites analyzed to characterize He diffusivity (Wolf et al., 1996) and yield identical closure temperatures.

(U-Th)/He ages from 79 to 17 Ma are clearly related to sample elevation (Figure 2, 3, Table 1). Southward along A-A', ages increase from 30 Ma at the base of the steep northern escarpment (430 m elevation) to 79 Ma at the summit (3290 m), then decrease to 40 Ma at 1420 m elevation on the southern edge of the block. Sample JS, across the Hot Springs fault from the block but at nearly the same elevation (1530 m), has a much older He age of 67 Ma. The age

| Sample | Elevation (m) | Latitude (N) | Longitude (W) | He (nmol/g) | U (ppm) | Th (ppm) | $F_T$ | Helium Age (Ma) |
|---|---|---|---|---|---|---|---|---|
| PS | 150 | 33°49.33' | 116°33.53' | 2.32 | 34.56 | 20.56 | 0.63 | 17.1 |
| SC | 430 | 33°52.71' | 116°41.21' | 3.81 | 26.28 | 29.90 | 0.70 | 30.0 |
| TP | 1275 | 33°51.29' | 116°49.93' | 5.38 | 20.46 | 21.38 | 0.74 | 52.5 |
| KW | 1420 | 33°42.57' | 116°43.09' | 5.28 | 27.00 | 33.02 | 0.70 | 39.6 |
| JS | 1530 | 33°38.85' | 116°41.45' | 5.32 | 16.70 | 17.50 | 0.70 | 67.0 |
| XL | 2070 | 33°51.65' | 116°43.70' | 2.36 | 9.83 | 13.17 | 0.67 | 50.5 |
| CI | 2070 | 33°50.82' | 116°43.52' | 5.80 | 21.10 | 21.38 | 0.85 | 48.0 |
| FR | 2575 | 33°49.92' | 116°43.02' | 6.35 | 22.02 | 22.46 | 0.77 | 55.7 |
| UT | 2605 | 33°48.78' | 116°38.27' | 5.52 | 30.06 | 27.12 | 0.80 | 35.0 |
| SJP | 3290 | 33°48.89' | 116°40.80' | 8.42 | 25.11 | 26.83 | 0.62 | 79.2 |

**Table 1.**

(U-Th)/He ages from Mt. San Jacinto. Of the the ten samples, eight (**SC**,**TP**,**KW**,**JS**,**SJP**,**CL**,**FR**,**UT**) are tonalites, one (**XL**) is a hornblende diorite, and one (**PS**) is a mylonitic tonalite from the lower plate of the Eastern Peninsular Ranges Mylonite Zone. Separate ~10 mg aliquots were analyzed for He and for U and Th. Replicate He measurements on all ten samples agree within analytical uncertainty (<1%), suggesting that 10 mg aliquots are sufficiently homogeneous to permit the analysis of separate aliquots for parent and daughter concentrations. Analytical procedures have been described elsewhere (Wolf et al., 1996). The estimated accuracy on (U-Th)/He ages obtained by these techniques is ±3%. Tabulated ages assume secular equilibrium for all intermediate daughters and have been corrected for alpha emission effects. A detailed study of the consequences of alpha emission in sample **CL** has been published elsewhere and provided the theoretical emission correction used here (Farley et al., 1996). During decay, alpha particles are ejected ~20 μm and can be lost from the edges of a crystal. By carefully measuring grain morphology, the fraction of alphas retained, or "$F_T$," can be calculated for each sample so that the ages can be corrected for this effect.

distribution on B-B' is similar, rising from 17 Ma at the base of the eastern escarpment (150 m) to the summit, then decreasing to 53 Ma at 1275 m on the western margin. Isochronal surfaces interpolated through the ages on each transect are indicated in Figure 2. On the north-south transect the isochrons are roughly parallel with a mean apparent dip to the south of ~1.5°. On the east-west transect the isochrons are also roughly parallel, with a mean apparent dip of ~6.5° to the west.

## 5.3 Discussion

He ages in the San Jacinto Mountains are substantially younger than ages obtained from any other chronometer and are the only ages which strongly covary with elevation. Both of these observations are consistent with the inferred low closure temperature of the system and relatively long residence of the rocks at temperatures at which He is only partially retained. We now consider the origin of the geographic variations in He age and discuss thermal histories for the San Jacinto Mountains that are consistent with the available thermochronometry.

Like apatite fission track ages, the He ages probably record the latest low temperature history of the range. However, because this is an essentially untested isotopic tool we briefly consider alternative explanations. Elevation-correlated variations in He retentivity as a consequence of chemical or petrological variations can be ruled out because 1) the plutonic complex is not zoned in this dimension (Hill, 1984); 2) the chemically distinctive hornblende

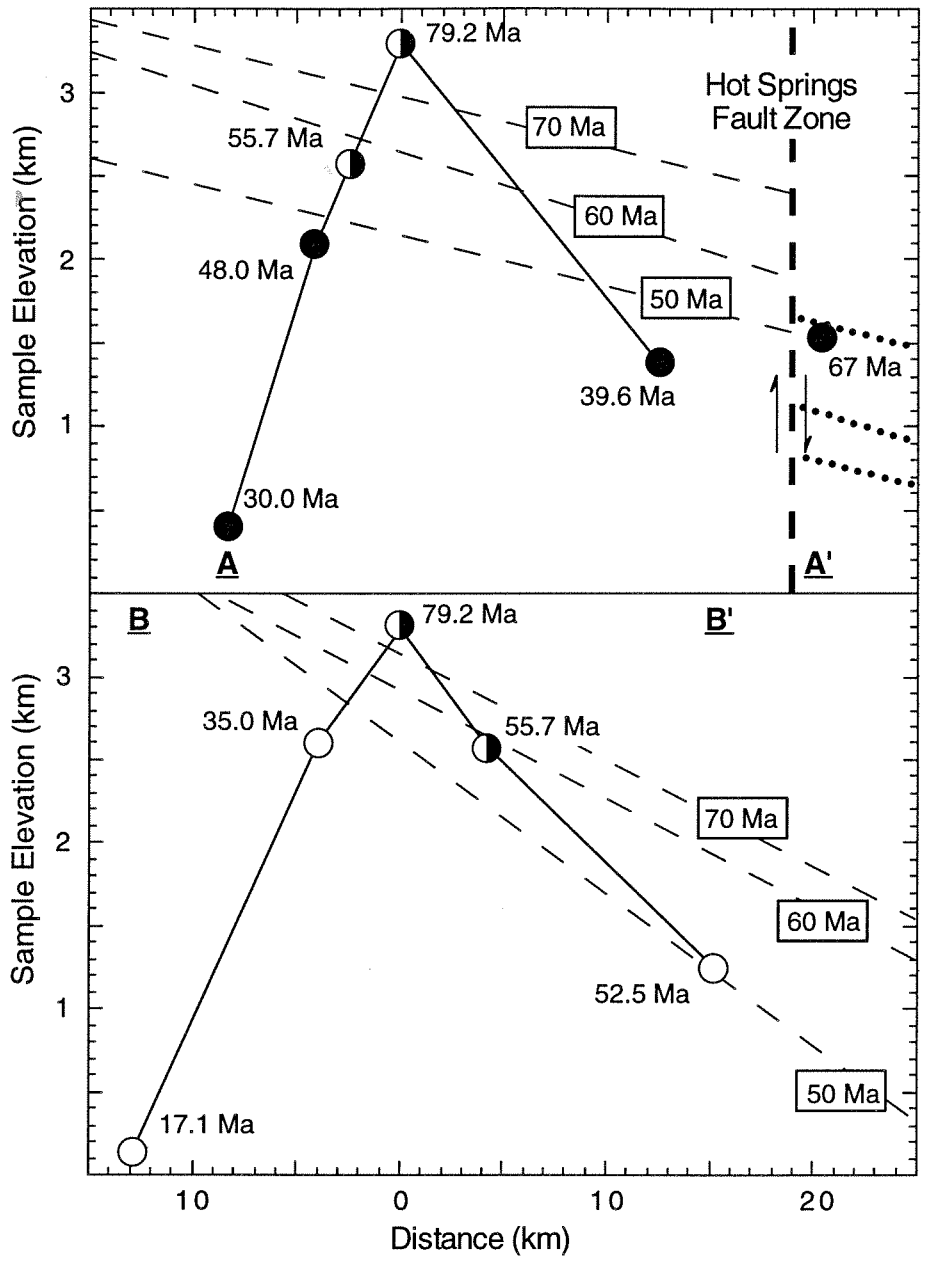


**Figure 2.**

Elevation of dated samples as a function of distance from the summit of San Jacinto peak along the two transects A-A' and B-B'. He ages are indicated beside each data point. The symbol style is the same as in Figure 1. Dashed lines are the traces of surfaces of equal He age interpolated within each transect (ages in boxes). Dotted lines are the inferred offset isochrons arising from vertical motion on the Hot Springs fault. Vertical exaggeration is 7.8x.

diorite xenolith (XL) yielded a He age indistinguishable from a nearby sample (CL) of the host tonalite; and 3) our laboratory measurements indicate that He retentivity in apatite is independent of chemistry and grain size over the range observed in these samples (Wolf et al., 1996). Nor can the correlation between sample elevation and He age be a result of diffusive He loss on the Earth's surface, with higher loss associated with the higher ambient temperatures at the base of the range compared to the summit. Even if the orographic temperature contrast existed for millions of years, such loss would yield only a few percent difference in age from base to summit using the diffusion data we reported previously (Wolf et al., 1996). It is most likely that He records primary cooling ages of these plutonic rocks.

A prominent aspect of the He age distribution is the tilted isochronal surfaces (Figure 2), indicating that rocks now exposed on the eastern and northern margins of the block cooled through the He partial retention zone later than those currently at the same elevation to the west and south. Assuming flat-lying isotherms beneath the block during cooling through ~75°C (a reasonable assumption, but possibly an oversimplification (e.g., Stuwe et al., 1995)), this observation can be attributed to tilting of the block after the rocks had begun to retain He. Taking the mean tilt implied by the isochrons on our two transects, the He ages imply 7°±2° of westward tilting about a horizontal axis bearing 193°. Such tilt is geologically reasonable and is in substantial agreement with independent observations. The steep eastern escarpment and the basin to the east of the range are indicative of extension, either Basin and Range evolution,

or associated with the recent (<5 Ma) opening of the Gulf of California. In an extensional environment, the footwall is often tilted upward to compensate for the removal of material in the hanging wall (Wernicke and Axen, 1988). Hornblende geobarometry indicates similar tilting, 15° ± 3.3°W on an axis bearing 161° ± 7.9° (Ague and Brandon, 1992). Tilting indicated by geobarometery is of a greater magnitude and about a slightly different axis than implied by the He ages; this discrepancy may arise from tilting that occurred after the hornblende system closed but prior to accumulation of radiogenic He in the apatite (between ~75° and 40°C). We also note that San Jacinto peak is capped by an isolated gentle plateau (Fraser, 1931) which does not appear to reflect this westward tilting. If this was an originally near horizontal erosion surface, then tilting predates its formation.

It is clear from Figure 2 that sample JS, lying south of the active Hot Springs fault zone, has a He age substantially older than suggested by projection of the isochronal surfaces through the fault. This discrepancy may be attributed to ~800 metres of vertical motion on this fault, which is consistent with observed local tectonic subsidence in San Jacinto and Garner valleys (Figure 1). Note that the age difference cannot be attributed to right-lateral motion on the Hot Springs fault, moving JS relative to the tilted isochronal surfaces within the San Jacinto block. Right-lateral motion would cause ages south of the fault to be younger than indicated by the projected isochronal surfaces, rather than older.

Plotted directly against elevation, the He ages form a broad scatter with

lower ages at lower elevations, a relationship seen most clearly for samples on the north-south transect (Figure 3). If our hypothesis that the block has been tilted after the He ages were established is correct, then tilt correction of our samples to their original structural levels will allow us to more directly interpret the block's cooling history. In Figure 3 we have computed pre-tilt structural depths relative to sample SJP (the summit of Mt. San Jacinto) using the tilt axis and magnitude indicated above. This correction increases the sampled structural depth to ~4.5 km, and moves all but one point to a nearly linear array when plotted against structural level. The outlier is the summit sample (SJP), which has an age substantially older than suggested by the trend of the other samples. The age profile in Figure 3 probably reflects the cooling history of the block and is comparable to one-dimensional fission track age-elevation profiles.

Unambiguous interpretation of low temperature thermal histories such as those provided by (U-Th)/He and apatite fission track dating requires more detailed geologic and chronometric information than is presently available for the San Jacinto Mountains, but some broad generalizations and comparisons can be made. Fission track age profiles similar to the distribution shown in Figure 2 have generally been interpreted in terms of cooling associated with exhumation. In the case of San Jacinto, evidence for substantial exhumation comes from the observation that rocks at the present summit were emplaced at crustal depths of ~10-15 km at ca. 92 Ma (Hill, 1984). The shallow slope of He ages plotted against structural level (Figure 3) suggest relative tectonic quiescence between 79 and 17 Ma, as any major uplift/cooling event would

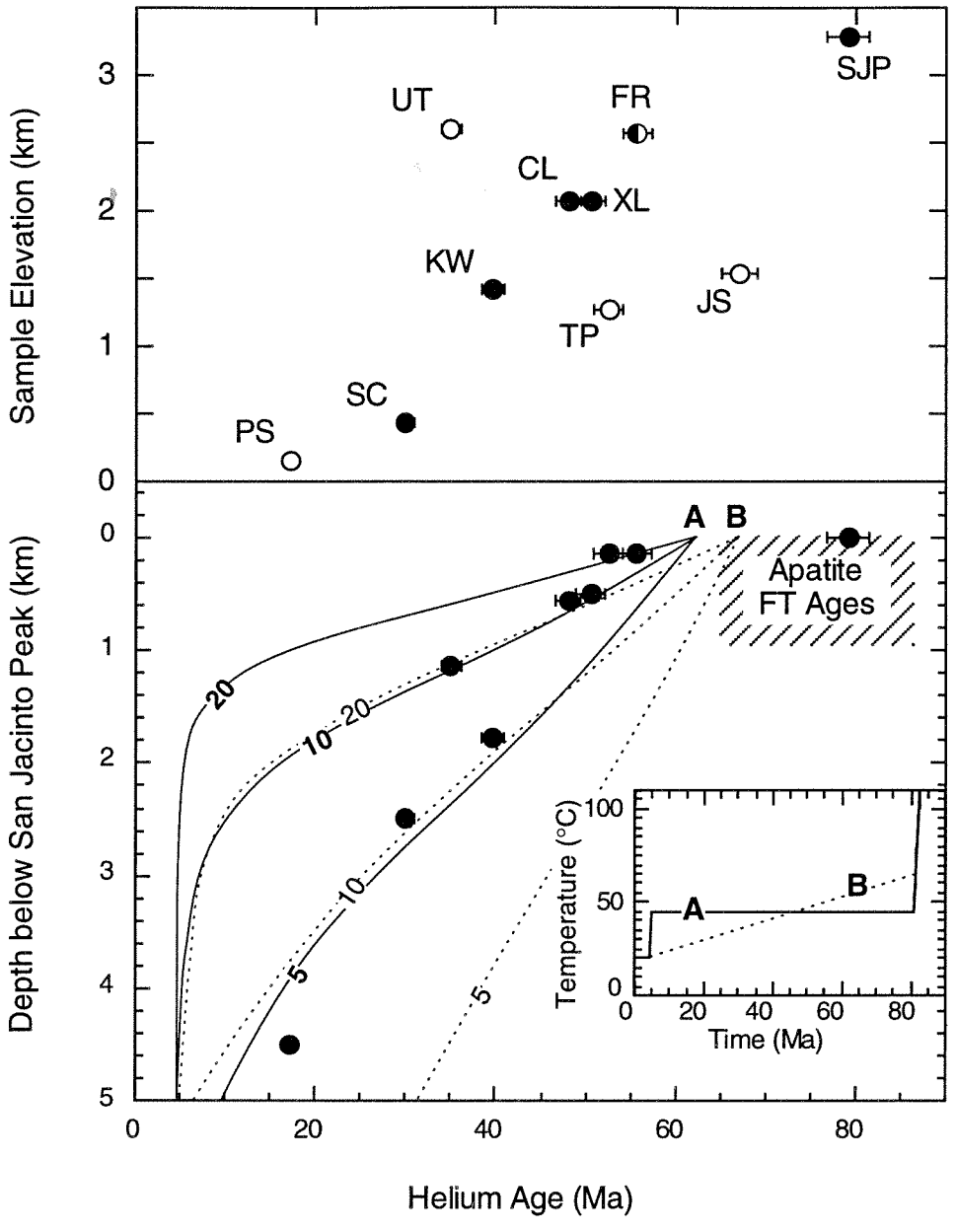


**Figure 3.**

(U-Th)/He ages plotted vs. elevation (top panel) and inferred tilt-corrected structural position relative to San Jacinto Peak (lower panel). Symbols and sample designations are the same as in Figure 1. The lower panel also shows the tilt-corrected apatite fission track ages from George and Dokka (1994) and model He age profiles computed using the temperature histories shown in the inset, the indicated geothermal gradients (in °C/km), and the diffusion characteristics of sample CL (Wolf et al., 1996).

yield ages approaching invariance with elevation. In this regard the He ages are in sharp contrast with apatite fission tracks ages from nearby on the mountain. George and Dokka (1994) report invariance of apatite fission track ages (75±8 Ma) on samples which span 2 km in elevation on the San Jacinto block, and argue for a rapid uplift and exhumation event associated with the Laramide Orogeny. However, if our observation of late-stage block tilting is correct, then the structural depth over which fission track ages were measured is smaller than the elevation difference. Using the same procedure applied to the He samples, we find that the fission track dated samples all lie structurally within 1 km of the summit of San Jacinto Peak (Figure 3). While rapid cooling may be indicated by the fission track data, our structurally deeper (and younger) samples suggest that much of the block remained at or below the helium partial retention zone (probably at depths > 3 km) at the time of the Laramide Orogeny. In addition none of the He ages are as young as 5 Ma, indicating that the recent uplift associated with the San Andreas fault system has not exhumed rocks from below the base of the helium partial retention zone. Evaluation of the degree of recent exhumation allowed by the He ages requires a more detailed examination of possible cooling histories.

The He age profile in Figure 3 could arise from a large number of different thermal histories. To show the sensitivity of the He system to cooling history and geothermal gradient, we compare our profile to model results for two reasonable histories similar to those proposed for the Sierra Nevada (Dumitru,1990), which probably had a comparable tectonic history prior to 5 Ma.

We used a numerical solution to the time-dependent He diffusion/production equation to calculate age-elevation profiles, assuming constant geothermal gradients of 5°, 10° and 20°C/km. Both thermal models have rapid cooling from magmatic temperatures until about 80 Ma to satisfy the cooling constraints derived from other chronometers, and to get the structurally highest samples retaining He in the latest Cretaceous to earliest Tertiary. In the first model we hold the temperature invariant from 80 to 5 Ma, at which time the entire block cools to 20°C. This corresponds to a shallow crustal block that remains static until rapid uplift associated with motion on the San Andreas fault system; the resulting age profile represents an exhumed He partial retention zone whose thickness is governed by the geotherm. As shown in Figure 3, the resulting age-elevation profiles are fairly shallow until ca. 5 Ma, when they become nearly invariant with elevation as a result of the onset of rapid cooling. For normal geothermal gradients these curves clearly do not match our observations, but for very shallow geotherms (5°C/km) the agreement is fair, largely because the record of rapid cooling is pushed to structural levels deeper than are exposed in the range.

In the second model we cool the block at a constant rate from 80 to 5 Ma, corresponding to slow and continuous erosional removal of overburden, again followed by cooling at 5 Ma. As with the first model, the agreement with observations is reasonable only for a shallow geotherm (10°C/km). Steeper geotherms compress the zone of He partial retention, and cause overly sharp curvature in the model profiles. In fact, a shallow geotherm is a robust

requirement for any successful thermal model involving monotonic cooling and a constant geothermal gradient. A geotherm in the range of 5-10°C lies at the low end of reasonable values and is lower than has been reported from nearby in the Peninsular Ranges (Henyey and Wasserburg, 1971), but note that very low geothermal gradients have been proposed for western North America in the Tertiary (Dumitru, 1990).

Although these models fit some aspects of the profile fairly well, neither can reproduce the rapid age drop from the summit sample to the next highest sample. It is difficult to imagine any simple history which could produce this result, raising the possibility that a one-dimensional cooling model with a constant geothermal gradient is an oversimplification of the real history. Alternatively this age might be inaccurate, possibly suffering from excess He, a phenomenon known to occur at least in some hydrothermal apatites (Lippolt et al., 1994). Further dating of samples from the vicinity of the summit of San Jacinto peak, and also at deeper structural levels (e.g., 3-4 km) are required to more fully evaluate the cooling history of this range.

## 5.4 Conclusions

Apatite (U-Th/He) ages in the San Jacinto Mountains range from 79 to 17 Ma and are much younger than those obtained by U/Pb, K/Ar and fission track dating. In addition, unlike these other ages the He ages correlate with elevation. The simplest interpretation of the He ages is that they record the latest low temperature thermal evolution of the San Jacinto block and reflect extended

residence of the block at temperatures where radiogenic He is only partially retained, i.e., between ~75° and 40°C. Variations of He age with structural position provide no evidence for proposed rapid cooling of the entire block during the Laramide Orogeny (George and Dokka, 1994). In addition, despite its suggestive geologic setting, the He ages, all in excess of 17 Ma, do not require dramatic tectonic uplift associated with convergence of the San Jacinto block with the Transverse ranges in the last 5 m.y. Independent of the block's cooling history, the precision available on He ages coupled with the correlation between He age and elevation allows us to suggest modest westward tilting of the block and substantial vertical motion on one of the block's bounding faults. Both the tilting and fault motion must have occurred when most of the exposed block was at fairly low temperatures (<75°C), such that He retention had begun. Further chronometric and geomorphologic investigations are in progress to more fully constrain the range's late stage thermal and tectonic evolution.

In agreement with laboratory observations (Zeitler et al., 1985; Wolf et al., 1996), this work demonstrates that apatite (U-Th)/He ages record geologically useful information in samples which have cooled slowly.

*Acknowledgments*

This work was supported by the National Science Foundation. Detailed reviews by Trevor Dumitru and Mark Brandon greatly improved this paper. We thank Brian Wernicke for helpful comments throughout the course of this work.

## 5.5 References Cited

Ague J., and Brandon M. (1992) Tilt and northward offset of Cordilleran batholiths resolved using igneous barometry. *Nature*, 360, 146-149.

Atwater T. (1970) Implications of plate tectonics for the Cenozoic tectonic evolution of western North America. *Geological Society of America Bulletin*, 81, 3513-3536.

Dumitru T. (1990) Subnormal Cenozoic geothermal gradients in the extinct Sierra Nevada magmatic arc: consequences of Laramide and post-Laramide shallow angle subduction. *Journal of Geophysical Research*, 95, 4925-4941.

Farley K., Wolf R., and Silver L. (1996) The effects of long alpha-stopping distances on (U-Th)/He ages. *Geochimica et Cosmochimica Acta*, 60, 4223-4230.

Fitzgerald P., and Gleadow A. (1990) New approaches in fission track geochronology as a tectonic tool: examples from the Trans-Antarctic Mountains. *Nuclear Tracks and Radiation Measurement*, 17, 351-357.

Fitzgerald P., Sorkhabi R., Redfield T., and Stump E. (1995) Uplift and denudation of the central Alaska Range: A case study in the use of apatite fission track thermochronology to determine absolute uplift parameters. *Journal of Geophysical Research*, 100, 20175-20191.

Fraser D. (1931) Geology of the San Jacinto Quadrangle south of San Gorgonio Pass, California. *Report of the State Mineralogist, California State Mining Bureau*, 27, 494-540.

George P., and Dokka R. (1994) Major late Cretaceous cooling events in the eastern Peninsular Ranges, California, and their implications for Cordilleran tectonics. *Geological Society of America Bulletin*, 106, 903-914.

Henyey T., and Wasserburg G. (1971) Heat flow near major strike-slip faults in California, *Journal of Geophysical Research.* 76, 7924-7946.

Hill R. (1984) Petrology and petrogenesis of batholithic rocks, San Jacinto Mountains, southern California. Ph.D. thesis, Pasadena, California Institute of Technology.

Hill R. (1988) San Jacinto intrusive complex. 1. Geology and mineral chemistry, and a model for intermittent recharge of tonalitic magma chambers. *Journal of Geophysical Research*, 93, 10325-10348.

Lippolt H.J., Leitz M., Wernicke R.S., and Hagedorn B. (1994) (U+Th)/He dating of apatite: experience with samples from different geochemical environments. *Chemical Geology*, 112, 179-191.

Silver L., and Hill R. (1986) U-Th-Pb microdiscordance in young zircons: a case study in the San Jacinto Mountains. *EOS, Transactions of the American Geophysical Union*, 67, 399-400.

Smith D., Morton D., and Miller F. (1991) Hornblende geobarometry and biotite K-Ar ages from the northern part of the Peninsular Ranges Batholith, Southern California. *Geological Society of America, Abstracts With Programs*, 23, A273.

Stuwe K., White L., and Brown R. (1994) The influence of eroding topography

on steady-state isotherms - application to fission track analysis. *Earth and Planetary Science Letters*, 124, 63-74.

Suppe J., and Armstrong R. (1973) Potassium-Argon geochronometry of Mesozoic igneous rocks in Nevada, Utah, and southern California. *Geological Society of America Bulletin*, 84, 1375-1391.

Wagner G.A., and Reimer G.M. (1972) Fission track tectonics: the tectonic interpretation of fission track ages. *Earth and Planetary Science Letters*, 14, 263-268.

Wernicke B., and Axen G. (1988) On the role of isostasy in the evolution of normal-fault systems. *Geology*, 16, 848-851.

Wolf R.A., Farley K.A., and Silver L.T. (1996) Helium diffusion and low temperature thermochronometry of apatite. *Geochimica et Cosmochimica Acta*, 60, 4231-4240.

Zeitler P.K., Herczig A.L., McDougall I., and Honda M. (1987) U-Th-He dating of apatite: a potential thermochronometer. *Geochimica et Cosmochimica Acta*, 51, 2865-2868.

## 5.A Appendix: The Potential for Helium Dating of Sphene, Allanite, and Zircon

### *5.A.1 Results from Tonalites of the San Jacinto Block*

Chapter 5 is an example of the application of apatite helium thermochronometry to an uplifted Mountain block, the San Jacinto mountains, California. The batholith is a well mapped rigid block which is petrologically homogeneous. Moreover, the crystallization and high temperature history have been well characterized by the use of the U/Pb (L.T. Silver, personal communication; Silver et al., 1979) and K/Ar methods (Armstrong and Suppe, 1973). Therefore, in some reconnaissance experiments, we used samples from the San Jacinto mountain block to ascertain the utility of (U-Th)/He dating of mineral phases other than apatite.

Using the methods described in chapter 2, we analyzed allanite, sphene, and zircon from a tonalite sample, CL. While the zircon and sphene show little or no effects of radiation damage, the allanite is clearly metamict (L.T. Silver, personal communication). We also analyzed sphene from other tonalites in the San Jacinto block (SC, SJP, KW, and PS) (Table 5A1). Initially, helium extraction was done at ~1050°C for 30 minutes as in the case of apatite (the temperature was calibrated using an optical pyrometer), but this required multiple reextraction steps at temperatures >1100°C. Samples whose quantitative helium extraction is suspect are labeled with an asterisk in Table 5A1. Samples which had reextraction steps at >1250°C provided no additional helium, and we assume quantitative helium extraction in these cases. Because

uranium, thorium, and helium were not run on the same aliquot, and quantitative helium extraction was not achieved in every case, there are considerable uncertainties on these analyses.

The sphene and allanite crystals were several hundred microns to >1 millimeter in diameter, and therefore require no significant alpha emission correction. The zircon was taken from a sieve fraction similar to one used in the alpha emission study (Farley et al., 1996; chapter 1, this volume); thus, to make an alpha emission correction, we used the value calculated for the previous study. Three sphene analyses on CL yield a mean age of 68 Ma. The helium age obtained from a single zircon analysis from CL is 72 Ma. A single allanite analysis from sample CL yields a helium age of 52 Ma. The sphene from CL did yield reproducible results, and CL was also the only sample for which we analyzed allanite and zircon. By using this reconnaissance study with other thermochronometric data, we can estimate the closure temperature for helium in these phases.

*5.A.2 Discussion of Preliminary Results*

Using the closure temperature formulation, we can plot the U/Pb, K/Ar, and (U-Th)/He apatite ages as a function of temperature for CL (Figure 5A1). The U/Pb analyses were previously conducted on CL (L.T. Silver, personal communication), and the K/Ar biotite and hornblende ages are extrapolated from samples collected in proximity to CL (Armstrong and Suppe, 1973). There are a limited number of K/Ar ages on biotite and hornblende from samples

| Sample | Mineral | Mass (mg) | He (nmol/g) | U (ppm) | Th (ppm) | $F_T$ | Helium Age (Ma) |
|---|---|---|---|---|---|---|---|
| CLs1 | sphene | 3.56 | 98.61 | 212.13 | 210.15 | 1 | 69 |
| CLs2 | sphene | 1.40 | 102.3 | 212.13 | 210.15 | 1 | 72 |
| CLs3 | sphene | 1.54 | 91.49 | 212.13 | 210.15 | 1 | >64* |
| CLa1 | allanite | 2.75 | 769.5 | 158.22 | 11000 | 1 | 52 |
| CLz1 | zircon | 1.76 | 190.2 | 702.15 | 197.36 | 0.65 | 72 |
| PSs1 | sphene | 2.86 | 9.64 | 28.40 | 21.98 | 1 | >53* |
| PSs2 | sphene | 2.18 | 11.0 | 28.40 | 21.98 | 1 | 60 |
| SJPs1 | sphene | 2.15 | 101.2 | 201.00 | 314.00 | 1 | >68* |
| SJPs2 | sphene | 2.64 | 123.5 | 201.00 | 314.00 | 1 | 82 |
| KWs1 | sphene | 2.64 | 68.66 | 118.00 | 217.50 | 1 | >74* |
| KWs2 | sphene | 2.91 | 82.7 | 118.00 | 217.50 | 1 | 90 |
| SCs1 | sphene | 1.40 | 51.64 | 104.30 | 213.50 | 1 | >61* |
| SCs2 | sphene | 1.74 | 76.35 | 104.30 | 213.50 | 1 | 90 |

* Refers to samples where quantitative helium extraction is suspect

**Table 5A1.**

Sphene, allanite, and zircon data from the San Jacinto Mountain block, California. U and Th concentration measurements were made by thermal ionization mass spectrometry on separate splits. Sphene and allanite grains were large enough that the alpha emission correction is <5%. The zircon was sieved in the passed 200 mesh fraction, and therefore, we use the alpha emission correction for the CL apatite Pass 200 mesh fraction described in Farley et al. (1996a).

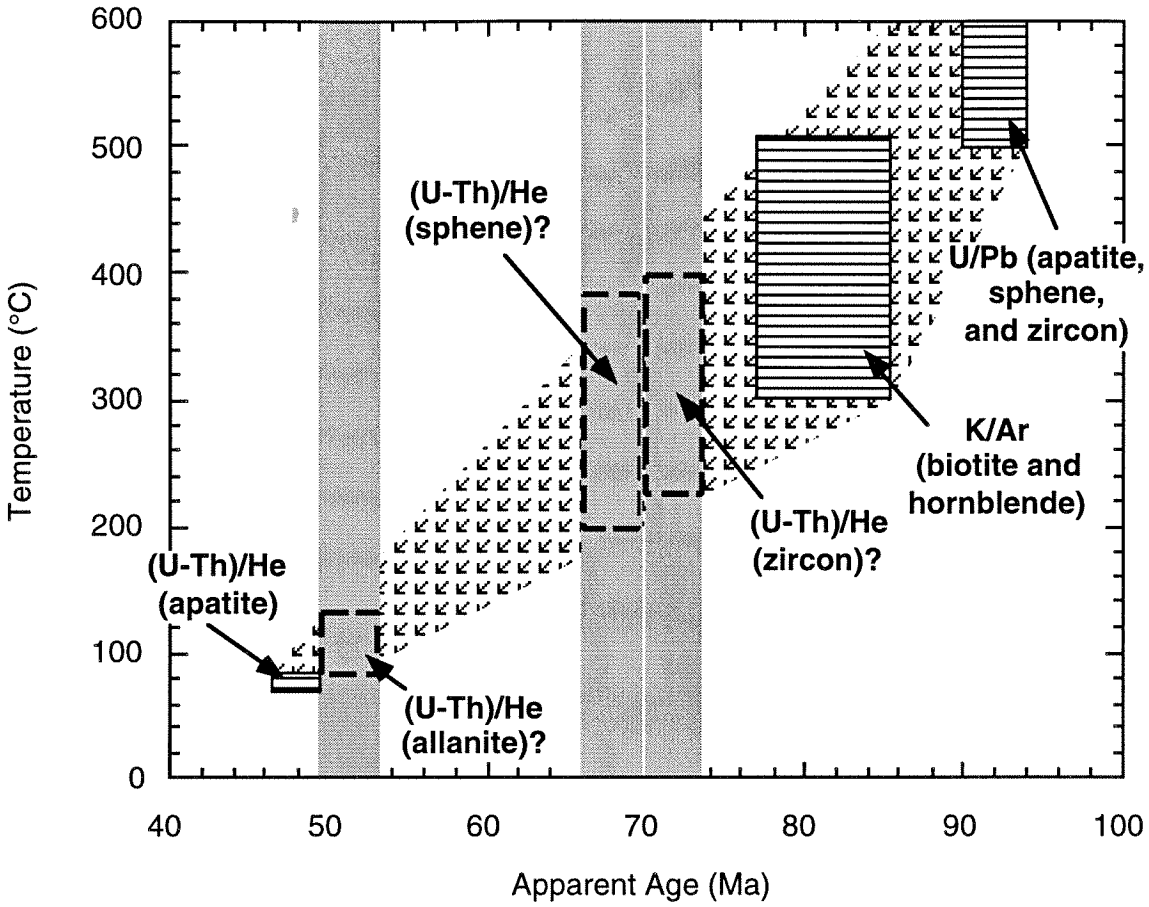


**Figure 5A1.**

U/Pb and helium age data from CL. U/Pb age is from L.T. Silver (personal communication). K/Ar data (Armstrong and Suppe, 1973) extrapolated from samples adjacent to CL. We use the mean age measured on replicate sphene analyses, and two single measurements of zircon and allanite. The grey bands represent the helium ages on sphene, allanite, and zircon, and they extend the length of the plot because their closure temperature is unknown. The width of the grey bands is schematic and does not represent an uncertainty. Assuming constant cooling (arrows), the intersection of the cooling path and the grey bands suggests a closure temperature for each of the phases (dashed boxes).

adjacent to CL. Even though biotite and hornblende have different closure temperatures (Harrison, 1981; Harrison and McDougall, 1985), the apparent ages measured on these phases from tonalites in proximity to CL are similar. Since we have to extrapolate these values to what we think the K/Ar apparent ages are on CL, we plot the data for both biotite and hornblende in one large group (Figure 5A1).

By plotting the allanite, sphene, and zircon helium ages on the same diagram, we can make some inferences about the relative helium retentivity of these phases. We assume that a constant rate of cooling occurs between the temperatures corresponding to the biotite and hornblende K/Ar ages and the apatite helium age. Because the helium ages on allanite, sphene, and zircon all lie between the K/Ar ages and the apatite helium age, their closure temperatures must be between 75°C (closure temperature for apatite, Wolf et al., 1996) and 310°C (closure temperature for biotite, Harrison and Mcdougall, 1985). With the assumption of a constant rate of cooling, we can infer that the closure temperature for sphene and zircon is probably in the ~225°C-350°C range. If we believe that the allanite helium age is not affected by metamictization, then the inferred closure temperature for allanite is in the ~100-200°C range.

### *5.A.3 Conclusions and Suggested Future Work*

Although the uncertainties are large, the sphene and zircon helium ages from CL are indistinguishable, suggesting that these two phases may have a

similar value for their closure temperatures. Both minerals are common accessory phases in igneous rocks, and both phases have higher uranium and thorium abundances than apatite. As a result, both phases tend to have higher concentrations of radiogenic helium than apatite, which makes the ability to analyze smaller samples such as single crystals much easier than apatite. Single crystal analyses are desirable because it is easier to handle a single grain than ten grains both in terms of analysis and making the alpha emission correction. Sphene tends to have a significantly larger grain size than zircon, and thus, the alpha emission corrections will be smaller. If the closure temperature of sphene and zircon is the same, sphene has greater utility for helium dating because of the relative alpha emission corrections. Allanite has a helium age which is only slightly greater than the apatite helium age. This may mean that allanite has a low closure temperature like apatite, or it may simply be an indication that the observed radiation damage to the allanite crystals has made helium more diffusive in the sample. The effect of radiation damage on helium diffusivity was previously observed in zircon by Damon and Kulp, (1957). This observation may have implications for the effects of radiation damage on diffusivity in allanite. Nonetheless, helium diffusivity from allanite may be affected by metamictization and, therefore, allanite may not be a reliable thermochronometer. High precision helium ages and incremental outgassing experiments are necessary to understand the helium retentivity of allanite, sphene, and zircon, so that these phases can be used for thermochronometry.

# Chapter 6

## Analytical Instrumentation

R.A. Wolf
K.A. Farley

### 6.1 Diffusion Experiments

*6.1.1 Introduction*

This section describes in detail the mechanical operations of the apparatus used for making helium diffusion experiments. We present a description of this instrumentation because it was a critical aspect of our ability to make incremental outgassing experiments, and it illustrates the factors we were concerned with when making these analyses. The development of a new method for diffusion measurements was critical to making high precision analyses at low temperatures (<100°C). Previous helium incremental outgassing experiments used methods derived primarily from argon diffusion experiments, and were geared towards diffusion at high temperatures (>200°C) over time increments of 30 minutes to an hour (Zeitler et al., 1987; Lippolt et al., 1994). In trying to improve on previous determinations, we were concerned with designing an instrument which would allow the ability to run long duration (up to three weeks) experiments at <100° and which would make the most precise temperature measurements possible. By making analyses at <100°C, we would greatly reduce the extrapolation to the closure temperature on an Arrhenius

plot. However, low temperature analyses required temperature steps which lasted as long as a few weeks in order to produce a significant amount of helium, and therefore, it was necessary to create an apparatus which would maintain thermal stability for up to a few weeks. We were concerned with the precision of the temperature measurement because during a 300°C temperature step, an uncertainty of a few °C is relatively small, but at 100°C an uncertainty of a few °C would result in profound uncertainties in the diffusivity. After many attempts, we designed a diffusion apparatus for making these analyses.

*6.1.2 Instrument Design*

Incremental outgassing experiments were conducted using a resistively heated furnace which slipped around the exterior of a stainless steel crucible which has a 3/4" outer diameter and a 3/8" inner diameter (Figure 1). The initial two experiments were made with a slightly different configuration than the later experiments. In the first two incremental outgassing experiments (CL1 and CL2, chapter 2), the samples were loaded into a sintered stainless steel capsule with a 1/4" diameter and a 0.5 μm pore space. The resistively heated coil in the furnace was ~3 cm long so that the hot zone in the furnace was much larger than the sample capsule. This ensured that the sample was uniformly heated in all directions. A slit was drilled into the bottom of the stainless steel crucible to house a K-type thermocouple, and the thermocouple resided ~0.5 cm from the sample capsule. The furnace temperature controller was regulated by this

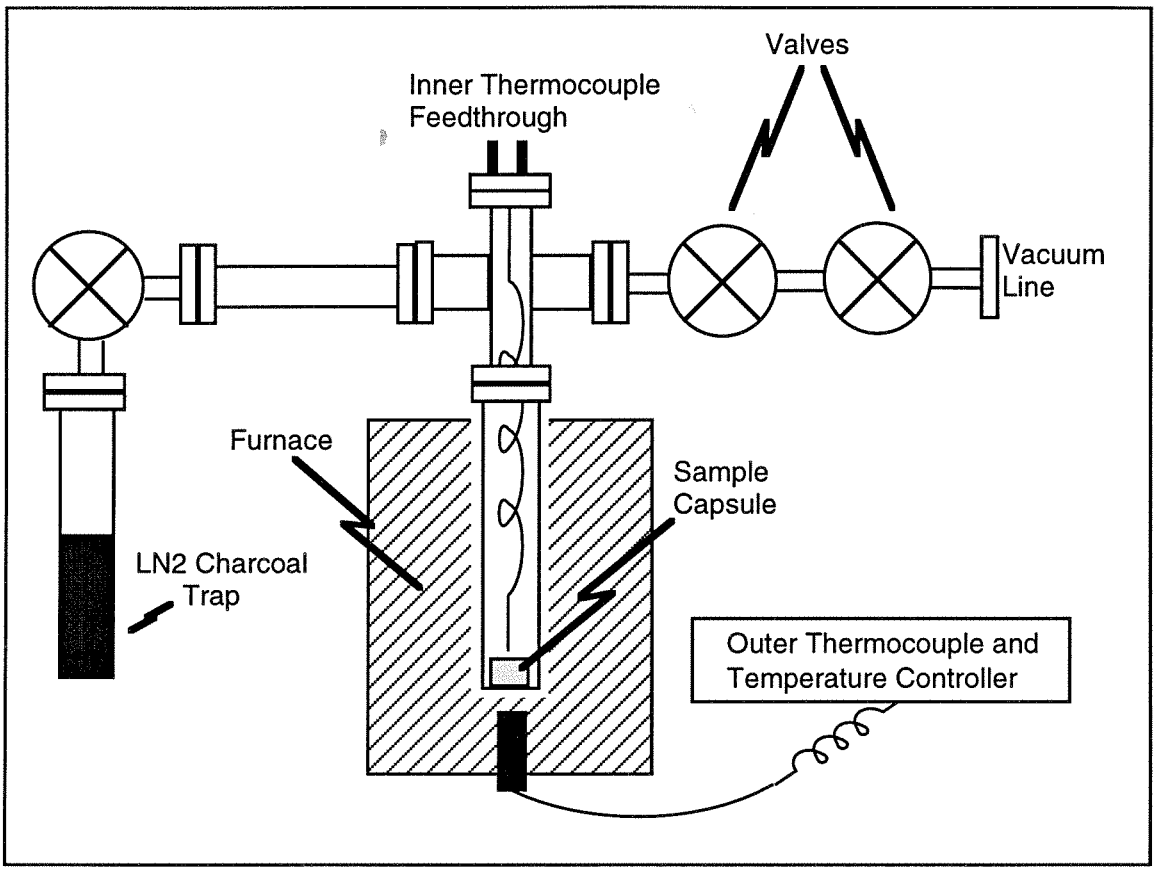


**Figure 1.**

Illustration of the diffusion apparatus. Only the outer thermocouple was used in the first two incremental outgassing experiments. The apparatus was changed to include an insulated in vacuo thermocouple which was in thermal contact with the apatite crystals.

thermocouple. One shortcoming of this configuration was that the time required to reach the setpoint was often several minutes to a half an hour. The first two experiments, CL1 and CL2, relied only on the exterior thermocouple as a measure of sample temperature. Unfortunately with this design, the effect on the sample temperature from an initial overshoot of the setpoint could not be resolved because we could not determine the effect of the thermal lag between the sample and the thermocouple. This resulted in large temperature uncertainties for experiments CL1 and CL2, and when there was an overshoot of the setpoint, it made it almost impossible to determine the appropriate temperature for the step.

To improve our precision on measuring the temperature, we added an invacuo K-type thermocouple (high precision rating for low temperatures) which was in close proximity to the grains. We changed our sample capsule to a copper cup to promote thermal equilibrium between the sample and the capsule. The thermocouple junction was made just inside the lip of the cup adjacent to the grains themselves. We retained the outer thermocouple to feed the temperature controller and to monitor the thermal lag between the outside of the crucible and the grains. We learned that there was indeed a significant thermal lag between the outer thermocouple and the invacuo thermocouple. We believe that the invacuo thermocouple improved our ability to measure the temperature of the sample, and we report a precision of ±1° to ±4°C on the temperature increments based on temperature oscillations during each step (Wolf et al., 1996; chapter 2, this volume).

*6.1.3 Conclusions*

As with any analytical technique, we may have achieved a high degree of precision, but not accuracy. However, we believe that we defined and addressed the most important problems surrounding low temperature diffusion experiments. We showed that it is possible to extract a significant amount of helium within a few degrees of the closure temperature. This greatly reduces the extrapolation to the closure temperature from laboratory data. Future instruments designed to improve on our system should do so by improving the ability to achieve the setpoint quickly and with no overshoot.

## 6.2 Quadrupole Vacuum Line

*6.2.1 Introduction*

The quadrupole vacuum line is an automated vacuum line connected to a quadrupole mass spectrometer used for measuring helium amounts (Figure 2), and it was built in the course of this work to have an instrument dedicated to helium thermochronology. The details on how helium ages are measured, either using the MAP 215-50 sector mass spectrometer or the Balzers QMS 064 quadrupole mass spectrometer, are described in sections of Chapters 2 and 4. The following is a description of the instrumentation that was built in the course of the thesis and used to make the analyses. The reason for creating a dedicated system for making these measurements was to reduce the number of $^4$He analyses on the MAP 215-50 sector mass spectrometer, but also determine

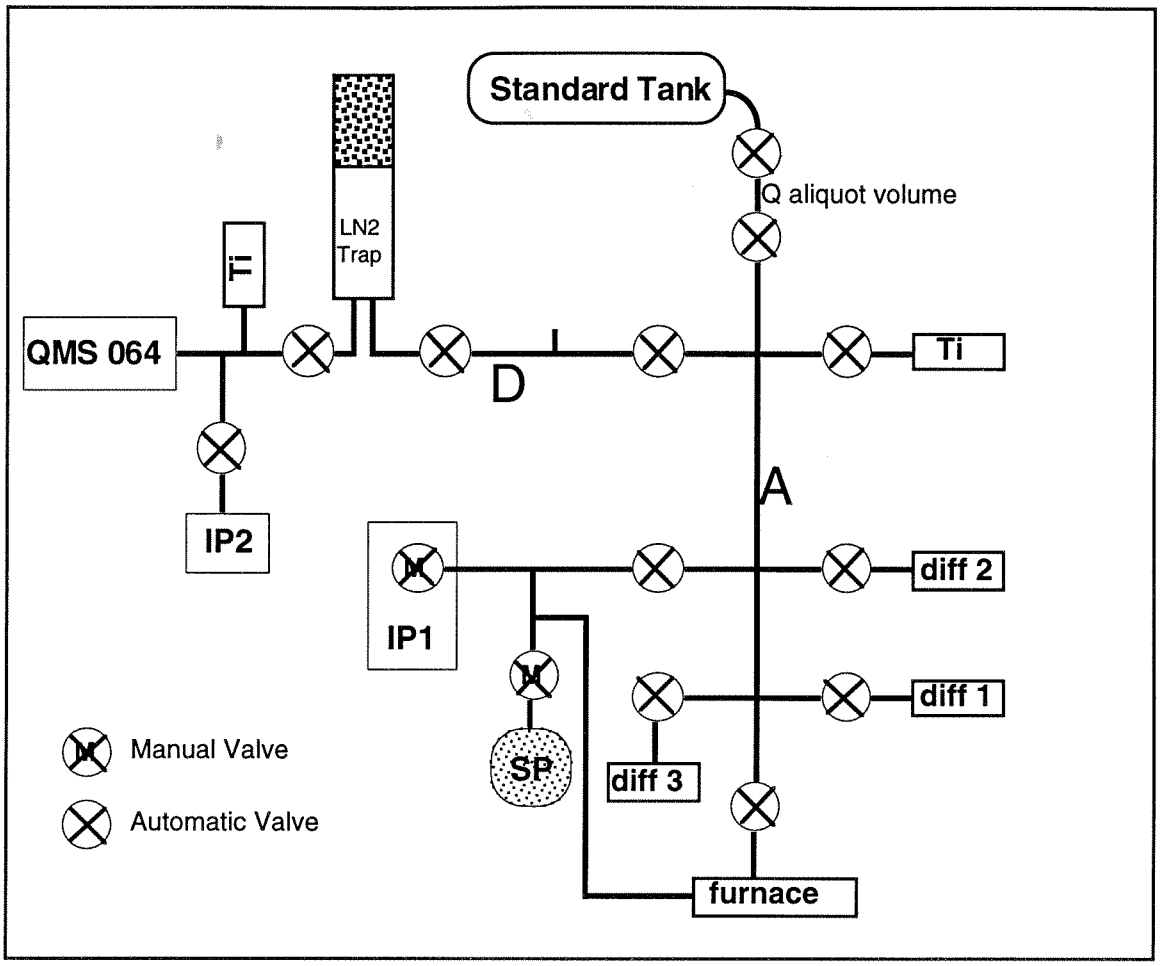


**Figure 2.**

Illustration of the helium thermochronometry vacuum line. QMS 064 is the quadrupole mass spectrometer, Ti represents the titanium getters, IP1 and IP2 are the ion pumps, SP is a sorption pump, and diff represents port for a diffusion apparatus. **A** is main line volume, **D** is the split volume used to reduce the amount delivered by a standard, and **Q** is the standard aliquot volume.

whether $^4He$ amounts could be measured with high precision on a less expensive, less complicated vacuum line using a quadrupole mass spectrometer.

*6.2.2 Instrument Design and Specifications*

Helium is measured using a quadrupole mass spectrometer, the Balzers QMS 064. The vacuum line is fully automated, and includes four ports which could be dedicated to diffusion experiments and one port for total outgassings. Nearly all the samples in chapter 4 were run using this vacuum line. The vacuum line itself, not including the electronics, takes up less than ~1 $m^3$. Samples and standards are purified using two titanium sponge getters and a flow-through charcoal trap held at liquid nitrogen temperatures to trap heavier species like $N_2$, $CO_2$, Ar, and $H_2O$. The titanium getters were added primarily to trap $H_2$, because $H_2$ was observed to interfere with the helium signal on the quadrupole, and large amounts of $H_2$ were being generated during sample heating and by the quadrupole filament.

Like the MAP 215-50 vacuum line, helium is measured by peak height comparison to a pure helium standard. The pure helium standard on this vacuum line was cross-calibrated against the working helium standard on the MAP 215-50 vacuum line (Wolf et al., 1996, chapter 2, this volume). Three separate cross-calibrations, corrected for tank depletion, demonstrate that the amount delivered by the standard is known to within 2%. The reproducibility of separate cross-calibrations is an additional confirmation of the standard tank

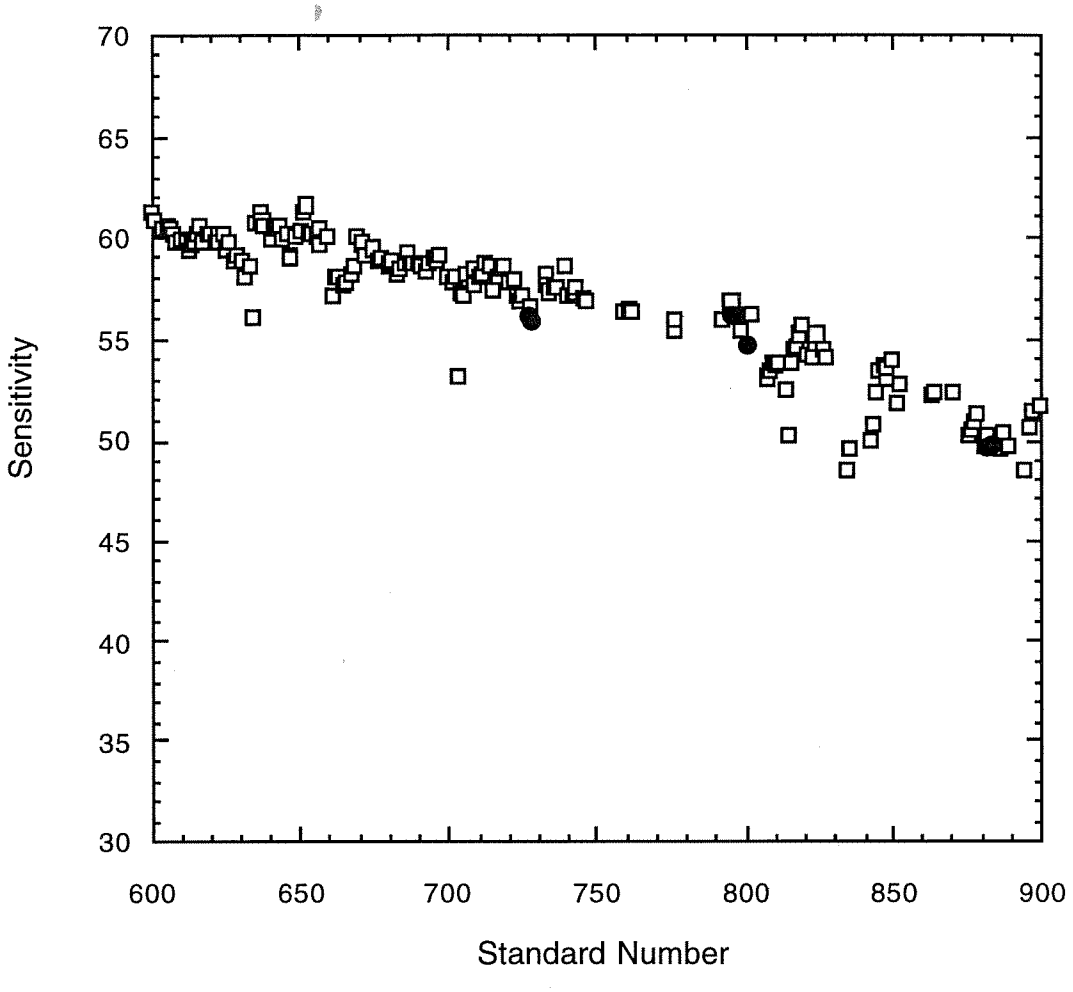


**Figure 3.**

Plot of the change in quadrupole sensitivty with time. Sensitivty is the ratio of the signal intensity to the known amount delivered by the standard (100%) (corrected for tank depletion). Boxes represent the change in sensitivity of the standard. Outliers are mostly related to saturation of the Ti getters. Circles represent cross calibration to another pure helium standard. Overlap of the two data sets suggests that the tank depletion correction is accurate.

depletion correction (Figure 3).

The reproducibility of standards becomes worse as sample size decreases. At ~3 pmol, the 1σ uncertainty on pure helium standards is 1.7%, but at ~0.1 pmol (comparable to the amount of helium delivered by many samples) the 1σ uncertainty is slightly better than 4%. This is to be compared with the estimated accuracy of helium measurements reported for the MAP 215-50 of better than 2% (Wolf et al., 1996a; chapter 2, this volume). Unlike the MAP 215-50, however, the pressure linearity of the quadrupole appears to be quite linear over a significant range of helium amounts (Figure 4).

The lower limit of our ability to make a helium measurement on a sample is determined by the helium blanks. A typical line blank on the quadrupole vacuum line is ~2 femtomol, but the blanks from a hot furnace form a Gaussian distribution about 12 femtomol (Figure 5). This is to be compared with furnace blanks of ~1 femtomol on the MAP 215-50 vacuum line. Future modifications will include a different furnace apparatus. The new furnace apparatus combined with repeated baking of the vacuum line and the quadrupole mass spectrometer itself may help drive the blanks down. We are also planning to add a cryogenic trap which can reach temperatures low enough to trap helium (<16°K) and allow us to analyze helium over a much smaller volume. The new trap will allow us to release helium into the quadrupole mass spectrometer without releasing other species like neon. This should also help lower the detection limit.

**Figure 4.**

Plot showing the pressure linearity of the quadrupole mass spectrometer. Standards are split using the different line volumes to deliver different amounts of helium. The amount delivered by the split fraction is known because the line volumes are known. If the ratio of the signal intensity to the known amount for each of the different splits of the standard is equivalent to the ratio of the signal intensity to the known amount in an unsplit standard, then the instrument has a linear response. Since standards are run over the course of many days, we normalize the standards to the average ratio of signal intensity to known amount for the unsplit standards for each day. By plotting this normalized ratio against the known amount delivered by the standards, we derive the pressure linearity for the instrument.

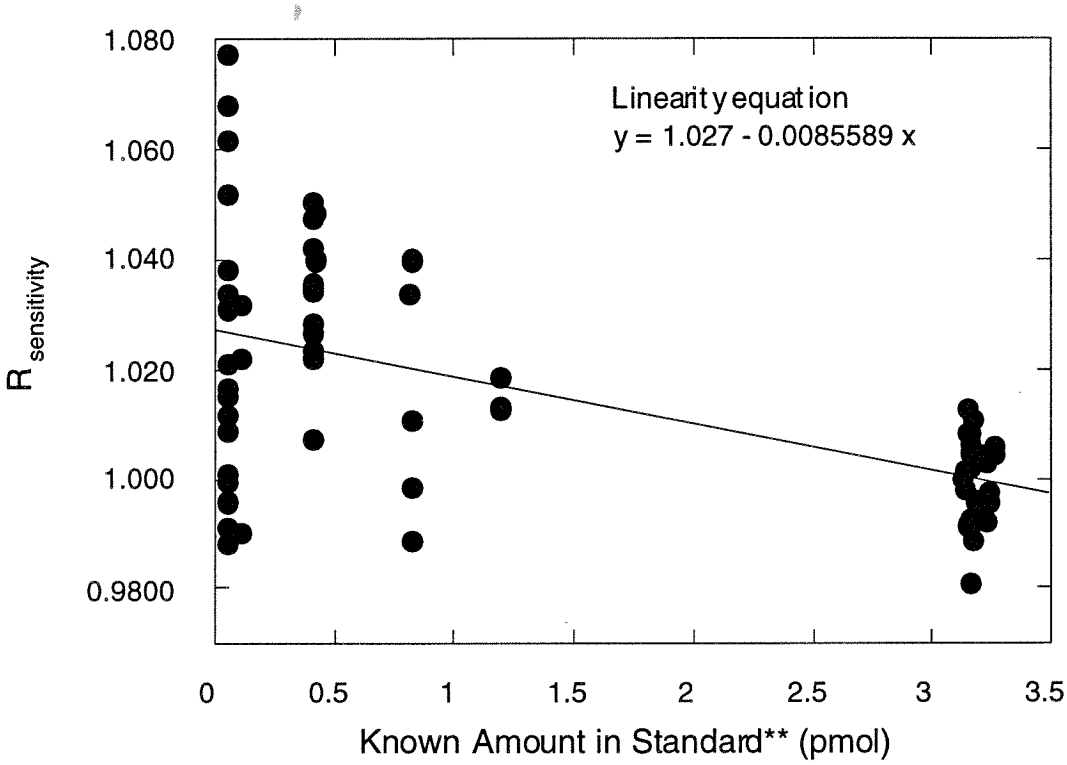


$$R_{sensitivity} = \frac{(\text{signal intensity/known amount})_{\text{standard split fraction}}}{(\text{signal intensity/known amount})_{\text{average of unsplit standards run on the same day}}}$$

** known amount in the standard split fraction [(pmol in each Q drawn, corrected for standard depletion) * known split fraction]

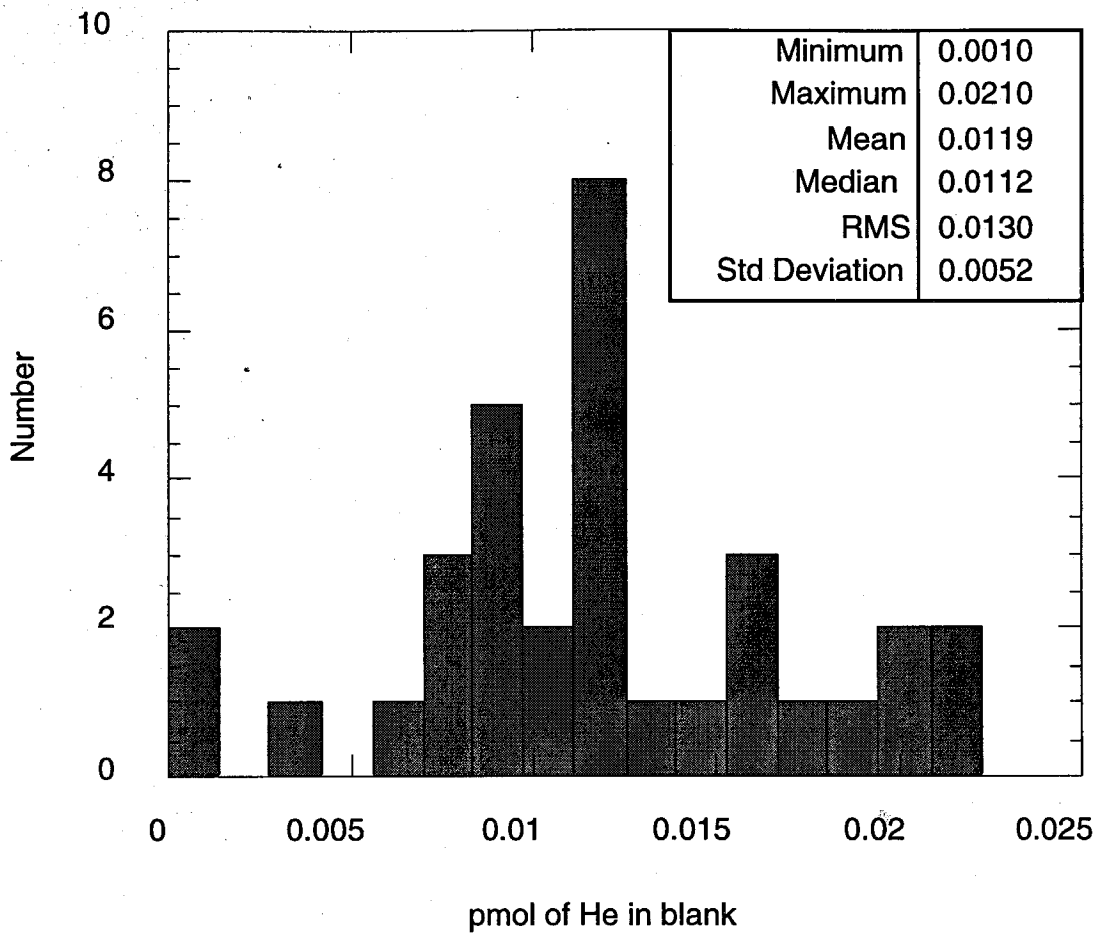


**Figure 5.**

Histogram of the blank measurements from the hot furnace. The mean value is about 12 femtomol with a standard deviation of about 5 femtomol.

### *6.2.3 Conclusions*

The quadrupole vacuum line is a demonstration that helium amounts at the level of ~0.1 pmol can be measured to better than 4% (1σ uncertainty) precision by peak height analysis using a quadrupole mass spectrometer. This is only slightly worse than the MAP 215-50 sector mass spectrometer. Unlike the MAP 215-50, we cannot measure $^3$He. However, the pressure non-linearity correction for the quadrupole is apparently less than for the MAP 215-50. Currently, the blanks are an order of magnitude higher on the quadrupole vacuum line, and thus, the detection limit is that much worse. However, we believe that we can drive the blanks down and lower the detection limit with some slight modifications. With these additional modifications, we may be able to achieve precision on helium analyses equal to the MAP 215-50.

# Appendix A

## Atypical Helium Retentivity in Metamorphic Rocks from the Gold Butte Block, Southeastern Nevada

R.A. Wolf
P.G. Fitzgerald
K.A. Farley

### A.1 Introduction and General Overview

Fission track ages from the Gold Butte block, Virgin Mountains, Nevada, distinctly resemble the base of the fission track partial annealing zone when plotted as a function of sample position relative to the Cambrian unconformity (Fitzgerald et al., 1991). Fission track ages become essentially invariant with sample position starting at a depth of 1.4 km below the Cambrian unconformity, indicating that the samples were rapidly cooled as the block was tilted and exhumed at ~15 Ma (Fitzgerald et al., 1991). To test whether the cooling event at ~15 Ma also cooled through the helium partial retention zone, and to compare fission track and helium ages from an exhumed mountain block which preserves the fission track partial annealing zone, we measured helium ages on the same apatite samples.

Although we anticipated to see apatite helium ages which were less than or equal to the apatite fission track ages, we observed poor reproducibility of helium ages and some which were greater than the apatite fission track age.

We also observed two samples which yielded helium during reextraction steps at higher temperatures, which had never been observed previously with apatite. We now believe that micro-inclusions of monazite are responsible for the high and irreproducible helium ages. The following is a description of the experiments conducted on the samples from Gold Butte, and the conclusions inferred from the observations.

## A.2 Results

Apatite (U-Th)/He ages were measured on six samples from the Gold Butte block, Virgin Mountains, Nevada, using the methods described in chapter 4 (Table A1). Initially there was poor reproducibility on all of the samples, and in some cases, helium ages were higher than fission track ages. This was surprising since diffusion experiments indicated that the apatite fission track annealing temperature was higher than the apatite helium closure temperature (Wolf et al., 1996a). Sample VM-03 was especially puzzling because two analyses of the sample yielded helium ages which were an order of magnitude older than the fission track age. Inclusions of minerals with a high index of refraction under polarized light had been observed in some of the apatites from all the Gold Butte samples, and it was suspected that the cause of the additional helium in VM-03 and poor reproducibility of helium ages from other samples was from inclusions.

To determine whether inclusions were responsible for the high apparent ages measured on VM-03, two additional splits, VM-03(III) and VM-03(IV), were

| Sample | Age | F | He nmol/g | U ppm | Th ppm |
|---|---|---|---|---|---|
| 1(I) | 63.7 | 0.82 | 3.22 | 10 | 6.0 |
| 1(II) | 39.3 | 0.83 | 2.07 | 10 | 7.0 |
| 1(III) | 35.3 | 0.81 | 2.20 | 12 | 8.0 |
| 1(IV)* | 29.5 | 0.80 | 1.98 | 13 | 8.7 |
| 10a | 16.5 | 0.79 | 0.47 | 4.9 | 7.6 |
| 10(I) | 13.5 | 0.81 | 0.36 | 4.4 | 7.2 |
| 10(III) | 15.1 | 0.85 | 0.42 | 4.2 | 7.9 |
| 10(IV)* | 13.1 | 0.83 | 0.35 | 4.2 | 7.3 |
| 2(I) | 37.3 | 0.85 | 5.46 | 30 | 9.3 |
| 2(II)* | 28.0 | 0.87 | 4.45 | 33 | 5.4 |
| 2(III)* | 31.3 | 0.84 | 5.32 | 36 | 6.7 |
| 3(I) | 130 | 0.80 | 12.0 | 16 | 22 |
| 3(II) | 148 | 0.79 | 9.30 | 11 | 17 |
| 3(III)** | 364 | 0.81 | 24.3 | 11 | 18 |
| 5(I) | 29.4 | 0.85 | 4.70 | 28 | 27 |
| 5(II) | 21.8 | 0.83 | 3.04 | 26 | 22 |
| 5(III) | 19.8 | 0.86 | 3.39 | 29 | 33 |
| 5(IV) | 30.5 | 0.86 | 4.90 | 28 | 30 |
| 5(V)** | 24.5 | 0.85 | 3.35 | 24 | 25 |
| 6(I)* | 16.4 | 0.88 | 1.09 | 14 | 0.5 |
| 6(II) | 30.1 | 0.87 | 2.18 | 15 | 1.3 |
| 6(III) | 13.4 | 0.85 | 1.31 | 21 | 1.1 |
| 6(IV) | 27.9 | 0.84 | 2.12 | 17 | 0.7 |
| 6(V)* | 16.9 | 0.83 | 1.98 | 26 | 1.4 |

| Sample | Ce ppm | La ppm | Y ppm | Nd ppm | Sm ppm |
|---|---|---|---|---|---|
| 1(I) | 1316 | 543 | 587 | 177 | 31 |
| 1(II) | 1376 | 576 | 488 | 171 | 28 |
| 1(III) | 1732 | 700 | 630 | 215 | 35 |
| 1(IV) | 1573 | 567 | 711 | 227 | 39 |
| 3(I) | 2068 | 740 | 803 | 260 | 42 |
| 3(II) | 1503 | 565 | 391 | 181 | 26 |
| 3(III) | 1396 | 527 | 478 | 179 | 28 |
| 5(I) | 1116 | 355 | 746 | 192 | 38 |
| 5(III) | 1539 | 525 | 745 | 236 | 41 |
| 5(IV) | 2008 | 655 | 913 | 320 | 56 |
| 5(V) | 1868 | 655 | 833 | 278 | 47 |
| 6(I) | 1073 | 286 | 1715 | 249 | 66 |
| 6(II) | 1083 | 300 | 1580 | 247 | 65 |
| 6(III) | 382 | 86 | 1861 | 117 | 43 |
| 6(IV) | 1423 | 382 | 1704 | 319 | 84 |
| 10(I) | 1077 | 368 | 434 | 153 | 27 |
| 10(III) | 1279 | 432 | 545 | 185 | 33 |
| 10(IV) | 981 | 322 | 451 | 147 | 26 |

* Included a reextraction step at a higher temperature

** Yielded additional helium during reextraction step

| | VM-01 | VM-02 | VM-03 | VM-05 | VM-10 | VM-06 |
|---|---|---|---|---|---|---|
| FT age (Ma) | 50 | 48 | 34 | 14 | 17 | 15 |
| Depth (km) | 0.1 | 0.6 | 1.2 | 3.6 | 6 | 9.5 |

**Table A1.**

(U-Th)/He age data from Gold Butte apatites. Rare earth element data measured by ICP-MS and determined by peak height comparison to U and Th. Fission track data (Fitzgerald et al., 1991) includes reconstructed sample depth below the Cambrian unconformity. Helium was analyzed by quadrupole mass spectrometry except in the case of samples 5(I), 5(II), 10(III), 1(I), 1(II), and 1(III) which were analyzed on the MAP 215-50 sector mass spectrometer.

prepared by picking apatite grains using a petrographic microscope under low power and polarized light (to exclude apatites which may be contaminated by inclusions). Even though the samples were picked under polarized light, additional helium was released from VM-03(IV) when reextraction steps were done at higher temperatures, suggesting that there may be inclusions which were undetected during grain picking. Prior to this experiment, reextraction steps were not done routinely. Following the experiment on VM-03(IV), reextraction steps were done on all of the apatite samples from Gold Butte. In addition to VM-03(IV), two other samples, VM-03(III) and VM-05(V), yielded additional helium during reextraction steps. Quantitative extraction at 800°C was achieved for aliquots from VM-01, VM-02, VM-06, and VM-10, but was never demonstrated on aliquots from VM-03 or VM-05.

To determine the cause of the abnormal helium retentivity in VM-03(IV), the grains which were analyzed for helium were mounted in epoxy and polished for SEM and electron microprobe analysis. SEM photos depict the presence of micron sized monazite inclusions in VM-03(IV) apatites (Figure A1). To better characterize the inclusions found in VM-03(IV), the monazite inclusions and the apatite were analyzed for major and trace elements by electron microprobe analysis (Table A2).

Apatite grains were indiscriminately picked from the other samples (none of which were previously outgassed for helium analysis) and were also analyzed by SEM and electron microprobe analysis to determine the presence mineral inclusions. Inclusions of monazite were observed in apatites from VM-

| | element weight % | | | | | | | | | ppm | | |
|---|---|---|---|---|---|---|---|---|---|---|---|---|
| Sample | Ca | F | P | Cl | Ce | Y | La | Nd | Sm | Th | U | TOTAL |
| Durango Apatite Standard | 38.6 | 3.39 | 17.8 | 0.42 | 0.44 | ND | 0.38 | 0.10 | ND | 227 | 45 | 99.66 |
| VM-03(IV)a (monazite inclusion a1) | 1.51 | 0.69 | 14.3 | 0.01 | 28.1 | 0.06 | 21.1 | 5.75 | 0.49 | 807 | 93 | 100.55 |
| VM-03(IV)a (monazite inclusion a2) | 1.21 | 0.70 | 14.2 | ND | 28.2 | 0.06 | 21.8 | 5.86 | 0.45 | 541 | ND | 100.97 |
| VM-03(IV)a (monazite inclusion a3) | 0.95 | 0.65 | 14.3 | ND | 28.5 | 0.04 | 22.3 | 5.81 | 0.49 | 860 | ND | 101.7 |
| VM-03(IV)a (host apatite) | 38.1 | 3.22 | 17.8 | 0.12 | 0.54 | 0.08 | 0.18 | 0.29 | 0.01 | 240 | ND | 98.65 |
| VM-03(IV)b (host apatite) | 38.8 | 3.27 | 18.1 | 0.10 | 0.27 | 0.02 | 0.12 | 0.10 | 0.00 | ND | 64 | 99.6 |
| VM-03(IV)b (host apatite) | 38.2 | 3.22 | 17.6 | 0.13 | 0.91 | 0.12 | 0.36 | 0.49 | 0.05 | ND | 15 | 99.4 |
| VM-03(IV)b (monazite inclusion b1) | 1.10 | 0.71 | 14.4 | 0.01 | 29.1 | 0.06 | 21.2 | 6.21 | 0.51 | 519 | 6 | 102.32 |
| VM-01 (apatite) | 39.7 | 3.64 | 18.0 | 0.05 | 0.31 | 0.02 | 0.06 | 0.11 | 0.02 | ND | ND | 101.01 |
| VM-06 (host apatite) | 40.0 | 4.12 | 18.0 | 0.03 | 0.01 | 0.03 | ND | 0.08 | ND | ND | ND | 101.42 |
| VM-10 (host apatite) | 37.9 | 3.05 | 17.6 | 0.63 | 0.34 | 0.20 | 0.08 | 0.28 | 0.08 | ND | ND | 98.29 |
| VM-05 (apatite) | 39.0 | 3.19 | 17.8 | 0.16 | 0.28 | 0.05 | 0.13 | 0.13 | ND | ND | 86 | 99.33 |
| VM-10 (monazite inclusion a1) | 1.01 | 0.86 | 13.5 | 0.06 | 26.0 | 1.23 | 11.7 | 12.8 | 2.10 | 540 | ND | 96.28 |
| VM-06 (xenotyme inclusion a1) | 5.09 | 0.89 | 14.7 | 0.01 | 16.4 | 5.31 | 4.58 | 14.8 | 3.81 | ND | 501 | 94.64 |
| VM-06 (xenotyme inclusion b1) | 0.52 | 0.16 | 14.1 | 0.01 | 2.74 | 26.0 | 0.83 | 3.32 | 1.61 | ND | 187 | 76.26 |
| VM-06 (xenotyme inclusion c1) | 0.88 | 0.60 | 13.4 | 0.02 | 22.1 | 2.00 | 6.28 | 17.6 | 3.59 | 79 | ND | 93.04 |

**Table A2.**

Electron Microprobe data from Gold Butte apatites and their inclusions. U and Th were determined by comparison to $UO_2$ and $ThO_2$ standards.

10 and inclusions of xenotyme were observed in VM-06. This does not preclude their existence in other samples, because inclusions simply may not have been exposed during polishing.

Helium was extracted from VM-03(III) at 800°C for 30 minutes and then reextracted five times at higher temperatures each time. The number of pmol of helium yielded at each step was 1.164, 0.324, 0.111, 0.142, 0.089, and 0.02. This indicates that at least ~40% of the total helium was derived from a more retentive source than apatite. The samples were dissolved in concentrated nitric acid and warmed in a drying oven and on a hot plate for several hours in an attempt to dissolve both the apatite and any potential monazite inclusions. Uranium and thorium were analyzed by isotope dilution on an ICP-MS as described in chapter 4 (Table A1). VM-03(III) yielded a helium age of 365 Ma, even though the fission track age was 34 Ma.

## A.3 Discussion

Using the electron microprobe data from monazites in VM-03(IV), we can make some approximate calculations to determine whether it is reasonable for monazite inclusions to be responsible for the 365 Ma helium age recorded on VM-03(III). We start by assuming that monazite is responsible for the aberrant helium age and that the monazite was dissolved with the apatite (i.e., uranium and thorium from monaizte and apatite were analyzed by ICP-MS). We assume a concentration of 900 ppm thorium and 200 ppm uranium for the monazite

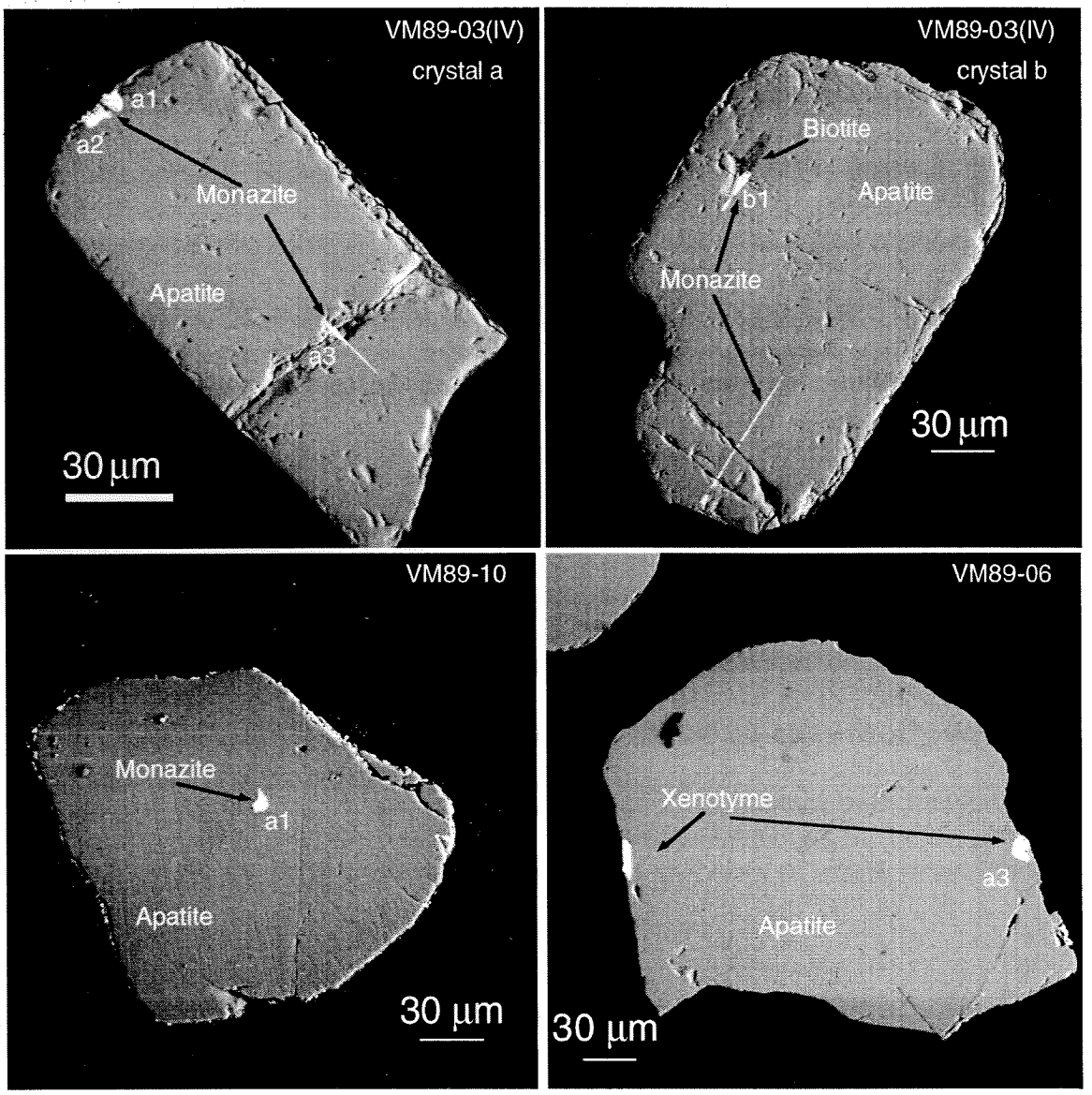


**Figure A1.**

Scanning electron microscope images of apatites from Gold Butte which depict the presence of monazite and xenotyme inclusions.

inclusions based on the maximum uncertainty of the electron microprobe analyses. We assume a mass fraction of monazite in the apatite and calculate the number of uranium and thorium atoms in the monazite (using 900 ppm Th and 200 ppm U). We choose a time over which we allow the uranium and thorium in the monazite to produce helium, and we calculate a number of helium atoms. We subtract the number of uranium, thorium, and helium atoms in the monazite from the ICP-MS and quadrupole mass spectrometer measured values, and we use the remaining number of uranium, thorium, and helium atoms to calculate a helium age for the apatite. With this model, we can vary the time for radiogenic ingrowth, the mass fraction of monazite, and also the fraction of helium atoms retained in the monazite after alpha emission (since the inclusions are quite small, the $F_T$ corrections should be quite large). We are limited in the assumed mass fraction of monazite inclusions both by what we observe under the SEM and by the measured amounts of uranium and thorium by ICP-MS.

If we assume that the uranium and thorium from the inclusions was analyzed and is part of the measured values from ICP-MS analysis, then the monazites must have retained helium for more than 34 Ma. Brady et al. (1996) showed that muscovite ages from samples collected at the same position relative to the Cambrian unconformity as VM-03 were 1.45 Ga. If the retentivity of helium in monazite is at least as great as the retentivity of argon in muscovite, then the monazite could have retained the ingrowth of 1.45 billion years of helium (excluding helium ejected into the apatite matrix during alpha emission).

If we use the calculations described above and allow monazite to retain helium for 1.45 Ga, then we could drive the age down to ≤34 Ma with a mass fraction of monazite of 2% and an $F_T$ for the monazite of 0.36. By these calculations, 96% of the helium we measured came from the monazite (~18 pmol), and 4% came from the apatite (~80 femtomol). There would be 1.36 pmol of uranium and 5.97 pmol of thorium in the monazite inclusions. This leaves 2.24 pmol of uranium and 3.06 pmol of thorium in the host apatite.

The emission correction for the calculation above may not be great enough, since the monazites are only microns across. If we want to lower the emission correction, then we must raise the mass fraction of the monazite in the apatite, raise the concentration of U and Th in the monazite, or increase the time allowed for radiogenic ingrowth. There is a balance between the fraction of inclusions, the emission correction, the helium age of the monazites, and the uranium and thorium concentration in the monazites. Nonetheless, we have shown in an approximate calculation that it is reasonable that the 365 Ma helium age measured on VM-03(III) could be the result of monazite inclusions which have retained helium since 1.45 Ga. However, it would be difficult to have monazite inclusions be responsible for the elevated helium ages and also have the monazite retain helium for much less than 1.45 Ga.

Monazite inclusions were not only observed in VM-03(IV). They were also observed in VM-10, and xenotyme was observed in VM-06. Even though inclusions were observed by SEM in these two samples, helium was not released during reextraction steps (although the samples analyzed by SEM

were never analyzed for helium). There were some elevated helium ages on VM-06 which could be explained by the presence of xenotyme, but VM-10 yielded consistently reproducible helium ages. The are a few possible explanations for this observation. It is possible that monazite has varying degrees of retentivity. Perhaps the monazite inclusions in VM-10 had a comparable diffusivity to apatite. This would explain the lack of helium yielded during reextraction steps. Another possibility is that the inclusions observed under the SEM in VM-10 were anomalous, and none of the replicates of VM-10 analyzed for helium ages actually contained monazite inclusions. Although we can speculate about the cause, we cannot explain the results based on our observations.

## A.4 Conclusions

In general, the results from the Gold Butte samples are difficult to understand, and we cannot conclude much about the thermal history of the block with any degree of certainty. However, there are two useful observations which have come from this work. The first is that two of the samples, VM-03 and VM-05, yielded additional helium during reextraction steps. This means that either the helium diffusivity from these apatites are aberrant as compared with other diffusion studies, or there are mineral and/or fluid inclusions which have a higher helium retentivity than apatite. VM-03(IV) contained monazite inclusions (observed by SEM analysis) which may be the cause of the additional retentivity. Calculations show that the monazite could cause the abnormally old

helium ages if it retained helium for >1.45 Ga. Although this is an interesting observation for the advancement of the helium dating method, it suggests that sample VM-03 is not suitable for comparison of apatite helium ages and apatite fission track ages from the Gold Butte block.

The second important observation from this work is that four of the samples never yielded additional helium during reextraction steps. In each case, only the youngest ages measured on the sample were ever reproduced. This may indicate that the older helium ages are the result of contamination from fluid and/or mineral inclusions. If we assume that the youngest ages are the accurate helium ages, then the helium ages are essentially in agreement with the interpretation of the fission track ages. The two helium ages near the Cambrian unconformity are less than the fission track ages and may represent the base of the helium partial retention zone. The two helium ages on samples several kilometers below the Cambrian unconformity are roughly equivalent to the fission track ages, suggesting that they represent rapid cooling and exhumation of the block at ~15-18 Ma. To precisely determine when the block was exhumed, it is necessary to collect samples from unmetamorphosed or lower grade rocks which may not have the complications of mineral inclusions and high helium retentivity exhibited by these samples. Certainly, a more comprehensive study is necessary to answer this question.

# Appendix B

## Characterization of Late Cenozoic Crust and Mantle Interaction Through the Analysis of Helium Isotopes in Basalts From the Central Great Basin, California

R.A. Wolf
K.A. Farley

### B.1 Introduction

Helium isotopic ratios are an unambiguous indicator of a mantle plume because $^3He/^4He$ ratios greater than 7-9 $R_A$ (where $R_A$ is the atmospheric $^3He/^4He$ ratio of $1.4 \times 10^{-6}$) are only found in rocks derived from a mantle plume source (this excludes $^3He/^4He$ which are elevated due to the production of cosmogenic $^3He$). To test the proposed hypothesis that there is a plume under the Central and Southern Great Basin, United States (Lachenbruch et al., 1994; Saltus and Thompson, 1995) or even that the Yellowstone plume is associated with extensional volcanism in the region (Parsons et al., 1994), we measured helium isotope ratios in olivine and pyroxene phenocrysts from Quaternary and late Tertiary basalts in the Central Great Basin, California.

In addition to determining the presence of a plume, helium in these basalts may help constrain, both temporally and spatially, the interactions between crust and mantle during a period of massive lithospheric thinning.

We studied basalts in a region bounded by the Coso volcanic field in the southwest, the Shoshone volcanics in the southeast, the basalts near Lathrop Wells in the northeast, and the Big Pine volcanic field in the northwest, including a few basalts from scattered vents in the high Sierra.

## B.2 Results

Helium isotopic ratios from olivine phenocrysts in lavas range from 7.7 $R_A$ (where $R_A$ is the atmospheric $^3He/^4He$ ratio of $1.4 \times 10^{-6}$) in the Coso volcanic field to 8.93 $R_A$ at the northern end of the Darwin Plateau (Table B1). These ratios are indistinguishable from those found in mid-ocean ridge basalts and support neither a mantle plume (high $^3He/^4He$) nor a crustal (low $^3He/^4He$) helium source. Major and trace element analyses were done on a few of the samples by XRF, ICP-ES, and ICP-MS at the Geological Survey of Canada (Table B2). The $SiO_2$ contents of these samples ranges from 48-57%, indicating that some of these rocks are not purely basaltic in composition and could be classified as andesites.

Pyroxenes from basalts whose age is greater than 4 Ma exhibit radiogenic helium (Figure B1). Figure B1 is a plot of sample age against $^3He/^4He$ ratio for olivines and pyroxenes. As part of this study, $^{40}Ar/^{39}Ar$ whole rock ages were measured on two of the samples, B1 and B2, by Dr. P.K. Zeitler at Lehigh University. The remaining ages are inferred by correlating our samples to samples whose ages are reported by Omerod (1988) and Schweig (1984,1982). In sample D1, the olivines yield a $^3He/^4He$ ratio of 8.1

| Sample | Phase | $^3He/^4He$ | Concentration (ncc/g) | Location | Latitude | Longitude |
|---|---|---|---|---|---|---|
| LAVAS | | | | | | |
| B1 | olivine | 8.2±.22 | 6.6 | Darwin Plateau | 36°30.50' | 117°33.88' |
| B2 | pyroxene | 0.16±.22 | 4.5 | Death Valley | 36°23.33' | 116°50.80' |
| B3 | olivine | 7.43±.29 | 7.5 | Coso | 35°50.05' | 117°52.50' |
| B4 | olivine | 7.7±.17 | 14 | Coso | 35°58.22' | 117°55.00' |
| B4 | pyroxene | 7.65±.3 | 13 | Coso | 35°58.22' | 117°55.00' |
| D1 | olivine | 8.1±.29 | 5.9 | Darwin Plateau | 36°24.44' | 117°48.07' |
| D1 | pyroxene | 3.5±1 | 1.2 | Darwin Plateau | 36°24.44' | 117°48.07' |
| D5-FL | olivine | 8.93±.3 | 4.1 | Darwin Plateau | 36°19.44' | 117°42.95' |
| BP8 | olivine | 7.4±.3 | 2.4 | Big Pine | 37°04.53' | 118°16.71' |
| LW13 | olivine | 8.26±.71 | 0.5 | Little Whitney | 36°21.63' | 118°19.29' |
| SH-1 | pyroxene | 0.92±.21 | 3.8 | Shoshone | 35°59.03' | 116°16.28' |
| RY-2 | olivine | 7.39±.75 | 15 | Ryan | 36°20.28' | 116°38.33' |
| XENOLITHS | | | | | | |
| WC11 | clinopyroxene | 7.4±.35 | 57 | Wacobacreek | 36°00.87' | 118°10.29' |
| WC11 | olivine | 8.99±.79 | 6.4 | Wacobacreek | 36°00.87' | 118°10.29' |
| W1 | orthopyroxene | 4.28±.44 | 2.4 | Wacobacreek | 36°00.87' | 118°10.29' |

**Table B1.**

Helium isotopic data for basalts from the central Great Basin, California. Two samples, BP8 and LW13, as well as the xenoliths were collected by Mihai Ducea.

| | B3 | B2 | SH-1 | RY-2 | D1 | B1 | B4 |
|---|---|---|---|---|---|---|---|
| Oxide | (weight %) | | | | | | |
| SiO2 | 54.70 | 57.30 | 56.50 | 54.30 | 50.10 | 48.10 | 53.40 |
| TiO2 | 1.64 | 1.58 | 1.47 | 1.90 | 1.74 | 1.43 | 1.84 |
| Al2O3 | 15.50 | 15.60 | 16.20 | 17.00 | 15.10 | 13.90 | 16.20 |
| FeO | 6.50 | 6.60 | 4.90 | 6.10 | 6.80 | 7.10 | 5.70 |
| MgO | 6.71 | 4.12 | 4.06 | 5.12 | 8.96 | 12.30 | 5.07 |
| MnO | 0.14 | 0.13 | 0.12 | 0.15 | 0.14 | 0.15 | 0.13 |
| CaO | 7.58 | 6.37 | 7.42 | 7.85 | 9.27 | 9.03 | 7.50 |
| Na2O | 3.64 | 3.59 | 3.66 | 3.50 | 3.09 | 2.81 | 3.76 |
| K2O | 1.63 | 2.42 | 2.01 | 1.70 | 1.28 | 0.79 | 1.71 |
| P2O5 | 0.10 | 0.21 | 0.27 | 0.39 | 0.30 | 0.27 | 0.18 |
| Element | (ppm) | | | | | | |
| Ba | 880 | 840 | 830 | 1100 | 540 | 400 | 920 |
| Ce* | 26 | 57 | 55 | 96 | 46 | 42 | 42 |
| Cl | 250 | 363 | 380 | 375 | 496 | 455 | 602 |
| Cr | 200 | 45 | 99 | 51 | 280 | 520 | 100 |
| F | 378 | 410 | 512 | 722 | 473 | 353 | 442 |
| Dy* | 2.20 | 3.50 | 3.50 | 3.70 | 3.30 | 3.40 | 2.90 |
| Er* | 1.20 | 2.00 | 1.90 | 1.90 | 1.70 | 1.90 | 1.60 |
| Eu* | 1.20 | 1.60 | 1.40 | 2.10 | 1.50 | 1.30 | 1.40 |
| Ga* | 18 | 19 | 19 | 21 | 16 | 15 | 20 |
| Gd* | 2.40 | 4.10 | 4.20 | 5.00 | 4.20 | 3.90 | 3.40 |
| Hf* | 4.30 | 6.30 | 5.00 | 7.00 | 3.40 | 3.00 | 4.50 |
| Ho* | | 0.73 | 0.71 | 0.73 | 0.66 | 0.69 | 0.60 |
| La* | 13 | 30 | 28 | 51 | 22 | 20 | 21 |
| Lu* | 0.24 | 0.35 | 0.34 | 0.31 | 0.27 | 0.29 | 0.27 |
| Mo* | 2.10 | 2.20 | 1.70 | 1.30 | 1.80 | 1.20 | 1.80 |
| Nb* | 18 | 23 | 18 | 26 | 27 | 13 | 20 |
| Nd* | 13 | 25 | 25 | 39 | 23 | 21 | 19 |
| Ni | 85 | 26 | 45 | 30 | 170 | 300 | 45 |
| Pb* | 10 | 13 | 12 | 10 | 4 | 3 | 9 |
| Pr* | 3 | 7 | 7 | 11 | 6 | 5 | 5 |
| Rb* | 25 | 59 | 37 | 27 | 21 | 9 | 27 |
| Sc | 20 | 19 | 21 | 21 | 24 | 25 | 19 |
| Sm* | 3 | 5 | 5 | 6 | 5 | 4 | 4 |
| Sr | 740 | 590 | 640 | 870 | 830 | 640 | 810 |
| Ta* | 2.3 | 3.3 | 3.6 | 4.5 | 4.9 | 2.2 | 2.0 |
| Tb* | | 0.6 | 0.6 | 0.7 | 0.6 | 0.6 | 0.5 |
| Th* | 2.9 | 7.2 | 5.7 | 6.4 | 2.5 | 2.2 | 3.6 |
| Tl* | 0.1 | 0.2 | 0.4 | 0.1 | 0.0 | 0.0 | 0.1 |
| Tm* | 0.2 | 0.4 | 0.3 | 0.3 | 0.3 | 0.3 | 0.3 |
| U* | 1.0 | 1.6 | 1.2 | 1.2 | 0.9 | 0.5 | 1.1 |
| V | 240.0 | 160.0 | 170.0 | 170.0 | 180.0 | 150.0 | 200.0 |
| Y* | 12.0 | 21.0 | 21.0 | 21.0 | 19.0 | 20.0 | 17.0 |
| Yb | 1.0 | 1.6 | 1.7 | 1.5 | 1.4 | 1.6 | 1.3 |
| Zr | 160 | 240 | 210 | 290 | 120 | 110 | 160 |

**Table B2.**

Major and trace element data for seven of the samples. Analyses were done at the Geological Survey of Canada by XRF and by ICP-ES. Elements labeled with an asterisk were done by ICP-MS.

$R_A$, and the pyroxenes have a $^3He/^4He$ ratio of 3.1 $R_A$. In the oldest sample, B2, the pyroxene yields a $^3He/^4He$ ratio <1 $R_A$. Such radiogenic values in pyroxene phenocrysts from relatively old basalts have been observed previously and likely reflect *post-eruptive* radiogenic ingrowth of $^4He$ from the decay of uranium and thorium, since the typical uranium and thorium concentration is higher in pyroxene than in olivine.

## B.3 Discussion

Consistent MORB-like helium isotope ratios do not support the proposed plume under the Great Basin, nor does it agree with the assertion that the Yellowstone plume could have influenced these rocks. However, despite their MORB-like helium, these volcanic fields are characterized by a broad range of dominantly enriched strontium (~0.704-0.708) and neodymium (as low as 0.51212) isotope ratios relative to depleted MORB mantle (Asmerom et al., 1994; Omerod, 1988).

To determine whether mixing between a depleted MORB mantle, DMM, source and a more enriched crustal source is a reasonable hypothesis, we made some model calculations (Figure B2). The curves in Figure B2 are bulk mixing between a MORB melt and a mantle lithospheric component with helium concentrations in the mantle lithospheric end member governed only by radiogenic ingrowth (i.e., no helium initially in the lithospheric end member). The plot assumes equivalent concentrations of strontium in both end members and 50 μcc/g of helium initially in the DMM end member (helium concentration

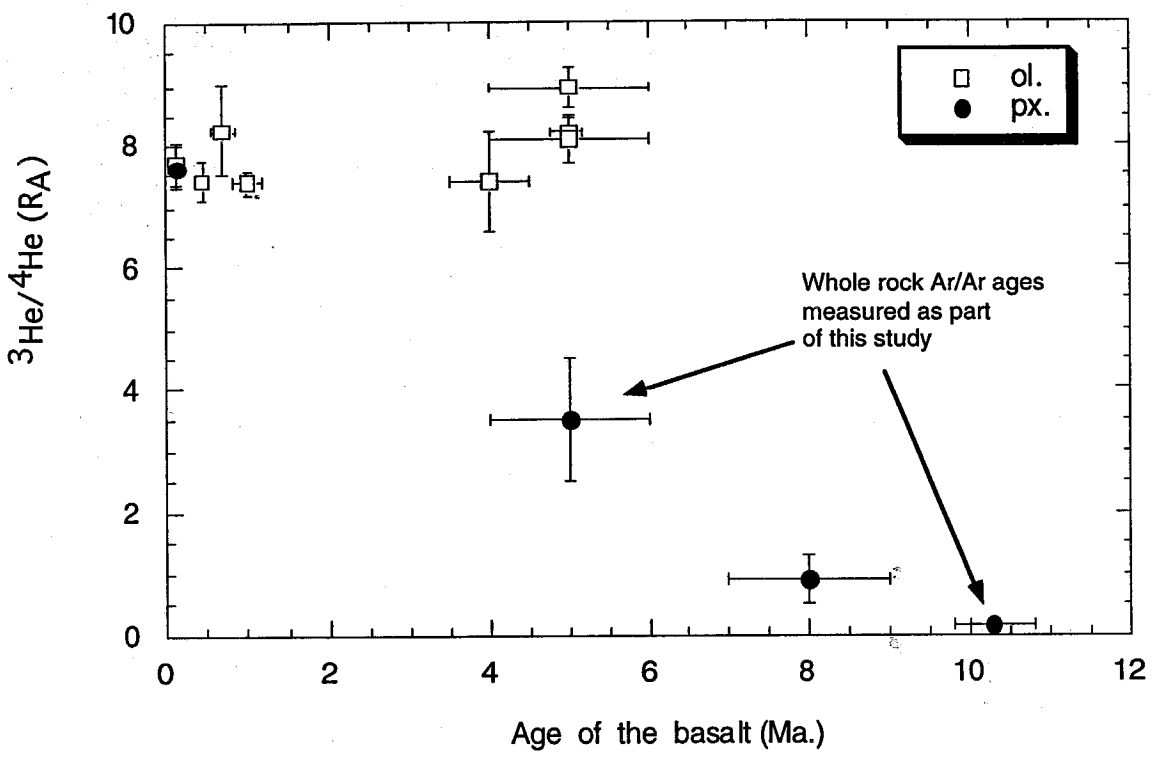


**Figure B1.**

Illustration of the effect of post-eruptive radiogenic ingrowth of $^4He$ into pyroxene, but not into olivine. This is the result of a higher average uranium and thorium concentration in the pyroxene phenyocrysts than in the olivine phenocrysts. All helium analyses were conducted by crushing of the phenocrysts under ultra-high vacuum to release helium trapped in the fluid inclusions. Two of the samples were dated by the Ar/Ar whole rock method as a part of this study by Dr. P.K. Zeitler. The remaining sample were correlated to samples whose ages are reported by Omerod (1988) and Schweig (1984,1982).

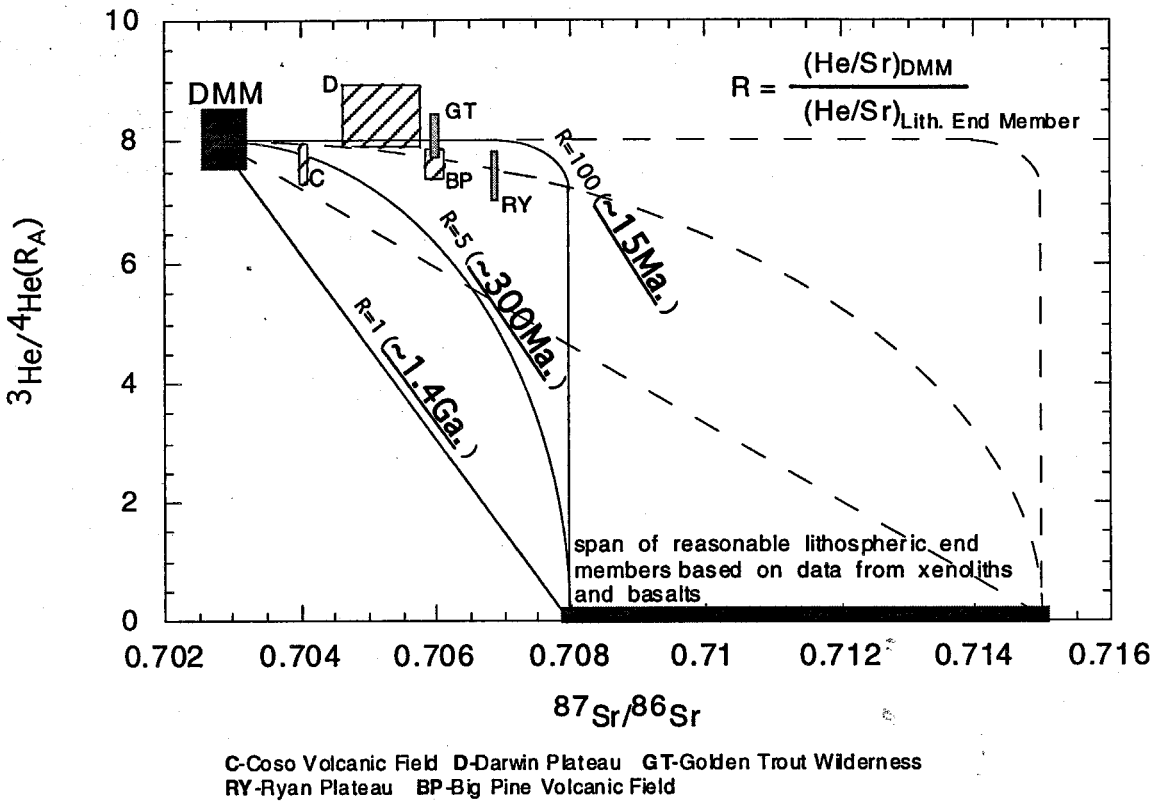


**Figure B2.**

Hypothetical mixing trajectories for helium and strontium between lithospheric and depleted mantle end members. The depleted mantle end member is assumed to have an initial concentration of helium of 50 µcc/g (Staudacher et al., 1989), and the lithospheric end member initially has no helium. Both end members are assumed to have the same strontium concentration. The range of strontium isotopic ratios for the lithospheric end member was inferred from Asmerom et al. (1994) and Omerod (1988). The strontium isotopic end member for the depleted mantle was taken from Zindler and Hart (1986).

taken from values for popping rocks, Staudacher et al., 1989). The range of strontium isotopic ratios used is derived from values obtained on basaltic and andesitic volcanic rocks in the region by Asmerom et al. (1994) and Omerod (1988). Ages on each mixing line give the age of the lithospheric end member, assuming a bulk lithospheric uranium concentration of 0.18 ppm and thorium concentration of 0.44 ppm (McDonough, 1990). In order for mixing to be reasonable, the age of the lithospheric end member would have to be less than a few hundred million years, and the actual age of the mantle lithosphere is likely to be >1.7 Ga (Reid and Graham, 1996). Based on our hypothetical mixing calculations, we do not see how Sr and He can be correlated. Moreover, a recent study suggests a positive correlation between helium and neodymium isotopic ratios (Reid and Graham, 1996), which is not consistent with our observations of consistently MORB-like helium. Although we cannot preclude this assertion for lack of neodymium analyses on our samples, we observe no correlation with helium and neodymium isotopic ratios when we compare our values with neodymium analyses reported on related flows. To fully ascertain whether our assertions are correct, it is necessary to make Sr and Nd analyses on our samples.

## B.4 Conclusions and Suggestions for Future Work

Helium isotopic ratios do not support a plume source under the central Great Basin. We observe consistent MORB-like helium ratios in volcanic rocks with apparently varied Sr and Nd isotopic ratios, and we cannot reconcile this

observation with simple mixing calculations. We suggest that there may be another mechanism which may cause helium to appear decoupled from Sr and Nd. We cannot fully answer questions regarding the interaction between Sr, Nd, and He without making more analyses which involve measurements of isotopes from all three elements on each sample.

# Conclusions and Future Work

*Thesis Summary*

This work represents the initial development of the (U-Th)/He thermochronometer. We have demonstrated that helium loss by alpha emission can be described quantitatively and proven analytically. We have shown that high precision, long duration diffusion experiments are an improvement on previous work and predict that helium retention in apatite occurs at a lower temperature than fission track annealing in apatite. Modeling of the diffusion data from incremental outgassing experiments using the full solution to the time varying radiogenic production/diffusion equation illustrates the effect of helium partial retention on apatite helium ages. This type of modeling is also a better method for characterizing helium ages than the closure temperature formulation because the closure temperature assumes a constant rate of cooling which is seldom the case at <100°C in the crust. Application of (U-Th)/He thermochronometry to the Cajon Pass Drillhole implies that laboratory diffusion experiments are applicable to natural systems and potentially provides new insight into the low temperature history of the Cajon Pass region. Finally, application of (U-Th)/He thermochronometry to the San Jacinto Mountain block yields new information about the recent thermal history of the block and demonstrates that apatite (U-Th)/He ages record useful and reliable geologic information. We have made the initial characterization of the system, modeled the system using laboratory data, and applied it to natural systems.

*New Avenues for (U-Th)/He Thermochronology*

The development of the (U-Th)/He thermochronometer will continue with higher precision analyses and diffusion experiments. Currently, there are a host of geologic problems which will benefit from (U-Th)/He thermochronometry because of its unique ability to record thermal histories below 100°C. It may help identify recent uplift along active faults or uplift rates for exhumed mountain blocks. Some preliminary investigations of basement rocks exposed at the surface near the Cajon Pass Drillhole indicate recent uplift (helium age of 2.8 Ma, work in progress) of these blocks which reside <1 km from the San Andreas fault. Since there is granitic basement exposed adjacent to Miocene and younger sediments along the entire Western San Bernardino Arch, this observation may be indicative of the recent uplift of basement blocks all along the Mojave Desert segment of the San Andreas Fault. More analyses are required to determine the full nature of the uplift history of the basement blocks, but this may be a case where the (U-Th)/He system is able to identify an important tectonic problem.

Future development of the (U-Th)/He method should also involve looking at a broader variety of apatites including sedimentary and metamorphic apatites. The data set from the Gold Butte block is a case where metamorphic apatite helium retentivity is inconsistent with igneous apatites. One interesting application of the (U-Th)/He method would be to examine the low temperature history of exhumed metamorphic core complexes and tilted ranges in the Great Basin, United States. However, if the diffusion behavior of metamorphic apatite

is not well understood, (U-Th)/He dating cannot be applied to this type of study. Another important use of the apatite (U-Th)/He method would be to investigate the maturation of sedimentary basins which can help determine hydrocarbon potential. In chapter 3, we describe the mathematical foundation for the time constants necessary to erase provenance helium. When helium ages exhibit the effects of provenance helium, this type of modeling can help to ascertain the maximum amount of heating which should correspond to the maximum amount of burial. In this way, sedimentary apatites can be used to understand basin evolution.

One of the most important new avenues for (U-Th)/He dating is the use of other mineral phases. Diffusion experiments on phases such as monazite, allanite, sphene, and zircon may provide new unique thermochronometers like apatite. We suggested that sphene has a closure temperature in the range of 225°-350°C, and it is the best phase for immediate future research. Currently, this could fill an important void in thermochronometry. The only other thermochronometers in this range are the $^{40}Ar/^{39}Ar$ method using micas and fission track counting of sphene. There are significant uncertainties in the annealing temperature of sphene and the closure temperature of micas. Therefore, the (U-Th)/He dating of sphene may provide an alternative high precision tool for understanding thermal histories in the crust occurring in the range of 225°-350°C, and would enhance our ability to understand low grade metamorphism and mid-crustal processes.

All of these research interests should be fulfilled to better our understanding of the low temperature history of the crust. However, like other thermochronometers, this technique is not perfect. The continued development of the method is critical for us to assess its limitations.

# Bibliography

Ague J., and Brandon M. (1992) Tilt and northward offset of Cordilleran batholiths resolved using igneous barometry. *Nature*, 360, 146-149.

Andrews J. N. (1985) The isotopic composition of radiogenic helium and its use to study groundwater movement in confined aquifers. *Chemical Geology*, 49, 339-351.

Atwater T. (1970) Implications of plate tectonics for the Cenozoic tectonic evolution of western North America. *Geological Society of America, Bulletin*, 81, 3513-3536.

Bender M. (1973) Helium-Uranium dating of corals. *Geochimica et Cosmochimica Acta*, 37, 1229-1247.

Bierman P. and Gillespie A. (1991) Range fires; a significant factor in exposure age determination and geomorphic surface evolution. *Geology*, 19, 641-644.

Brady R.J. (1996) arge magnitude Miocene extension in the Lake Mead region. *Geological Society of America Annual Meeting, Denver, Abstract Volume*, A-449.

Carslaw H.S. and Jaeger J.C. (1959) Conduction of Heat in Solids. 2ed., Oxford, Clarendon Press, 510p.

Cermak V. Huckenholz H.G., Rybach L., Schmid R., Schopper J.R., Schuch M., Stoffler D., and Wohlenberg J. (1982) Numerical Data and Functional Relationships in Science and Technology: Physical

Properties of Rocks. volume 1, subvolume a, New York, Springer-Verlag, p.315.

Climatological Data (1995) Publication of the California Division of Mines and Geology and the National Oceanic and Atmospheric Administration, 99, no.1-13.

Corrigan J. (1991) Inversion of apatite fission track data for thermal history information. *Journal of Geophysical Research*, 96, 10347-10360.

Craig H. and Lupton J. E. (1981) Helium-3 and mantle volatiles in the ocean and the oceanic crust. In *The Sea*, Vol. 7 (ed. C. Emiliani), J. Wiley and Sons, 391-428.

Crank J. and Nicolson (1947) *Proc. Camb. phil. Soc. math. phys. Sci.*, 43, 50p.

Crank J. (1975) The mathematics of diffusion, 2nd ed., Oxford, [Eng]: Clarendon Press, 414p.

Crowley K., Cameron M., and Schaefer R. (1991) Experimental studies of annealing of etched fission tracks in fluorapatite. *Geochimica et Cosmochimica Acta*, 55, 1449-1465.

Damon P. E. and Green W. D. (1963) Investigations of the helium age dating method by stable isotope dilution technique. In *Radioactive Dating*, IAEA. 55-71.

Damon P.E. and Kulp J.L. (1957) Determination of radiogenic helium in zircon by stable isotope dilution technique. *Trans. Am Geophys. Union*, 38, 945-953.

Dibblee T.W. (1967) Areal geology of the western Mojave Desert, California.

*U.S. Geological Survey Professional Paper*, 522, 153p.

Dodson M. H. (1973) Closure temperatures in cooling geological and petrological systems. *Contrib. Mineral. Petrol.*, 40, 259-274.

Dokka R. (1984) Fission track geochronologic evidence for late Cretaceous mylonitization and early Paleocene uplift of the northern Peninsular Ranges, California. *Geophysical Research Letters,* 11, 46-49.

Dumitru T. (1990) Subnormal Cenozoic geothermal gradients in the extinct Sierra Nevada magmatic arc: consequences of Laramide and post-Laramide shallow angle subduction. *Journal of Geophysical Research*, 95, 4925-4941.

Ehlig P.L. (1988) Geologic Structure near the Cajon Pass scientific drillhole. *Geophysical Research Letters*, 15, 953-956.

Fanale F. P. and Kulp J. L. (1962) The helium method and the age of the Cornwall, Pennsylvania magnetite ore. *Economic Geology,* 57, 735-746.

Fanale F. P. and Schaeffer O. A. (1965) Helium-uranium ratios for Pleistocene and tertiary fossil aragonites. *Science*, 149, 312-317.

Farley K.A., Wolf R.A., and Silver L.T. (1996a) The effects of long alpha stopping distances on (U-Th)/He ages. *Geochimica et Cosmochimica Acta*, 60, 4223-4230.

Farley K.A., Blythe A.E., and Wolf R.A. (1996b) Apatite helium ages: comparison with fission track ages and track length derived thermal models. *American Geophysical Union Fall Meeting, San Francisco, Abstract Volume*, 77, F644-F645.

Fechtig H. and Kalbitzer S. (1966) The diffusion of argon in potassium bearing solids. In Potassium-Argon Dating, ed. by O. A. Schaeffer and J. Zahringer, Springer, 68-106.

Ferreira M., Macedo R., Reynolds J., Riley J., and Rowe M. (1975) Rare gas dating. II. Attempted U-He dating of young volcanic rocks from the Madiera Archipelago. *Earth and Planetary Science* Letters, 25, 142-150.

Fitzgerald P.G., Sorkhabi R.B., Redfield T.F., and Stump E. (1995) Uplift and denudation of the Central Alaska Range: A case study in the use of apatite fission track thermochronology to determine absolute uplift parameters. *Journal of Geophysical Research*, 100, 20175-20191.

Fitzgerald P.G., Fryxell J.E., and Wernicke B.P. (1991) Miocene crustal extension and uplift in southeastern Nevada: Constraints from fission track analysis. *Geology*, 19, 1013-1016.

Fitzgerald P.F. and Gleadow A.J.W. (1990) New approaches in fission track geochronology as a tectonic tool - examples from the Transantarctic Mountains, *Nuclear Tracks and Radiation Measurements*, 17, 351-357.

Fleischer L., Price P.B., and Walker R.M. (1975) Nuclear tracks in solids: Principles and applications. University of California Press, Berkeley, 605p.

Fraser D. (1931) Geology of the San Jacinto Quadrangle south of San Gorgonio Pass, California. *Report of the State Mineralogist, California State Mining Bureau*, 27, 494-540.

George P. and Dokka R. (1994) Major late Cretaceous cooling events in the eastern Peninsular Ranges, California, and their implications for Cordilleran tectonics. *Geological Society of America Bulletin*, 106, 903-914.

Gilleti B. J. and Kulp J. L. (1955) Radon leakage from radioactive minerals. *American Mineralogist*, 40, 481-496.

Gleadow A.J.W. and Duddy I.R. (1981) A natural long-term annealing experiment for apatite. *Nuclear Tracks and Radiation Measurements*, 5, 169-174.

Gleadow A.J.W., Duddy I.R., and Lovering J.F. (1983) Fission track analysis: a new tool for the evaluation of thermal histories and hydrocarbon potential. *Austral. Petrol. Expl. Assoc. Journal*, 23, 93-102.

Goodwin L.B. and Renne P.R. (1991) effects of progressive mylonitization on Ar retention in biotites from the Santa Rosa Mylonite Zone, California and thermochronologic implications. *Contributions to Mineralogy and Petrology*, 108, 283-297.

Green P.F., Duddy I.R., Gleadow A.J.W., Tingate P.R., and Laslett G.M. (1985) Fission track annealing and the form of the arrhenius plot. *Nuclear Tracks and Radiation Measurements International Journal of Radiation Applications and Instrumentation Part D*, 10, 232-328.

Green P., Duddy I., Gleadow A., Tingate P., and Laslett G. (1986) Thermal annealing of fission tracks in apatite: 1. A qualitative description. *Chemical Geology,* 59, 237-253.

Green P.F., Duddy I.R., and Laslett G.M. (1988) Can fission track annealing in apatite be described by 1st order kinetics. *Earth and Planetary Science Letters*, 87, 216-228.

Green P.F. (1988) The relationship between track shortening and fission track age reduction in apatite: combined influences of inherent instability, annealing, anisotropy, length bias, and system calibration. *Earth and Planetary Science Letters*, 89, 335-352.

Green P.F., Duddy I.R., Laslett G.M., Hegarty K.A., Gleadow A.J.W., and Lovering J.F. (1989) Thermal annealing of fission tracks in apatite 4: Quantitative modelling techniques and extension to geological timescales. *Chemical Geology*, 79, 155-182.

Graham D. W., Jenkins W. J., Kurz M. D., and Batiza R. (1987) Helium isotope disequilibrium and geochronology of glassy submarine basalts. *Nature,* 326, 384-386.

Harrison T.M. (1981) Diffusion of $^{40}Ar$ in hornblende. *Contrib. Mineral. Petrol.*, 78, 324-331.

Harrison T.M. and McDougall I.D. (1985) Diffusion of (super 40) Ar in biotite; temperature, pressure and compositional effects. *Geochimica et Cosmochimica Acta*, 49, 2461-2468.

Henyey T., and Wasserburg G. (1971) Heat flow near major strike-slip faults in California. *Journal of Geophysical Research*, 76, 7924-7946.

Hill R. (1984) Petrology and petrogenesis of batholithic rocks, San Jacinto Mountains, southern California. PhD, California Institute of Technology.

Hill R. (1988) San Jacinto intrusive complex. 1. Geology and mineral chemistry, and a model for intermittent recharge of tonalitic magma chambers. *Journal of Geophysical Research*, 93, 10325-10348.

Holm D.K. and Dokka R.K. (1993) Interpretation and tectonic implications of cooling histories: An example from the Black Mountains, Death Valley Extended Terrane, California. *Earth and Planetary Science Letters*, 116, 63-80.

House M.A., Wernicke B.P., Farley K.A., and Dumitru T.A. (1997) Cenozoic thermal evolution of the central Sierra Nevada from (U-Th)/He thermochronometry. submitted to *Earth and Planetary Science Letters.*

Hurley P. M. (1954) The helium age method and the distribution and migration of helium in rocks. In Nuclear Geology (ed. H. Faul), Wiley, 301-329.

James E.W., and Silver L.T. (1988) Implications of zeolites and their zonation in the Cajon Pass Deep Drillhole, *Geophysical Research Letters* , 15, 973-976.

Kohn B.P., Saltus R.W., and Gleadow A.J.W. (1994) Thermotectonic history of the Cajon Pass Deep Drillhole, southern California: an apatite fission track study. *Abstracts from the Eigth International Conference on Geochronology, Cosmochronology, and Isotope Geology, U.S. Geological Survey Circular*, 1107, 176.

Lachenbruch A.H., Sass J.H., Clow G.D., and Weldon R.J. (1995) Heat flow at Cajon Pass, California, revisited. *Journal of Geophysical Research*, 100, 2005-2012.

Lachenbruch A.H., Sass J.H., and Morgan P. (1994) Thermal regime of the Southern Basin and Range Province 2: Implications of heat flow for regional extension and metamorphic core complexes. *Journal of Geophysical Research*, 99, 22121-22133.

Lachenbruch A.H. and Sass J.H. (1992) Heat-flow from Cajon Pass, fault strength, and tectonic implications. *Journal of Geophysical Research*, 97, 4995-5015.

Lippolt H.J., Leitz M., Wernicke R.S., and Hagedorn B. (1994) (U+Th)/He dating of apatite: experience with samples from different geochemical environments. *Chemical Geology*, 112, 179-191.

Lippolt H. J. and Weigel E. (1988) $^{4}He$ diffusion in $^{40}Ar$ retentive minerals. *Geochim. et Cosmochim. Acta*, 52, 1449-1458.

Lovera O., Richter F., and Harrison T. (1989) The $^{40}Ar/^{39}Ar$ thermochronometry for slowly cooled samples having a distribution of domain sizes. *Journal of Geophysical Research*, 94, 17917-17935.

Lovera O., Richter F., and Harrison T. (1991) Diffusion domains determined by 39Ar released during step heating. *Journal of Geophysical Research*, 96, 2057-2069.

Lutz T.M. and Omar G. (1991) An inverse method of modelling thermal histories from apatite fission track data, *Earth and Planetary Sciences Letters*, 104, 181-195.

Lyons J.I. (1988) Volcanogenic iron oxides, Cerro de Mercado and vicinity, Durango, Mexico. *Economic Geology*, 83, 1886-1906.

McDonough W.F. (1990) Constraints of the composition of the continental lithospheric mantle. *Earth and Planetary Science Letters*, 101, 1-18.

Mcdougall I., and Harrison M.T. (1989) Geochronology and thermochronology by the $^{40}Ar/^{39}Ar$ method. Oxford University Press, Oxford, 212p.

McDowell F. and Keizer R. (1977) Timing of mid-Tertiary volcanism of the Sierra Madre Occidental between Durango City and Mazatlan, Mexico. *Geological Society of America, Bulletin*, 88, 1479-1487.

Meisling K.E. and Weldon R.J. (1989) The Late Cenozoic tectonics of the northewestern San Bernardino Mountains, southern California. *Geological Society of America Bulletin*, 101, 106-128.

Miller M.G., and Weldon R.J. (1992) A lateral ramp origin for the north trending segment of the Squaw Peak fault, Cajon Pass, California. *Journal of Geophysical Research*, 97, 5153-5165.

Naeser C. and Fleischer R. (1975) Age of the apatite at Cerro de Mercado, Mexico: a problem for fission track annealing records. *Geophysical Research Letters,* 2, 67-70.

Noble L.F. (1954) The San Andreas fault zone from Soledad Pass to Cajon Pass, California. *Bulletin of the California Division of Mines and Geology*, 170, 32-48.

Ormerod D.S. (1988) Late to post-subduction magmatic transitions in the western Great Basin, United States of America. Ph.D. Thesis, The Open University.

Osullivan P.B. and Currie L.D. (1996) Thermotectonic history of Mt. Logan, Yukon Territory, Canada: Implications of multiple episodes of middle to late Cenozoic denudation. *Earth and Planetary Science Letters*, 144, 251-261.

Parsons T., Thompson G.A., and Sleep N.H. (1994) Mantle plume influence on the Neogene uplift and extension of the United States western Cordillera. *Geology*, 22, 83-86.

Pratson E.L., Anderson R.N., Dove R.E., Lyle M., Silver L.T., James E., and Chappell B.W. (1992) Geochemical logging in the Cajon Pass Drillhole and its application to a new, oxide, igneous rock classification scheme. *Journal of Geophysical Research*, 97, 5167-5180.

Reynolds R.E. (1985) Tertiary small mammals in the Cajon Valley, San Bernardino, California, R.E., ed., in Geologic Investigations along Interstate 15, Cajon Pass to Mannix Lake, California. *Western Association of Vertebrate Paleontologists Field Trip Guidebook*, 60th Meeting, Redlands California, San Bernardino County Museum, 49-58.

Roberts S.V. and Burbank D.W. (1993) Uplift and thermal history of the Teton Range (Northwestern Wyoming) defined by apatite fission track dating. *Earth and Planetary Science Letters*, 118, 295-309.

Rutherford E. (1905) Present problems in radioactivity. *Popular Science,* May, 1-34.

Saltus R.W. and Thompson G.A. (1995) Why is it downhill from Tonopah to Las Vegas: A case for mantle plumes. *Tectonics*, 14, 1235-1244.

Sass J.H., Lachenbruch A.H., MosesT.H., and Morgan P. (1992) Heat Flow from a Scientific Research Well at Cajon Pass, California. *Journal of Geophysical Research*, 97, 5017-5030.

Sass J.H., Lachenbruch A.H., Galanis Jr., S.P., Munroe R.J., and Moses T.H. (1986) An analysis of thermal data from the vicinity of Cajon Pass, California. *U.S.G.S. Open File Report*, 86-468, 47p.

Schweig E.S. (1982) Late Cenozoic stratigraphy of the Darwin Plateau, Inyo County, California/ M.S. Thesis, Stanford University, 85p.

Schweig E.S. (1984) Neogene tectonics and paleogeography of the southwestern Great Basin, California. Ph.D. Thesis, Stanford University, 229p.

Sharp R.V. (1966) Ancient mylonite zone and fault displacements in the Peninsular Ranges of Southern California. *Geological Society of America Special Paper*, 101, 333p.

Sharp R.V. (1979) Some characteristics of the Eastern Peninsular Ranges Mylonite Zone. *U.S.G.S. Open-File Report 79-1239*, 258-267.

Silver L., Taylor H., and Chappell B. (1979) Some petrological, geochemical and geochronological investigations of the Peninsular Ranges Batholith near the international border of the USA and Mexico. In *Mesozoic Crystalline Rocks* (ed. P. Abbot and V. Todd). Geological Society of America Guidebook, Annual Meeting, San Diego.

Silver L., and Hill R. (1986) U-Th-Pb microdiscordance in young zircons: a case study in the San Jacinto Mountains. *EOS, Transactions of the American Geophysical Union*, 67, 399-400.

Silver L.T. and James E.W. (1988) Geologic setting and lithologic column of the Cajon Pass Deep Drillhole. *Geophysical Research Letters*, 15, 941-944.

Silver L.T., James E.W., and Chapple B.W. (1988) Petrological and geochemical investigations at the Cajon Pass deep drillhole. *Geophysical Research Letters*, 15, 961-964.

Simpson C. (1984) Borrego Springs - Santa Rosa mylonite zone: a late Cretaceous west-directed thrust in Southern California. *Geology,* 12, 8-11.

Smith D., Morton D., and Miller F. (1991) Hornblende geobarometry and biotite K-Ar ages from the northern part of the Peninsular Ranges Batholith, Southern California. *Geological Society of America, Abstracts With Programs*, 23, A273.

Staudacher T., Sarda P., Richardson S.H., Allegre C.J., Sagna I., and Dmitriev L.V. (1989) Noble gases in basalt glasses from a Mid-Atlantic Ridge topographic high at 14°N: geodynamic consequences. *Earth and Planetary Science Letters*, 96, 119-133.

Stuwe K., White L., and Brown R. (1994) The influence of eroding topography on steady-state isotherms - application to fission track analysis. *Earth and Planetary Science Letters*, 124, 63-74.

Strutt R. (1908) The accumulation of helium in geologic time. *Roy. Soc. London Proceedings*, 81A, 272-277.

Strutt R. (1909) The leakage of helium from radioactive minerals. *Roy. Soc. London Proceedings*, 82A, 166-169.

Suppe J., and Armstrong R. (1973) Potassium-Argon geochronometry of Mesozoic igneous rocks in Nevada, Utah, and southern California. *Geological Society of America Bulletin*, 84, 1375-1391.

Trull T. W., Kurz M. D., and Jenkins W. J. (1991) Diffusion of cosmogenic 3He in olivine and quartz: implications for surface exposure dating. *Earth and Planetary Science Letters*, 103, 241-256.

Trull T.W., Brown E.T., Marty B., Raisbeck G.M., and Yiou F. (1995) Cosmogenic $^{10}Be$ and $^{3}He$ accumulation in Pleistocene beach terraces in Death Valley, California, USA - implications for cosmic-ray exposure dating of young surfaces in hot climates. *Chemical Geology*, 119, 191-207.

Turekian K., Kharkar D., Funkhouser J., and Schaeffer O. (1970) An evaluation of the U-He method of dating bone. *Earth and Planetary Science Letters*, 7, 420-424.

Wagner G.A., and Reimer, G.M. (1972) Fission track tectonics: the tectonic interpretation of fission track ages. *Earth and Planetary Science Letters*, 14, 263-268.

Wagner G.A., Gleadow A.J.W., and Fitzgerald P.G. (1989) The significance of the partial annealing zone in apatite fission track analysis - projected

track lenght measurements and uplift chronology of the Transantarctic Mountains. *Chemical Geology*, 79, 295-305.

Warnock A.C., P.K. Zeitler R.A. Wolf, and Bergman S.C. Low-Temperature Thermochronometry using the Apatite (U-Th)/He Method. submitted to*Geochimica et Cosmochimica Acta.*

Wernicke B., and Axen G., 1988, On the role of isostasy in the evolution of normal-fault systems. *Geology*, 16, 848-851.

Weldon R.J. (1986) The late Cenozoic geology of Cajon Pass : implications for tectonics and sedimentation along the San Andreas fault. Ph.D. Thesis, California Institute of Technology, 400p.

Weldon R.J., Meisling K.E., and Alexander J. (1993) A speculative history of the San Andreas fault in the central Transverse Ranges, California, in The San Andreas fault system: displacement, palinspastic reconstruction, and geologic evolution. ed. by Powell, R.E., R.J. Weldon, and Matti, J.C., *Memoir of the Geological Society of America*, 178, 161-198.

Wolf R.A., Farley K.A., and Silver L.T. (1996a) Helium diffusion and low temperature thermochronometry of apatite. *Geochimica et Cosmochimica Acta*, 60, 4231-4240.

Wolf R.A., Kass D.M., and Farley K.A. (1996b) The sensitivity of the apatite (U-Th)/He system to thermal history. *American Geophysical Union Fall Meeting, San Francisco, Abstract Volume*, 77, F644.

Wolf R.A., Farley K.A., and Silver L.T. (1997) Assessment of (U-Th)/He thermochronometry: the low temperature history of the San Jacinto mountains, California. *Geology*, 25, 65-68.

Woodburne M.O. and Golz D.J. (1972) Stratigraphy of the Punchbowl Formation, Cajon Valley, southern California. *University of California Publ. Geol. Sci.*, 92, 57p.

Woodhead J. A., Rossman G. R., and Silver L. T. (1991) The metamictization of zircon: radiation dose-dependent structural characteristics. *American Mineralogist,* 76, 74-82.

Young E., Myers A., Munson E., and Conklin N. (1969) Mineralogy and geochemistry of fluorapatite from Cerro de Mercado, Durango, Mexico. *United States Geological Survey, Professional Paper*, 650-D, D84-D93.

Zeitler P. K., Herczig A. L., McDougall I., and Honda M. (1987) U-Th-He dating of apatite: a potential thermochronometer. *Geochimica et Cosmochimica Acta*, 51, 2865-2868.

Ziegler J. F. (1977) Helium: Stopping powers and ranges in all elemental matter. Pergamon.

Zindler A. and Hart S. (1986) Chemical geodynamics. *Annual Review of Earth and Planetary Sciences*, 14, 493-571.

# ERRATA

There is an error in the plot which illustrates how a forest fire affects helium retentivity (page 102). The depth scale is incorrect; scale values should be increased by a factor of 2. Thus, the depth to which helium retention would be significantly affected by a fire lasting 10 minutes is ~3 cm instead of ~1.5 cm, while that affected by an hour long fire is ~9 cm instead of ~4.5 cm. The conclusion that typical forest fires should not significantly affect apatite helium ages remains unchanged.